CHARACTERISATION AND OPTIMIZING OF ULTRASOUND TRANSDUCERS FOR BREAST CANCER DIAGNOSIS AND THERAPY

Juhana Pirinen

Bachelor's Thesis

Bachelor's degree

Savonia
University of Applied Sciences

SAVONIA UNIVERSITY OF APPLIED SCIENCES **THESIS**
Abstract

Field of Study Technology, Communication and Transport			
Degree Programme Degree Programme in Electronic Engineering			
Author(s) Juhana Pirinen			
Title of Thesis Characterisation and Optimizing of Ultrasound Transducers for Breast Cancer Diagnosis and Therapy			
Date	13 July 2011	Pages/Appendices	79/4
Supervisor(s) Arto Toppinen, Benedikt Kohout			
Client Organisation/Partners Karlsruhe Institute of Technology			

Abstract

The characteristics of an ultrasound transducer have to be optimized in order to enhance the performance to a maximized level. In this thesis the influence of the geometrics and materials of the transducer on the behaviour of the transducer was studied.

The characteristics of the ultrasound transducer were researched and the finite element analysis (FEA) simulation model of the transducer was optimized. The work was carried out within the Ultrasound Computer Tomography (USCT) project by the Institute for Data Processing and Electronics (IPE) in Karlsruhe Institute of Technology (KIT), Germany.

The optimization of the model included fitting the material parameters and the damping of the model to a measured transducer by comparing the impedance absolute values. The model was also enhanced in accuracy by strategically condensing the meshing of the simulation model.

Simulations with varying parts of the transducer's dimensions were conducted and analyzed. As a result, some behaviour in the transducer was linked to the material parameters and/or to the geometry of the transducer.

Keywords
ultrasound transducer, ultrasound computer tomography, finite element analysis

SAVONIA-AMMATTIKORKEAKOULU **OPINNÄYTETYÖ**
Tiivistelmä

Koulutusala Tekniikan ja liikenteen ala			
Koulutusohjelma Elektroniikan koulutusohjelma			
Työn tekijä(t) Juhana Pirinen			
Työn nimi Ultraäänimuuntimien karakterisointi ja optimointi rintasyövän diagnosointiin ja hoitamiseen			
Päiväys	13.07.2011	Sivumäärä/Liitteet	79/4
Ohjaaja(t) Arto Toppinen, Benedikt Kohout			
Toimeksiantaja/Yhteistyökumppani(t) Karlsruhen teknillinen instituutti			

Tiivistelmä

Ultraäänimuuntimien ominaisuudet täytyvät olla optimoidut että ultraäänitomografian suorituskyky voidaan nostaa maksimaaliselle tasolle. Opinnäytetyössä selvitettiin ultraäänimuuntimien geometrian ja materiaalien vaikutusta ultraäänimuuntimien käyttäytymiseen.

Ultraäänimuuntimen erityispiirteet selvitettiin ja muuntimen äärellisten elementtien analyysin (FEA) simulaatiomalli optimoitiin. Työ suoritettiin Karlsruhen teknillisen instituutin (KIT) Ultrasound Computer Tomography (USCT) –projektissa Saksassa.

Mallin optimointi tapahtui sovittamalla mallin materiaaliparametrit ja vaimennus oikeaan ultraäänimuuntimeen ja vertaamalla mitattuja ja simuloituja impedanssin itseisarvoja. Mallia tehtiin myös tarkemmaksi strategisesti tiivistämällä simulaatiomallin elementtiverkkoa.

Simulaatioita, joissa varioitiin osia muuntimesta suoritettiin ja tuloksia analysoitiin. Työn tuloksena osa muuntimen käyttäytymisestä pystyttiin yhdistämään materiaaliparametreihin ja/tai muuntimeen geometriaan.

Avainsanat
ultraäänimuunnin, ultraäänitietokonetomografia, äärellisten elementtien analyysi

ACKNOWLEDGEMENTS

This thesis was conducted for the USCT project at the Institute for Data Processing and Electronics of Karlsruhe Institute of Technology in Leopoldshafen, Germany in spring 2011.

I would like to express my gratitude for my supervisors Arto Toppinen in Savonia University of Applied Sciences and especially for Benedikt Kohout in Karlsruhe Institute of Technology for guidance and the possibility to conduct this thesis. I would also like to thank Nicole Ruiter and all the other people included in the USCT project.

Most of all I would like to thank my family and friends for being so supportive during my studies through the years.

CONTENTS

ABBREVIATIONS AND NOTIONS

2D	Two dimensional
3D	Three dimensional
A/D	From analog to digital
APDL	ANSYS Parametric Design Language
CAE	Computer Aided Engineering
DAQ	Data Aqcuisition
Dipole	Pair of electric point charges of equal magnitude and opposite sign
Element	Individual particle of the model
FEA	Finite Element Analysis
FEM	Finite Element Method
GPU	Graphics Processing Unit
GUI	Graphic User Interface
IPE	Institute for Data Processing and Electronics
Isotropic	Uniform in all orientations
KIT	Karlsruhe Institute of Technology
Lamb waves	Elastic waves in solid media in the plane of plate normal to the direction of wave propagation
Mammography	Examination of human breast by X-ray
Mesh/meshing	Arrangement of the nodes in simulation model
Metastasis	Spread of a disease from one organ to another
Node	Interconnection point of the elements in simulation model
Palpation	Physical examination by feeling the object with hand
Polarization	Vector quantity indicating the electric dipole moment
PU	Lead-zirkonite-titanate mixed ceramic
TAS	Transducer Array System
TMM	Ceramic thermoset polymer composite
Tomography	Technique used to obtain an image of a selected plane section
Transducer	Device that converts energy from one type to another (commonly sensor/detector)
USCT	Ultrasound Computer Tomography

1 INTRODUCTION

Cancer is a leading cause of death worldwide and in 2008 more than 7.5 million people died of cancer. More than 12.6 million cancer incidences were recorded that year, 1.4 million of them were breast cancers. Breast cancer is the most common cancer in women and second most frequent after lung cancer in both sexes. In 2008 half a million people died of a cancer in a breast. [1]

At Karlsruhe Institute of Technology (KIT) a new methodology for early breast cancer detection is being researched. The project called USCT, from “Ultrasound Computer Tomography”, develops a device to detect tumors at an early stage in a human breast by the means of ultrasound tomography. [2]

In ultrasound tomography a set of ultrasound transducers are used to send ultrasonic waves to an object like in Figure 1. When the waves hit the object they pass through, rebound, scatter and are intercepted by the receiving transducers. The resulting signal is then processed with the sending signal with computer algorithms to create a visualisation of the object. [3]

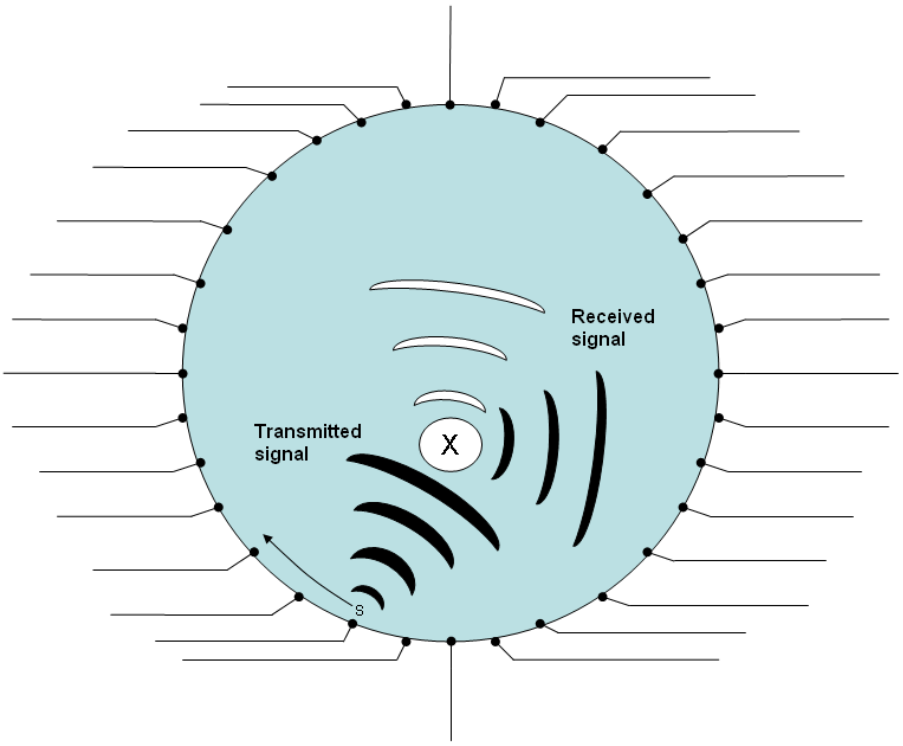

FIGURE 1. 2D sketch of a sound wave propagating to an object X

The characteristics of the transducers have to enable a preferred signal to be sent and to have a good reception in receiving signals. The electrical and the acoustical impedance have to fit the system, the created sound pressure has to be strong enough and the bandwidth must be wide enough to cover the used frequency area.

“The ideal medical transducer has high sensitivity, generates short acoustic pulses, and has properties that match the electrical impedance of a practical transmitter/receiver.” (Hunt et al. 1983, 463.)

Optimizing the transducer can be done by making material and structural changes to the transducer. While the changes and their effects on the behaviour of the transducer could be researched by building prototype models, it is often not feasible to do so because the manufacturing process is always quite time and money consuming. Also for the manufacturing of a prototype by hand is prone to errors there would have to be a whole series built. Therefore Finite Element Method (FEM) simulations are used first to confirm that the modifications for the transducers could provide wanted results.

In this thesis the use of the ANSYS software to simulate a transducer is discussed and provided with results from modifying the transducer structure and materials. The knowledge of physical phenomena, documentation skills, basic knowledge of scripting languages and MatLab programming as well as electronics manufacturing were needed to conduct this thesis.

2 USCT

2.1 USCT project

The USCT project (logo in Figure 2) is a project carried out in KIt is Institute for Data Processing and Electronics (IPE). Its goal is to obtain a detection of a breast tumor in an early stage of the disease. The objective is to detect tumors smaller than 5 mm in diameter. This can be achieved by creating a 3D image of the inside of a breast. Early detection of the cancer is important because at early stage the disease is easier to treat and metastases are not yet formed. Many breast cancer incidents go unnoticed at the early stage because the tumor is often too small to be recognised by palpation or by mammography. Also the X-ray mammography works well only for elderly patients due to their less dense breast tissue. Often the lump in a breast is the first sign of the cancer that the patient or a doctor notices. With the USCT diagnosing device the tumor may be recognized at early stage before metastases are formed and from patients of all ages without the ionizing effect of the X-ray mammography. Unlike the results from X-ray, the results from USCT imaging are unambiguous and comparable. [4]

FIGURE 2. USCT logo

2.2 Ultrasound Imaging

Ultrasound imaging is commonly used only as second look diagnosis in healthcare, because of its tendency to produce images that are difficult to interpret due to reduced image quality by noise and shadowing effects. However, a good quality 3D image is possible to create by using a setup where a reservoir of ultrasound transducers surrounds the object in water to be imaged. Then each transducer in its turn transmits a pulse signal while the other transducers receive all transmitted, scattered and reflected

signals. This leads, however, to a massive data rate depending on the setup size and sampling rate. The image can be restored by using robust image restoration methods. The image processing is one of the key areas in the USCT project. In Figure 3 there is a reconstructed image of breast phantom taken with USCT I-device. [4] [5]

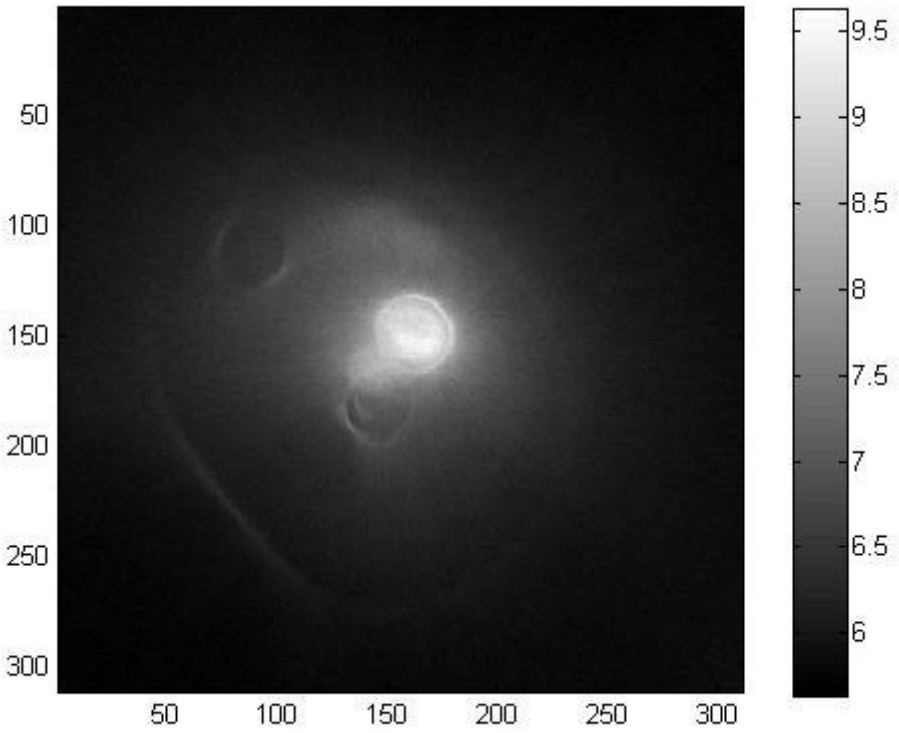

FIGURE 3. Reconstructed image of breast phantom taken with USCT I-device

2.3 The Imaging Apertures

The first USCT device (Figure 4) built at KIT in 2004 has 384 emitting and 1536 receiving ultrasound transducers on a surface of a cylinder 18 cm in diameter and 15 cm in height. The cylinder, which is filled with water, can be rotated in six steps making 2304 emitter and 9216 receiver virtual positions. The transducers are grouped in to array systems of eight emitters and 32 receivers. The device has an embedded signal generator allowing the emitters to be excited digitally for 256 samples at 40 MHz. The received signals are directed to a dedicated DAQ system which consists of nine 9U Eurocard boards out of which one is for controlling the DAQ and data handling. The other eight are for A/D-conversion and signal processing. The digital signal processing is carried out by an array of four Altera FPGAs. [6]

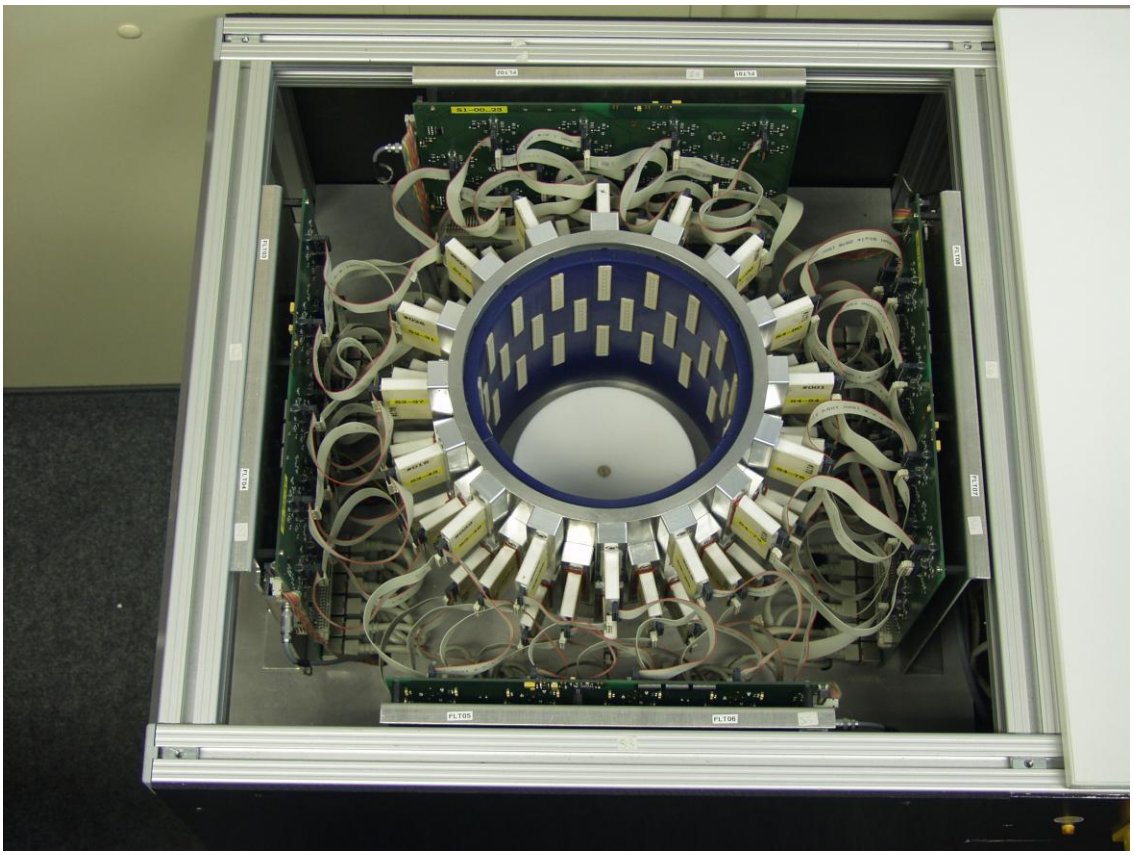

FIGURE 4. The first USCT 3D-imaging aperture, the USCT I

After proving the feasibility of the method with the first aperture, the second generation of the USCT device, USCT II (Figure 5), for pre-clinical studies was built. The shape of the aperture was changed to a semi-ellipsoid for more optimal imaging results. The USCT II has 628 emitting and 1413 receiving transducers and movement of the setup creates further transducer positions. The working principle is the same as in the first USCT but the TAS and the data aqcuisition (DAQ) system have been modified. Parallel data processing has been also taken into account in the hardware for reducing the data acquisition time. [7]

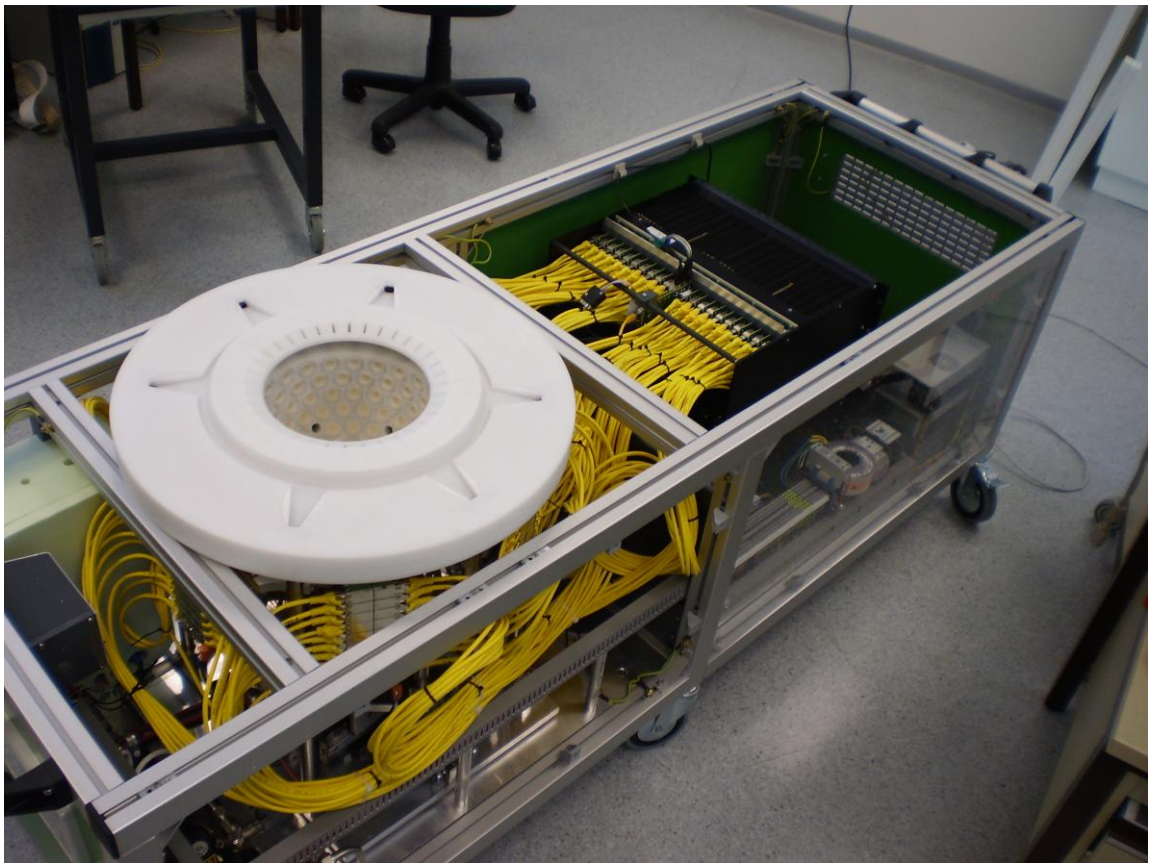

FIGURE 5. The USCT II aperture

3 ULTRASOUND TRANSDUCERS

Ultrasound is sound that has frequency over the limit of human hearing, commonly denoted as 20 kHz. Piezoelectric transducers have piezoelectric material that pick up the sound waves and convert it to electrical energy or when excited with alternative current or voltage, produce ultrasound by vibrating. This is due to the electromechanical interaction in piezoelectric materials. [8]

Most ultrasound transducer systems used in medical imaging comprise of an array or a matrix of piezoelectric transducer elements. They are used to send a short pulse wave to the imaged object and then gather the resulting signal. The same transducer can be used to send and receive the pulse, but in the USCT project there are designated transducers for both tasks. A matching layer to the propagated media and/or a backing is/are often, although not always, used.

In an ultrasound imaging system, the transducer is perhaps the single most important component. The USCT transducers are in-house built piezoelectric (PZT) ultrasound transducers with a sub-diced matrix structure. The diced rods are surrounded by a polyurethane (PU) filler material and towards the water load there is a matching layer. Behind the PZT there is backing made out of polyurethane. The transducer is sealed with connecting electronics inside a metal tube for protection, like in Figure 6. [8]

FIGURE 6. USCT transducer

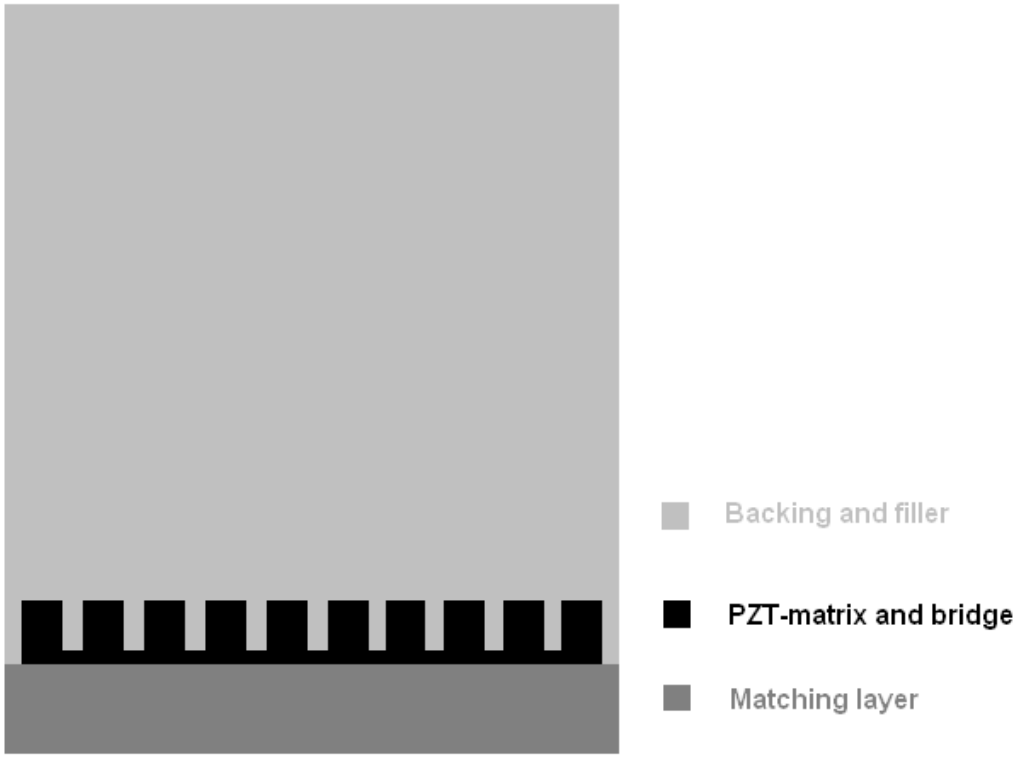

FIGURE 7. Vertical cut of a transducer

Contacts are bonded to transducer rods so that it becomes a transducer array system (TAS). In TAS, there are 13 sets of independently working elements out of which four sets are sending and nine sets are receiving. In Figure 7 there is a vertical cut sketch of the transducer and in Figure 8 is a horizontal cut sketch of the transducer with the sending and receiving sets marked.

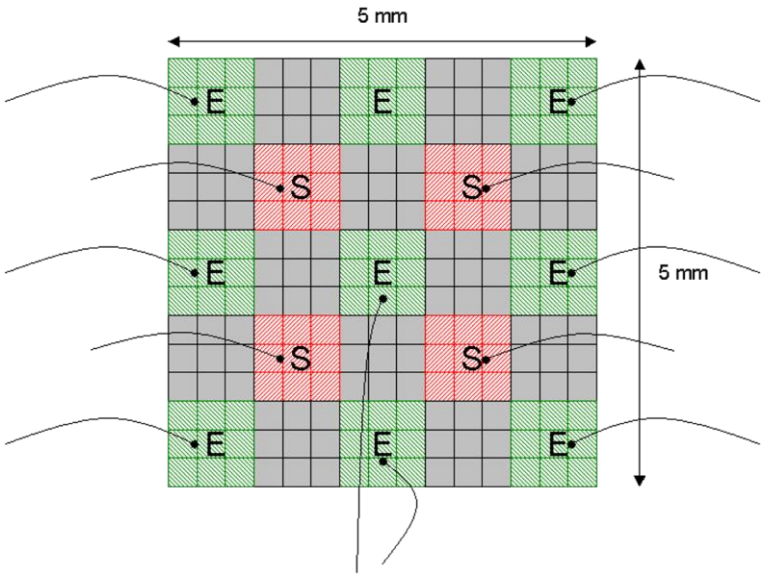

FIGURE 8. Transducer Array System with four senders (S) and nine receivers (E)

3.1 Equivalent Circuit

A transducer can be demonstrated as electromechanical equivalent circuit. It is based on the analogies of mathematical descriptions between electric and mechanical phenomena. The analogies come from similarities in equations that describe the behaviour of electrical and mechanical systems. One of the most commonly used equivalent circuits, the Mason's equivalent circuit, is in Figure 9. The quantities in the figure are as follow:

F_B: force on the back face
F_L: force on the front face (radiating surface)
V: voltage across the electrodes in transducer
I: current through the electrodes in transducer
C_0^S: clamped capacitance of the piezoelectric plate
A: area of the electrodes
Z_0: characteristic acoustic impedance of the piezoelectric material
β: propagation constant
h_{33}: piezoelectric constant

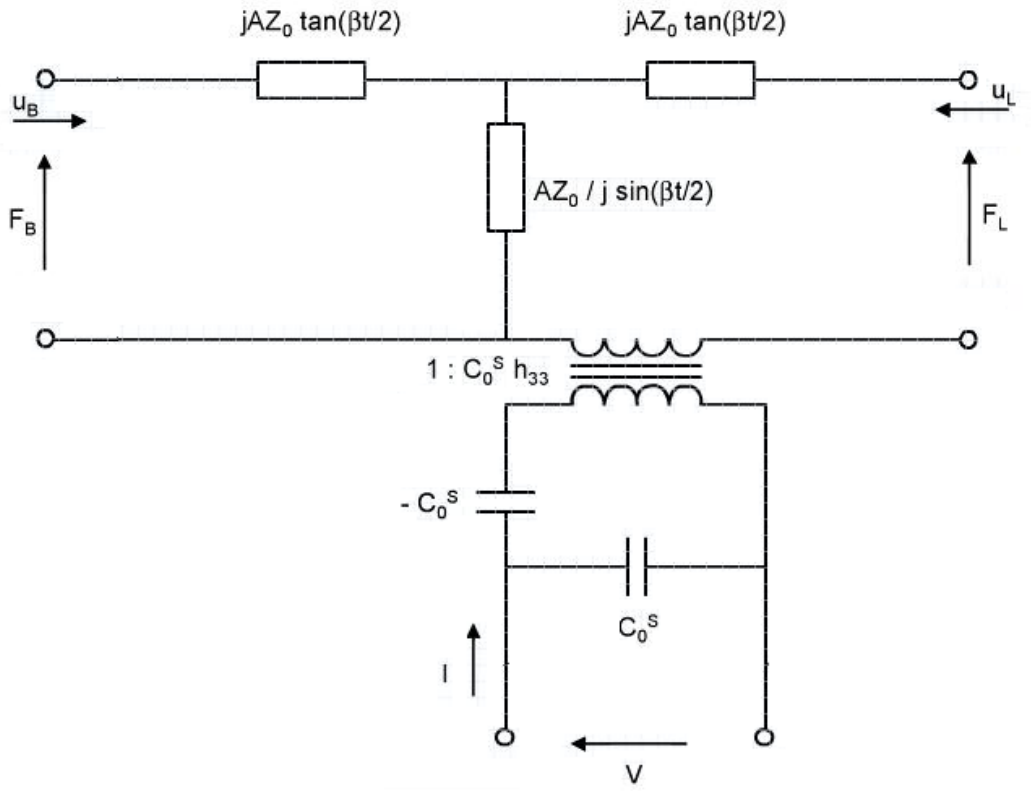

FIGURE 9. Mason's equivalent circuit of a thickness mode transducer

In the circuit the electrical port is coupled through an ideal transformer to a T network which represents the acoustic propagation of the piezoelectric material. The mechanical ports are on the ends of the T-network. The negative capacitance and the ideal transformer account for the electromechanical coupling. [9]

Equivalent circuit models are widely used in researching ultrasound transducers, but they cannot replace the FEA done with simulation software. At best they offer a basis for limited amount of theoretical calculations that can be used to examine the mechanical behaviour of the transducer and one-dimensional plane waves travelling in the transducer. From the simulations, not only the mechanical and electrical data can be retrieved, but also a set of very specific three-dimensional details. Equivalent circuit models are also valid only for specific types of PZT structures with defined electrodes and this sets limitations for the models. In the equivalent circuit the transducer is always represented more or less as a whole system whereas from the simulations it is possible to look at a single fragment and its influence on other fragments. [10] [11]

3.2 Transducer Electrical Impedance

The electrical impedance of an ultrasound transducer is easier to simulate than sound pressure, which would need a big volume of propagated media to be simulated as well. The impedance tells a lot about transducers behaviour. Resonances can be concluded from the impedance graph. And from the shape, width and magnitude of the resonance one can tell a lot about the properties of the transducer. The materials, shape and the size of the active element determine the resonance frequencies. In general, thicker element has lower resonance frequency than a thinner element of same shape.

Disregarding mechanical losses, when an ultrasound transducer resonates (series resonance), its current has maximum value and so the impedance has minimum value. At resonance, the impedance is purely resistant. Anti-resonance (parallel resonance) occurs when impedance reaches its maximum value (admittance is minimum). Transducer has its best response between the resonance and anti-resonance points, the maximum being at resonance point. [12]

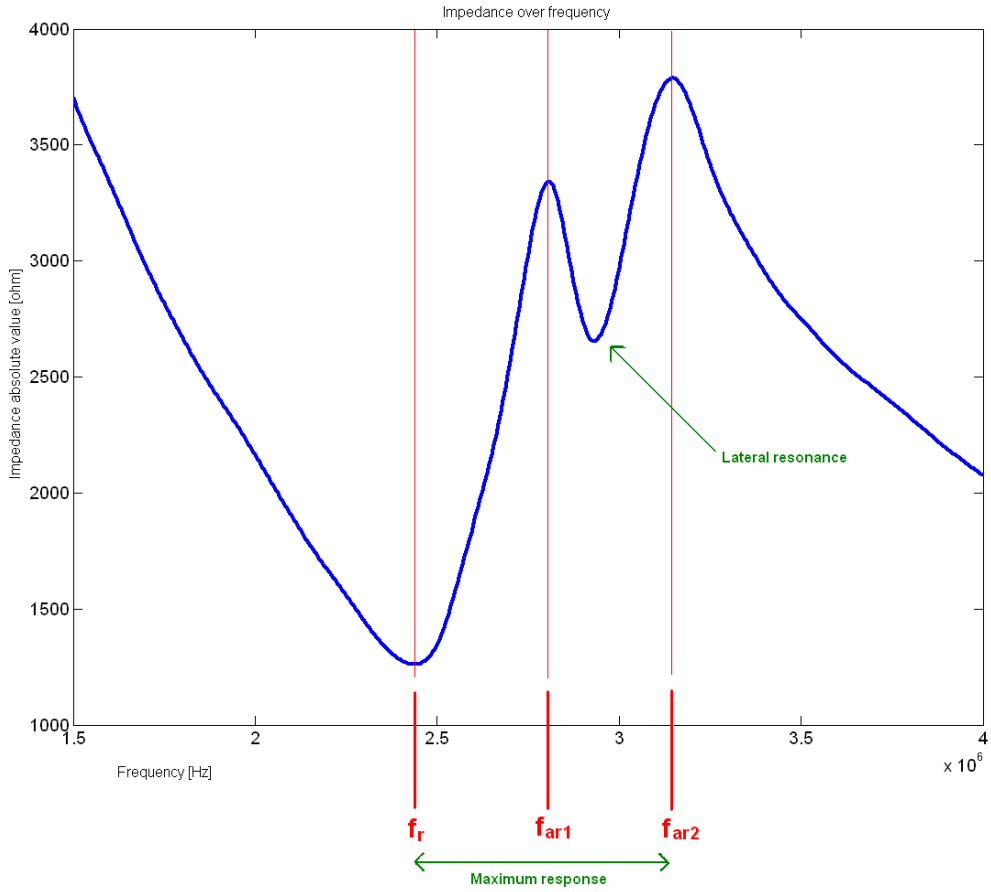

FIGURE 10. Measured ultrasound transducer impedance absolute value graph

Figure 10 has a typical impedance absolute value curve for a USCT test transducer. In between 1.5 and 4 MHz there's two local minimums and two local maximums. The first minimum, f_r is the thickness mode resonance point. The second local minimum is the lateral resonance between the two anti-resonance points, f_{ar1} and f_{ar2}.

3.3 PZT Matrix

The piezoelectric part of the transducers used in USCT TAS is made from PZT material. PZT is artificially produced piezoelectric ceramic with high piezoelectric constant. It consists of many piezoelectric crystallites with areas where electric dipoles are aligned. The orientation of the areas is random and the material is isotropic until it is polarized. [13]

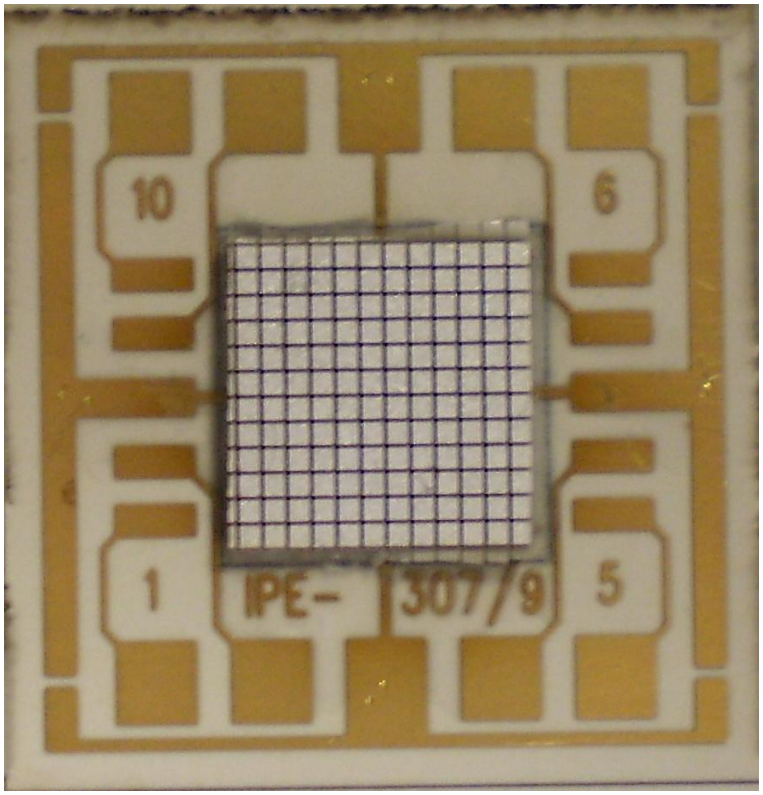

FIGURE 11. Structured PZT matrix placed on a test circuit board

The PZT is polarized in thickness direction towards the sending wave so that it operates by longitudinal effect and oscillates in thickness mode. For longitudinal effect the amount of charges inside the PZT is strictly proportional to the applied force [14]. The PZT has a sub-diced matrix of elements, or rods. The rods have a common part called bridge connecting them from the base. The electrodes are placed at the bottom of the bridge

and on top of the rods. In Figures 11 and 12 is the PZT before and after the bonding. The outmost rods in the matrix are not excited, they only provide similar coupling environment for the active rods.

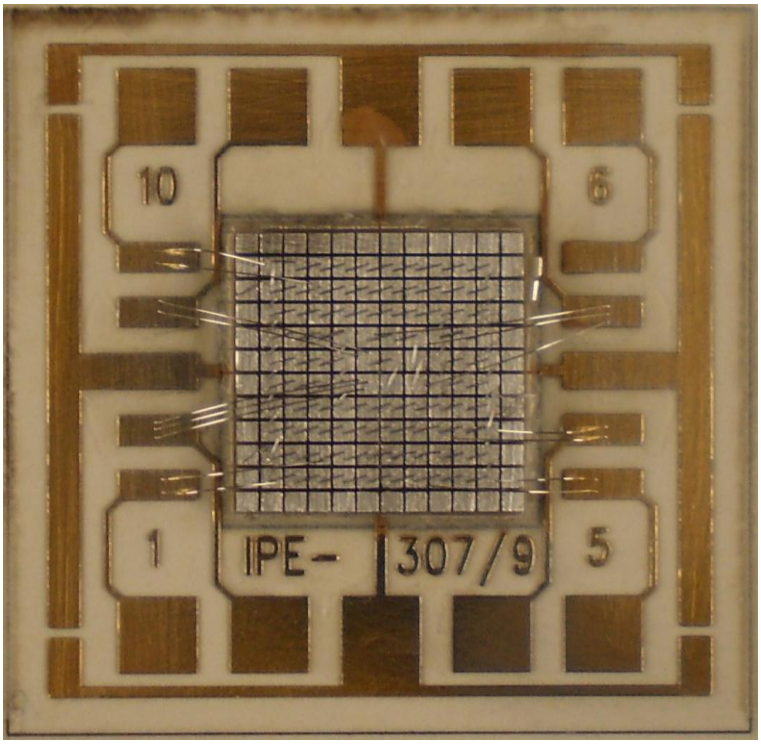

FIGURE 12. PZT-rods bonded to a test circuit board

3.4 Filler and Backing

The PZT rods are covered in polyurethane, filling the surrounding area and the spacing between the rods. There is also a layer of polyurethane on top of the rods making a lossy backing, which attenuates the sound waves coming to “wrong direction”, hence making avoidance of false echoes coming from the backing. It also acts as a support for the structure. In the test transducers the backing is 2 cm thick. In the transducers used in the USCT II it is around the electronics as well. Figure 13 shows an USCT transducer being filled with polyurethane.

FIGURE 13. USCT transducer being filled with polyurethane

The use of a backing can widen the bandwidth, but also might have the effect of increasing the transmission loss. The acoustic impedance of the backing should match that of the PZT to effectively absorb the sound waves. If most of the sound waves are attenuated by the backing, the transducer will have a shorter pulse and decreased sensitivity. [15]

Grewe et. al. describe the attenuation in the backing:

Attenuation is the loss of acoustical energy and is mainly due to two mechanisms:

1) *scattering of acoustic energy (Rayleigh, diffusion, and stochastic) and*
2) *absorption losses from thermoelastic effects, inelastic hysteresis, relaxation, and dislocation damping.*

(Grewe et al. 1990, 506.)

3.5 Matching Layer

In the direction of the sending and receiving wave there is a matching layer to match the acoustic impedance of the transducer to water. The characteristic acoustic impedance of

the PZT is ~28 MRayl and for water it is 1,5 MRayl. Would there be a big mismatch in the acoustic impedance; the energy of the ultrasound in the water would be reduced. The matching layer's acoustical impedance must be in between the impedance of the water and the PZT matrix. The matching layer also brings the series and parallel resonances closer together so that the transducer is only not sending with maximum power but also receiving with good sensitivity. [10]

There are three principles that have to be taken in to account when designing a matching layer for ultrasound transducer:

1. $Z_{ML} = \sqrt{Z_{PZT} Z_{Meedium}}$
2. $d_{ML} = n \cdot \frac{\lambda_{ML}}{4}; n = 1,3,5,...$
3. Attenuation = minimum

where Z_{ML} is the characteristic acoustic impedance of the matching layer, Z_{PZT} is the characteristic acoustic impedance of the PZT-matrix, Z_{Medium} is the characteristic acoustic impedance of the medium where the sound waves are sent, d_{ML} is the thickness of the matching layer and λ_{ML} is the wavelength of the matching layer. [16]

There is very limited source of materials with suitable impedance and when the frequency gets higher, the one fourth of a wavelength gets shorter and therefore producing of the matching layer comes more difficult. So even the attenuation increases, it is often suitable to have ¾ of wavelength thick matching layer. This is the case with the USCT test transducers which are made for measurement and testing purposes. They have a ¾ wavelength matching layer made out of TMM4-material, which is the material of the electronic board the PZT is connected to. The transducers used in the aperture however have a matching layer thinner than ¾ of wavelength so that they can be used with several different frequencies. Without a matching layer or with a very thin matching layer all frequencies are transmitted equally, but without the gain in sound pressure produced by the matching layer. [16]

4 SIMULATION

4.1 Software

The FEM analysis of the transducer was done by using ANSYS Mechanical software. ANSYS Mechanical is a product of CAE simulation software provider ANSYS Inc. ANSYS Mechanical has complete set of elements behaviour, material models and equation solvers for a wide range of engineering problems. It has full support for not only piezoelectric, but also for acoustic, thermal-structural and thermoelectric analyses. Figure 14 shows a screen capture from ANSYS Mechanical APDL and Figure 15 has the plot of the transducer in ANSYS. [17]

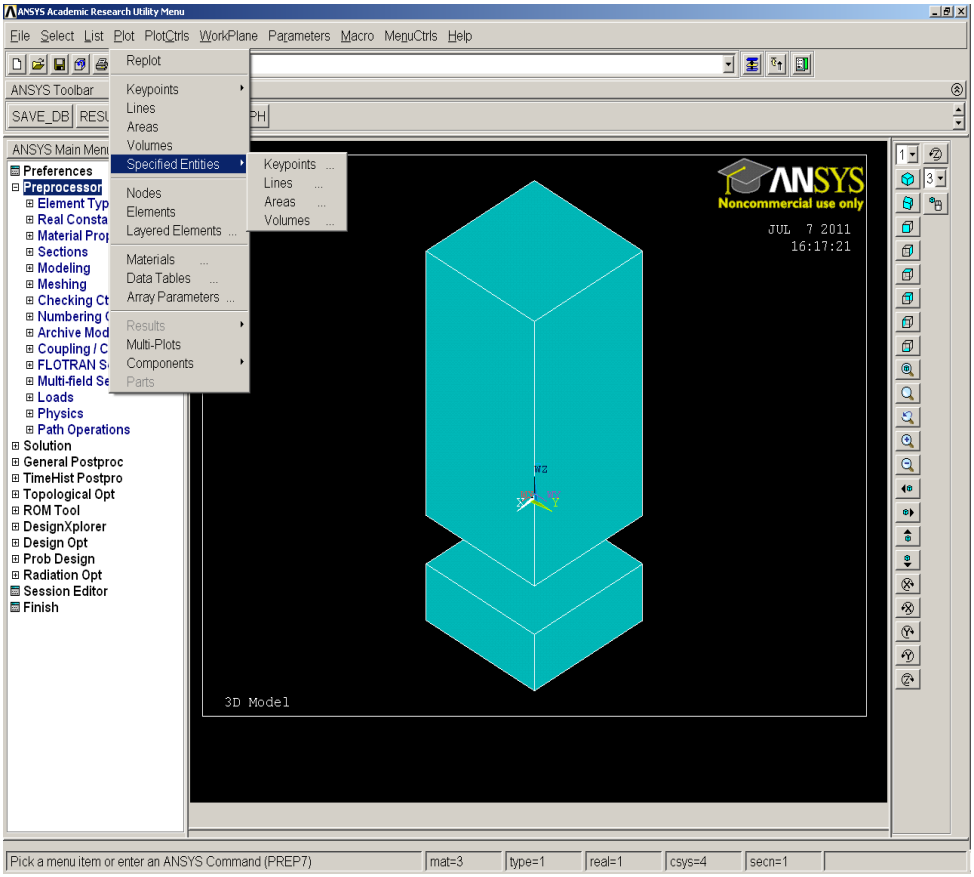

FIGURE 14. Screen capture from ANSYS Mechanical APDL 13.0

ANSYS products use a scripting language called ANSYS Parametric Design Language (APDL). The structure of the language is similar to Fortran 77. Shared libraries from Fortran 77 and ANSI standard C can be used in APDL. The products also have a GUI from where the commands are also translated to APDL code. So the end user can either

use the GUI, APDL code or both. The APDL code can be entered straight to a command line or it can be inserted as a batch file. [17]

Batch files generated in notepad were used to build the analyses of the transducer. This proved to be an efficient method, because several solutions could be solved consecutively. The results of consecutive solutions were saved independently for later examination. Nodal and elemental behaviour was studied in ANSYS using the GUI, and the electrical data was stored in separate files and was examined in MATLAB-software by MathWorks Inc. A MATLAB program was written for easy access and plotting of the data, the code can be found in appendix 1.

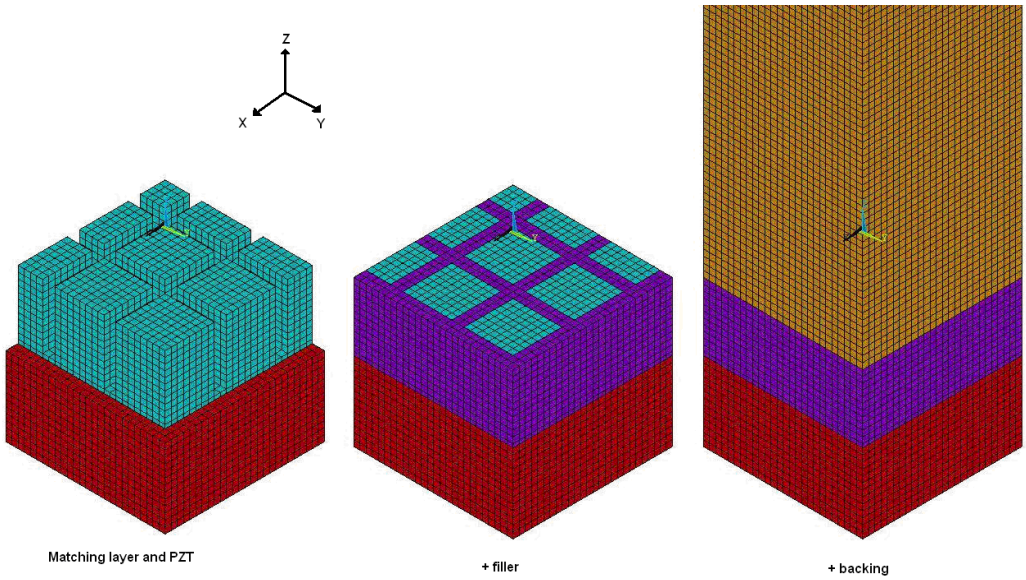

FIGURE 15. Transducer viewed in ANSYS Mechanical

4.2 Simulation Model and Analysis

The batch file consists of several sections:

1. Element modelling
2. Model building
3. Meshing and merging
4. Creating symmetry
5. Damping
6. Defining loads
7. Defining analysis
8. Postprocessing

4.2.1 Element Modelling

Element and material properties have to be defined for different materials and/or geometrical sections in the model. Element type has to be defined and different element types enable different kind of analyses. The structure of the element is also different for different element types.

The element types can be sectioned by:

1. Matter type: solids, fluids, shells, joints, contacts, effects, surfaces and others (such as contacts, links, circuits, pipes etc.).
2. By coupled fields: structural, acoustic, thermal, electromagnetic and others.
3. Dimension: 2D or 3D.
4. Element shape.
5. Number of nodes.

Material properties depend on the material type, but density has to be defined for all materials. For example piezoelectric material has dielectric constants, the elastic coefficient matrix and the piezoelectric matrix whereas anisotropic elastic materials have only the elastic coefficient matrix.

In the simulation model of the transducer, SOLID5 element type was used. SOLID5, shown in Figure 16, has a 3D magnetic, thermal, electric, piezoelectric and structural field capability with limited coupling between the fields. The element is eight node - cuboid with up to six degrees of freedom at each node.

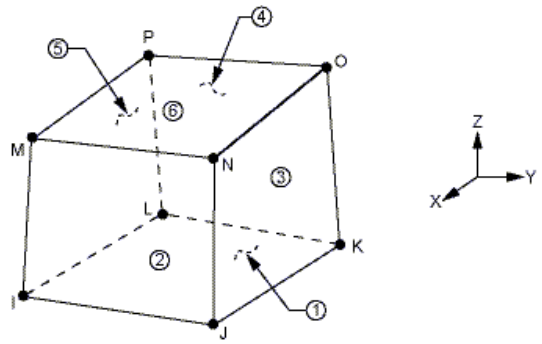

FIGURE 16. SOLID5 element in ANSYS

Density and permittivity were defined for all materials, piezoelectricity matrix and elastic coefficient matrix as a structural table for the PZT and elastic coefficient matrix as stiffness constants for isotropic materials (PU and TMM4).

4.2.2 Model Building

In the model building section all of the structural dimensions are defined and the transducer is built from set of volumes, each of which has correspondent material type specified. Since the transducer is symmetrical in XY-plane (Z being the direction of propagated sound waves), it is only necessary to build a quarter model of the transducer and mirror the remaining three quarters by the means of symmetry boundaries. Symmetry is built in model building section by cutting the whole transducer in Z-direction to a quarter piece of the transducer. The boundaries are added later at the symmetry-section. Figure 17 illustrates the symmetry in the transducer model.

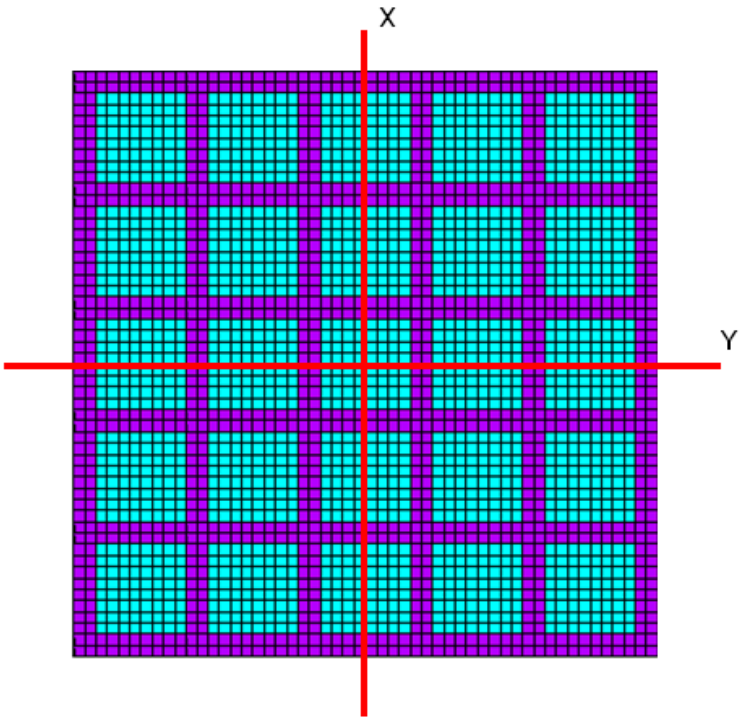

FIGURE 17. The transducer is symmetrical in XY-plane

4.2.3 Meshing and Merging

Meshing the model creates elements and nodes from the meshed volumes. Meshing can be done in several ways resulting in different sized and shaped elements in the model. In this case, rectangular cuboid elements were preferred because of their ability to produce more accurate results compared to pyramid elements. The original model had constant sized elements of 50x50x50 µm. Later in this thesis, the size of the elements is discussed further.

Merging the keypoints and nodes “glues” the model together. All coincident and equivalently defined items are merged.

4.2.4 Creating Symmetry

After the model is appropriately meshed and merged, the symmetry boundaries can be defined. In this case, the boundaries are set to X- and Y-axes on the cut sides of the transducer.

4.2.5 Damping

For the analysis, damping must be defined. There are several ways for several situations to define damping in ANSYS. The damping can be material dependent or constant. For the transducer model, Rayleigh damping was used. In Rayleigh damping the matrix [C] is calculated by using alpha and beta constants, α and β, to multiply the mass matrix [M] and stiffness matrix [K]: $[C] = \alpha[M] + \beta[K]$. [18]

4.2.6 Defining Loads

Electrical loads are set as voltages across the PZT-rods. Voltage constraints are defined to the nodes on top of the volumes of the rods and on the bottom of the volumes of the transducer’s bridge. In this case a potential of 40 V is applied on top of the rods and 0 V on the bottom of the bridge. Each load is also numbered and defined as a set of coupled degree of freedom.

4.2.7 Defining Analysis

Analysis type, range and output are defined and the equation solver is selected in this section of the code. Harmonic analysis was used in analysing the transducer, but also static, buckling, modal, transient, substructure and spectrum analyses are available in ANSYS Mechanical. Harmonic analysis can be done in full mode, reduced mode or in mode superposition mode. Several variational technology methods that are based on the same algorithm used in full method are also available. A normal full analysis was used in this case. The range was set to start before the resonance area and to stop after the anti-resonance area depending on what was studied. Most simulations were studied between 1.5 to 3.5 MHz.

There are several iterative solvers and a sparse direct equation solver for harmonic analysis in ANSYS. A sparse solver was selected for this analysis, because it combines both speed and robustness. It can be run in shared or distributed memory parallel mode and it also supports GPU accelerator capability. It requires more memory than the iterative solvers to obtain optimal performance because optimally it is run totally in-core. However, this is not a problem, since the computing hardware used for the simulations has enough in-core memory for quite large solutions.

4.2.8 Postprocessing

In the postprocessing section, all the required nodal and/or elemental results are gathered and if necessary calculated, displayed and written to a file. From the transducer analyses, nodal displacement in the matching layer was retrieved from the corresponding nodes, charge and current data were retrieved from the loaded rods, and impedance and power were calculated from the current and voltage.

4.3 Starting Point

This thesis continues and enhances an existing simulation model for the USCT transducer [3]. The material parameters had been fitted, so that the impedance of the model would fit the measurements from a real life transducer as well as possible. The impedance curve from the model, compared with measured impedance is shown in Figure 18. This model has been the basis for conducting this thesis work in examining

the behaviour of the transducer when some of the parameters and geometry are changed.

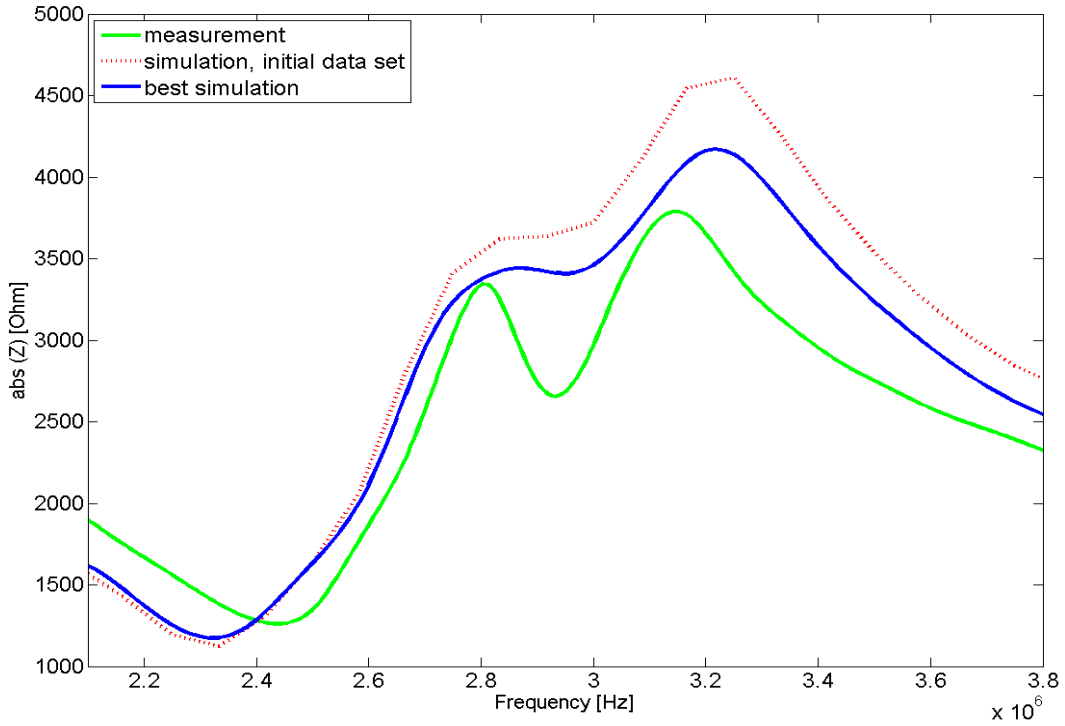

FIGURE 18. The starting point model's impedance absolute value compared to a measuring

However, there were errors concerning the building of the model. Closer look at the meshing revealed that not all of the nodes in the mesh were connected to each other due to bad meshing parameters. This made the model to have "cuts" when the improperly connected nodes would half tear away from the surface and in inside.

Another error was when applying the voltage to the symmetry model incorrectly caused the active rods to have different voltage potential. The model was a 5x5 matrix with the inner nine rods excited with voltage. Due to symmetry, a quarter model with an appropriate boundary conditions was built. In the quarter model, there is one full and one quarter of a rod and two halves of a rod active. Instead of applying the same voltage to all of the active rods, the voltage was applied with respect to the size of the rods.

Unfortunately some of the work was done before these errors came to knowledge, so a portion of the work had to be redone. Having an incorrect model also meant that the material parameters had to be reconsidered and fitted again.

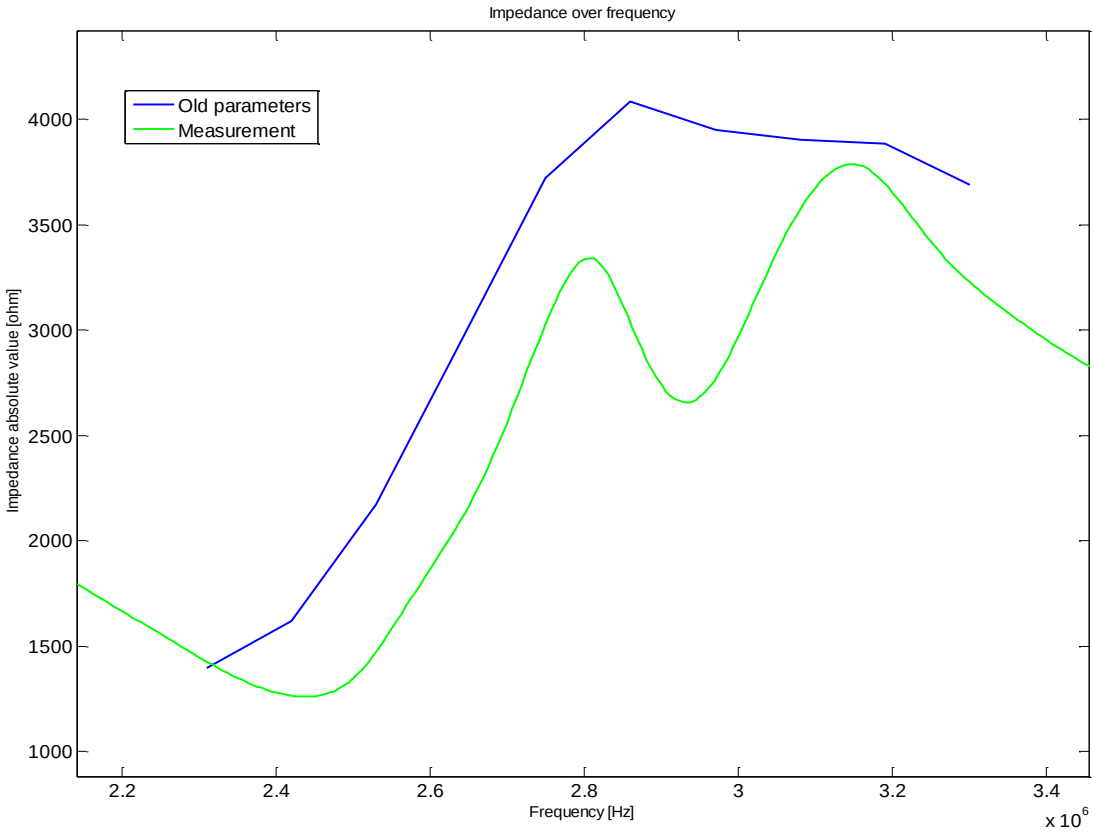

FIGURE 19. Impedance absolute value of a corrected model with old parameters

In Figure 19 is the impedance absolute value curve from a model where the meshing and voltage errors are corrected, but the material parameters are the same as in starting point model. Compared to Figure 18, even though having fewer simulation steps (measurement points), it is visible why the parameters had to be optimized again.

5 IMPLEMENTATION AND RESULTS

5.1 Optimizing the Model

The ANSYS-model of the ultrasound transducer was optimized to represent the real life transducer by adjusting the material parameters, damping and meshing of the model. Material parameters from the datasheet were used as a starting point.

The simulations show that most material parameters affect the electrical impedance of the transducer. This applies to both absolute value and the phase of the impedance. The greatest influence was seen near the anti-resonance (or lateral resonance) frequencies as would be expected because the material parameters have a big influence on the lateral resonances in the transducer due to their effect on the speed of wave travel. Influence near the resonance area on the other hand was relatively small and damping had mostly effect on the extreme values as was expected. Different meshings of the model were noted to have more effect on the absolute value of the impedance especially in between the first and second anti-resonance peaks.

Simulated impedance was compared to measured impedance from a real life transducer. It should be noted that the transducer in question has fluctuation in the dimensions due to fabrication process. This means that the simulated transducer may not match the real life transducer 100%, but will represent results accurately enough.

5.1.1 Effects of Single Material Parameters

Because of the variation of the material parameters from the datasheet values in the real life transducer, the effect of the parameters on the impedance of the transducer was studied. Because the most important part of the transducer is the piezo matrix, the piezo parameters were varied first. Simulations where a single material parameter of the piezo was varied ±5% from the datasheet values were conducted. The effects of the parameters can be seen in Table 1, where the arrows represent the change. The broader arrow means a bigger change where the narrow arrow means a slight change.

TABLE 1. Effect of the PZT material parameters to the impedance.

Parameter	**Variation**	**Res Effect**		**Anti-res Effect**	
Datasheet values		Abs. value	Phase	Abs. value	Phase
	+5%	⇑	-	⇑	-
ρ = 7800 kg/m^3	-5%	-	⇒	↓	⇒
	+5%	-	-	-	-
ε11 = 930	-5%	-	-	-	-
	+5%	-	-	⇓	-
ε33 = 857	-5%	-	-	⇑	-
	+5%	-	-	-	-
e13 = -7.15 N/Vm	-5%	-	-	-	-
	+5%	-	-	-	-
e15 = 11.9 N/Vm	-5%	-	-	-	-
	+5%	-	-	-	-
e33 = 13.7 N/Vm	-5%	↑	←	-	←
	+5%	↓	-	⇓	←
C11 = 1.23E11 N/m^2	-5%	↑	-	⇑	←
	+5%	-	-	↓	-
C12 = 7.67E10 N/m^2	-5%	-	-	↑	-
	+5%	↑	←	⇑	←
C13 = 7.025E10 N/m^2	-5%	↓	→	⇓	→
	+5%	-	⇒	↓	⇒
C33 = 9.711E10 N/m^2	-5%	⇑	⇐	⇑	⇐
	+5%	-	-	-	-
C44 = 2.226E10 N/m^2	-5%	-	-	-	-
	+5%	-	-	-	-
C66 = 2.315E10 N/m^2	-5%	-	-	-	-

5.1.2 Enhancing the Meshing

Meshing the ANSYS-model creates elements containing nodes throughout the model. The size and the shape of the elements can be varied to produce an accurate 3D-model. Optimally the element size should be reduced until it does not affect the results. However reducing element size increases the number of nodes thus increasing the simulation time. It was seen desirable for the model to pass a single step with harmonic analysis in under ten minutes. This can only be achieved by compromising the accuracy of the simulation or by using high power super computer to run the simulations.

While the original meshing of the ANSYS-model, with 50 µm elements, can be condensed to a certain degree, the computer used in simulations, with 16 Intel Xeon 2.5 GHz processors, sets limitations. In the other direction the limits for the maximum element size are set by the Nyquist theorem.

The Nyquist theorem suggests that the sampling rate must be twice or more larger than the highest frequency in the original signal. Adapting the theorem to wavelength produces

$$f_{disc} \geq 2 * f_{\max} \Leftrightarrow \frac{c}{\lambda_{disc}} \geq 2 * \frac{c}{\lambda_{\max}} \Rightarrow \lambda_{disc} \leq \lambda_{\max} / 2 \qquad (1)$$

where f_{disc} is the sampling frequency, f_{max} is the maximum frequency in signal, c is the speed of sound in material, λ_{disc} is the wavelength of the sampling frequency and λ_{max} is the wavelength of the maximum frequency.

With the maximum frequency of 4 MHz and the speed of sound in piezo material of 3528 m/s we get minimum value for the wavelength of the sampling frequency as follow:

$$\lambda_{\max} = \frac{c}{f_{\max}} = \frac{3528 \ m/s}{4 \ MHz} = 0.000882 \ m \Rightarrow \lambda_{disc} \leq 0.000882 \ m/2$$
$$\Leftrightarrow \lambda_{disc} \leq 0.000441 \ m \qquad (2)$$

With the same maximum frequency, we get for the polyurethane (speed of sound: 1931 m/s): $\lambda_{disc} \leq 0.000241$ m.

Another length to compare the element length to is the wavelength of a shear wave. Shear wave velocity c_s can be calculated for the PZT as a square root for the relation between an elastic constant c^E_{44} and density ρ.

$$c_s = \sqrt{\frac{C_{44}^E}{\rho}} = \sqrt{\frac{2.226 * 10^{10} \frac{N}{m^2}}{7.80 * 10^3 \frac{kg}{m^3}}} = 1689.333 \ m/s \approx 1690 \ m/s \qquad (3)$$

Thus the shear wavelength λ_s at 4 MHz is

$$\lambda_s = \frac{1689.33 \ m/s}{4 \ MHz} = 0.000422 \ m \qquad (4)$$

which makes the Nyquist wavelength for the shear wave in PZT half of that; 211 µm.

The original ANSYS-model has element length of 50 µm, which can be seen to represent the wavelength of the sampling rate. Since the element length, at 50 µm, is 8.8 times smaller than the Nyquist wavelength for the PZT and 4.8 times smaller than for

polyurethane and finally 4.2 smaller than the Nyquist shear wavelength, it is sufficiently small. [10]

The original model however, becomes restricted when parts of the model go in the scale of equal or below twice the element size. In this scale the model will only have two elements (or three nodes) per direction and the force distributions are not represented correctly.

In the original simulation model this happens in the filler part and in the bridge part. The spacing between the piezo rods defines the smallest width and length in the element and the thickness of bridge defines the smallest height.

While the default element length could be reduced from 50 µm for the whole model, it would result in multiplied simulation time and result file size. Since 50 µm element length is sufficient in the large parts of the model and reducing it there would not significantly better the model, it is better to shrink the elements only where needed. So the meshing of the model was improved with strategically positioned condensing in the mesh and it was compared to the original meshing and denser meshing with 25 µm elements.

Having different sized elements in the model means that the junctions between the areas with different element sizes must be carefully planned. It must be made sure that every corner of an element is connected to a corner of another element, because the corners have nodes that need to be interconnected in order to make a working solid model. If the nodes are not connected the simulation will have erroneous results.

There are two ways to regionally condense the elements correctly. One way is to use elements that are not cuboids; this however is not recommended due to possible erroneous behaviour caused by the shape of the elements. The easiest, and the only way to do it without changing the shape of an element from rectangular cuboid, is to cut the model in to sections that go through the model in the direction of the axes. Then the sections that contain parts with small dimensions can be meshed with smaller elements and the other sections can be meshed with larger elements while still preserving the connection between the corners of the elements.

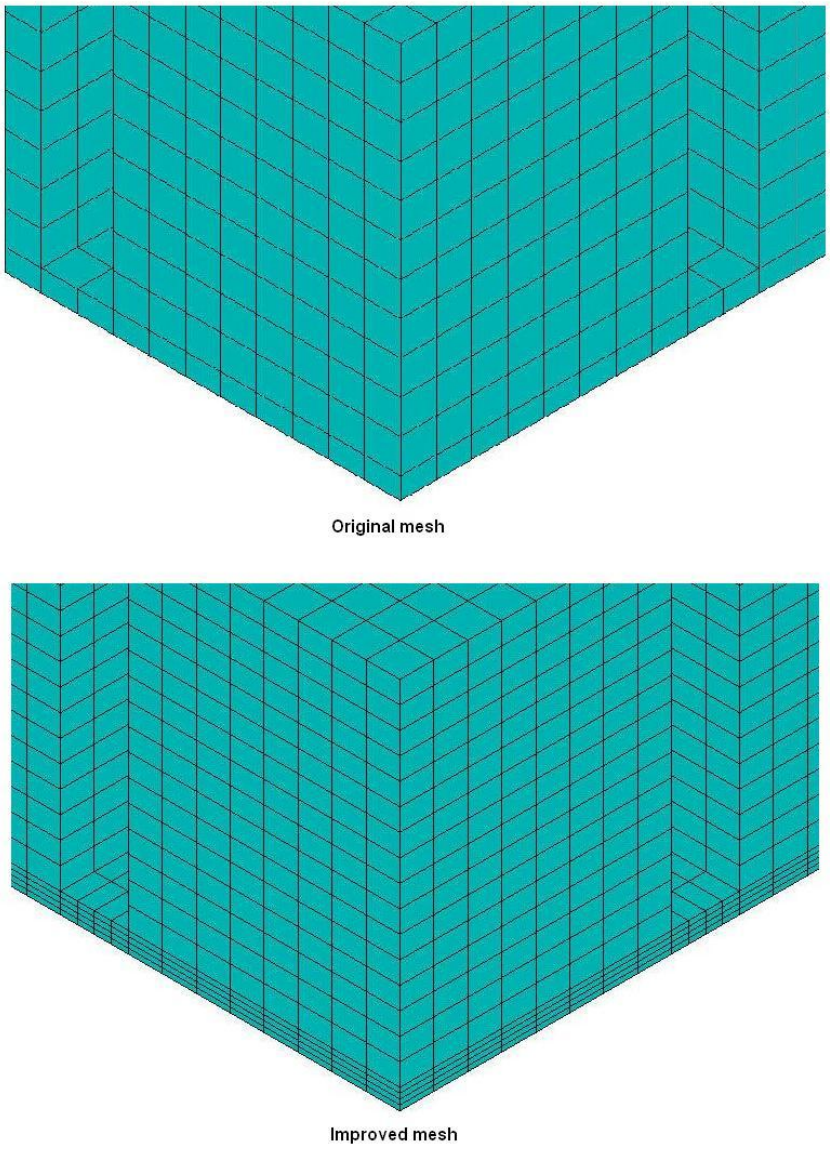

FIGURE 20. Original and improved mesh of piezo rodd and bridge showing the need for smaller elements

The only problem with using this method is that the sections where small dimensioned parts are located also contain parts with larger dimensions, those thus being unnecessarily meshed into small elements as well. In the simulations made of the transducer this does not produce much problem because the volume of the unnecessarily condensed elements stays small enough to have minimalistic effect in simulation time and results size and it can be compensated by slightly enlarging the other elements for example in the backing area. Figures 20 and 21 illustrate the difference between the original and the improved meshing.

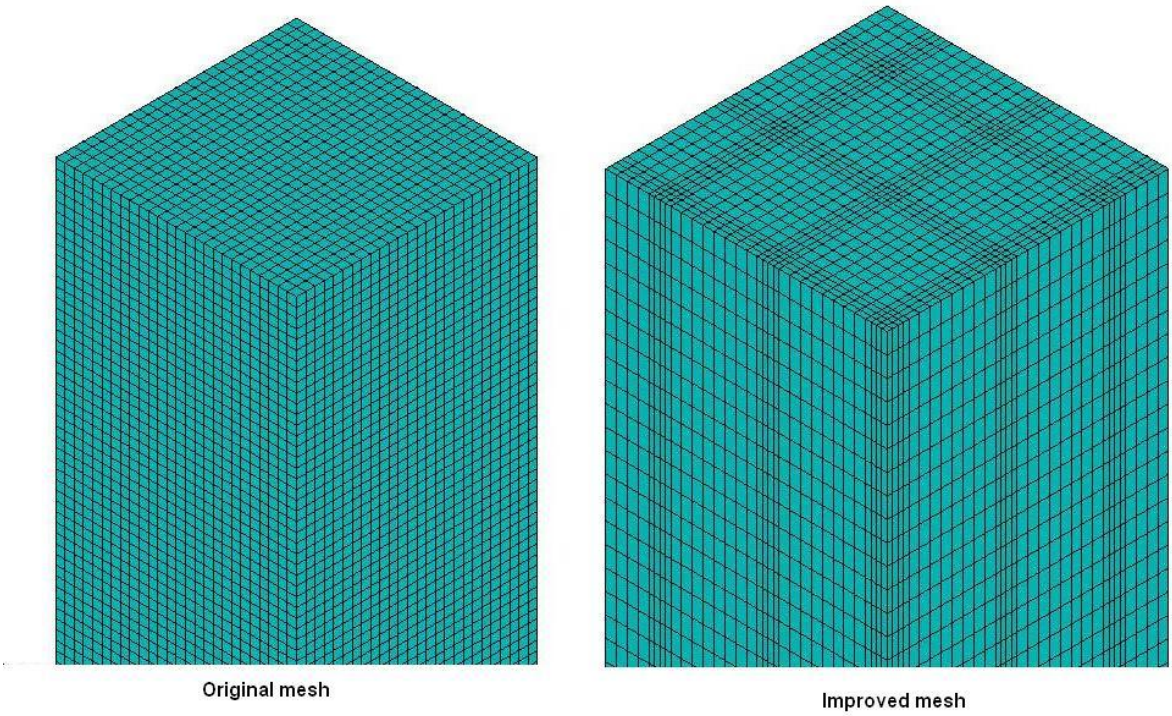

FIGURE 21. Original and improved mesh of backing showing unnecessarily small elements in grid

The effect of the element size in XY-direction was studied by constructing a model with elements of 25 µm in XY-direction and strategically condensed mesh in z-direction. It was then compared to a model with elements of 50 µm in XY-direction and strategically condensed mesh in z-direction. Figure 22 shows that reducing the element length in XY-direction to 25 µm affects the impedance of the model only very nominally.

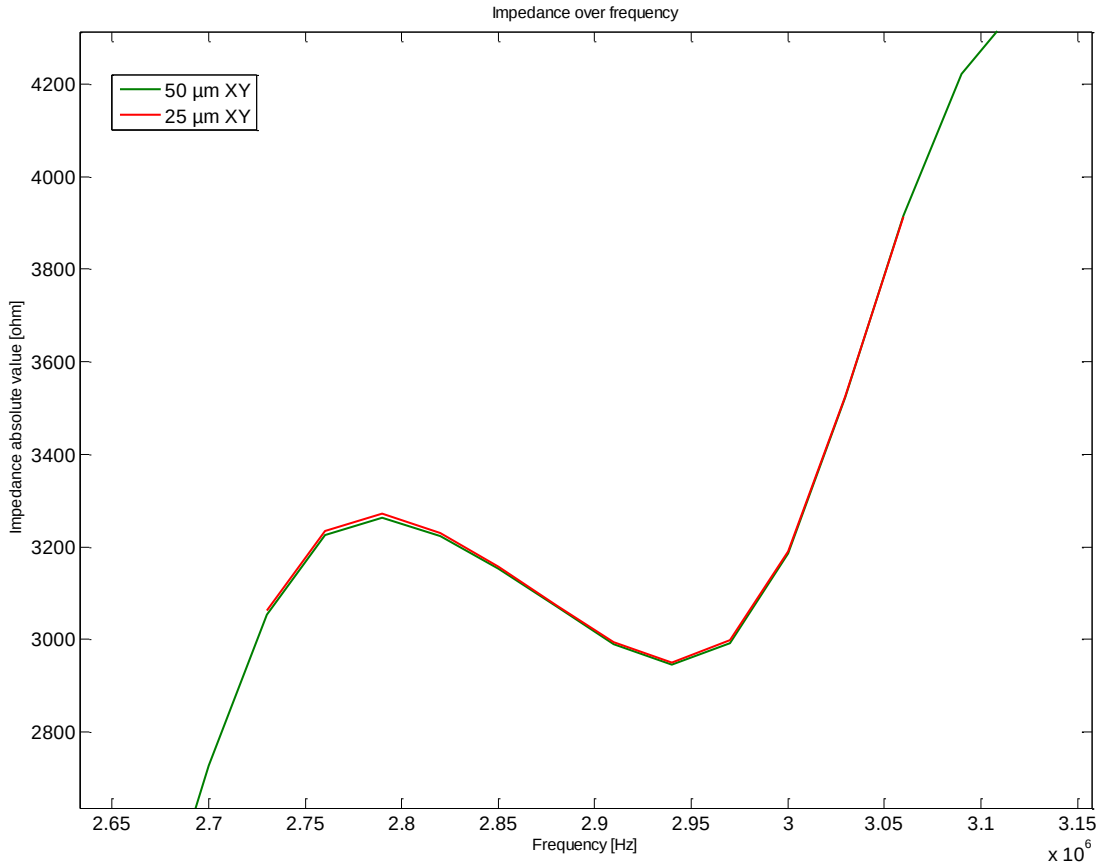

FIGURE 22. Comparison of the impedance with 25 µm and 50 µm XY-mesh

Models with constant element lengths of half and double of the original 50 µm and a model with original length but wedge elements in filler were built. Simulations with strategically condensed mesh and constant element size models were conducted and the results were valuated in accordance of the accuracy and elapsed time. The resulting impedance curves are in Figure 23 and the time consumption in Table 2.

The mesh with 100 µm element lengths and the mesh with wedge elements in filler produce so inaccurate results that they can not be used to simulate a transducer this size. The mesh with 25 µm element lengths on the other hand makes the simulation times unbearable so it has to be ruled out as well. Strategically condensed meshing is more accurate than the meshing with 50 µm elements and the difference in time is small enough to be left unconsidered. Out of the different meshing types studied the strategically condensed meshing is clearly the most suitable.

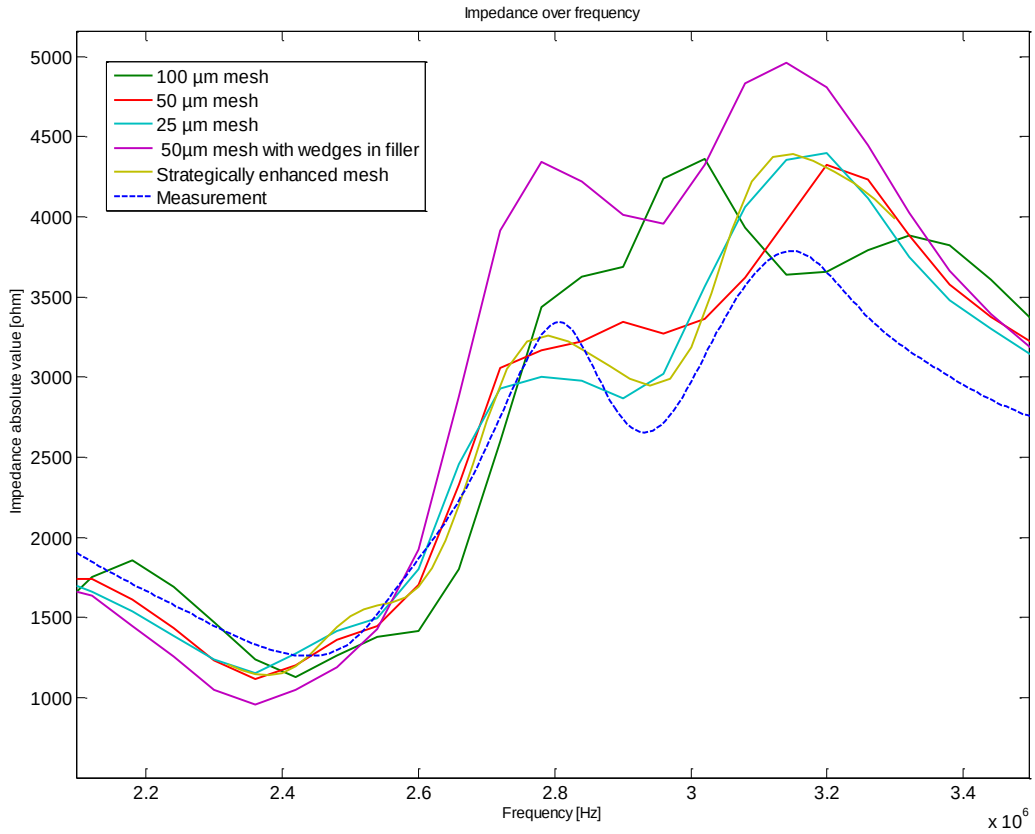

FIGURE 23. Comparison of the impedance absolute value with different meshing types

TABLE 2. Comparison of simulation times for different meshing types

Mesh size and type	100 µm constant	50 µm constant	25 µm constant	50 µm constant, wedges in filler	Strategically condensed
Time of one simulation* step	10 s	3 min 40s	1h 10min 30s	4min 40s	5min 50s

**Harmonic response analysis*

Comparing the impedance from the improved meshing model to the original meshing model and measured real life transducer show that although the material parameters and the damping is optimized for the original meshing the new model is accurate in representing the real life transducer. Some behaviour seen in the measurements from a real life transducer come visible in the simulations only with the improved model.

5.1.3 Improving the Model by Further Adjusting the Material Parameters and Damping

After the meshing was enhanced, the material parameters and damping were adjusted to a preferred level. Original alpha-damping was $8.617*10^5$ s and beta-damping was

$2.879*10^{-9}$ s^{-1}. After varying the damping from 50% to 100%, it was decided that a damping of 70% from the original matches best for the natural damping of the real life transducer caused by measuring and physical phenomena such as friction and drag etc. The effect of damping for the impedance of the transducer can be seen in Figure 24.

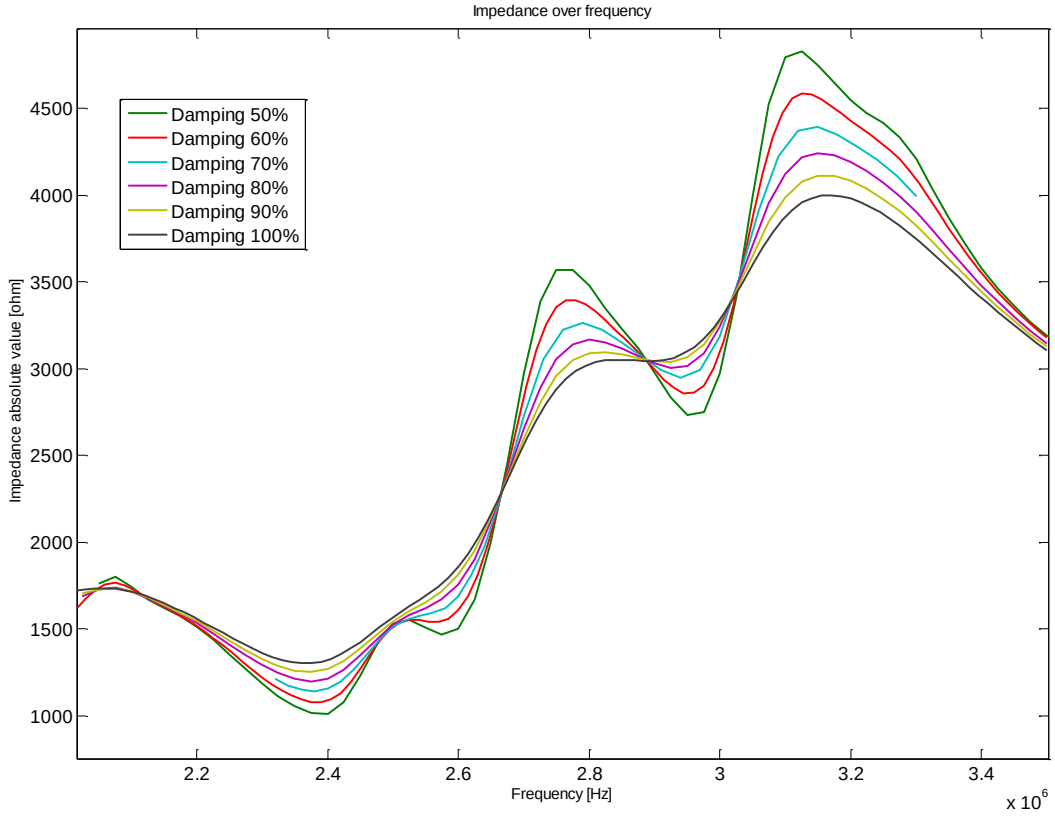

FIGURE 24. Damping's effect for impedance

The material parameters were varied ±5% from the previous optimization. Because the enhanced meshing had big effect to the anti-resonance area, the impedance near the anti-resonance was studied first in order to find suitable parameter variations to get it closer to the measured impedance. Table 3 has the data from these simulations. Variations were then combined by choosing the wanted effects from the table.

TABLE 3. Effects of the material parameters to the enhanced model's impedance at anti-resonances.

Parameter	**Variation**	**Effect compared to enhanced model**			
		1st Antires		**2nd Antires**	
PZT		Abs. value	Phase	Abs. value	Phase
ρ	+5%	⇑	←	↑	⇐
	-5%	⇓	-	↓	⇒
ε11	+5%	-	-	-	-
	-5%	-	-	-	-
ε33	+5%	↓	-	⇓	-
	-5%	↑	-	⇑	→
e13	+5%	-	-	-	-
	-5%	-	-	-	-
e15	+5%	-	-	-	-
	-5%	-	-	-	-
e33	+5%	⇓	→	⇑	→
	-5%	⇑	←	⇓	←
C11	+5%	⇓	→	↓	→
	-5%	⇑	←	↑	←
C12	+5%	↓	-	↓	-
	-5%	↑	-	↑	-
C13	+5%	⇑	⇐	⇑	⇐
	-5%	⇓	→	⇓	⇒
C33	+5%	⇓	→	⇓	⇒
	-5%	⇑	←	⇑	⇐
C44	+5%	-	-	-	-
	-5%	-	-	-	-
C66	+5%	-	-	-	-
	-5%	-	-	-	-
Polyurethan		1st Antires Effect		2nd Antires Effect	
ρ	+5%	⇓	⇒	-	⇒
	-5%	⇑	⇒	⇑	-
E-Modulus	+5%	⇑	→	⇑	→
	-5%	⇓	→	⇑	→
Poisson-ratio μ	+5%	⇓	→	↓	→
	-5%	⇑	-	⇑	-
εr	+5%	-	-	-	-
	-5%	-	-	-	-
TMM4		1st Antires Effect		2nd Antires Effect	
ρ	+5%	⇓	⇐	⇑	⇐
	-5%	⇑	⇒	⇓	⇒
ε33	+5%	-	-	-	-
	-5%	-	-	-	-
E	+5%	⇑	⇒	⇓	⇒
	-5%	⇓	⇐	⇑	⇐

Then a number of combinations of the parameter variations were tried out resulting in several distinct impedance curves, some of them shown in Figure 25. At this point the behaviour of the impedance near the resonance area was regarded as well. Again parameters were varied to get satisfying impedance output from the whole frequency area of interest; the frequency and the absolute value of the resonance were especially fitted to match the measurement. The resulting material parameter dataset can be seen in Table 4 and the impedance curve in Figure 26. The optimizing problem is such that it could be solved easier with optimization software if there was one available. Since the parameter optimization was done empirically, the number of simulations needed to get this result ascended to more than 140.

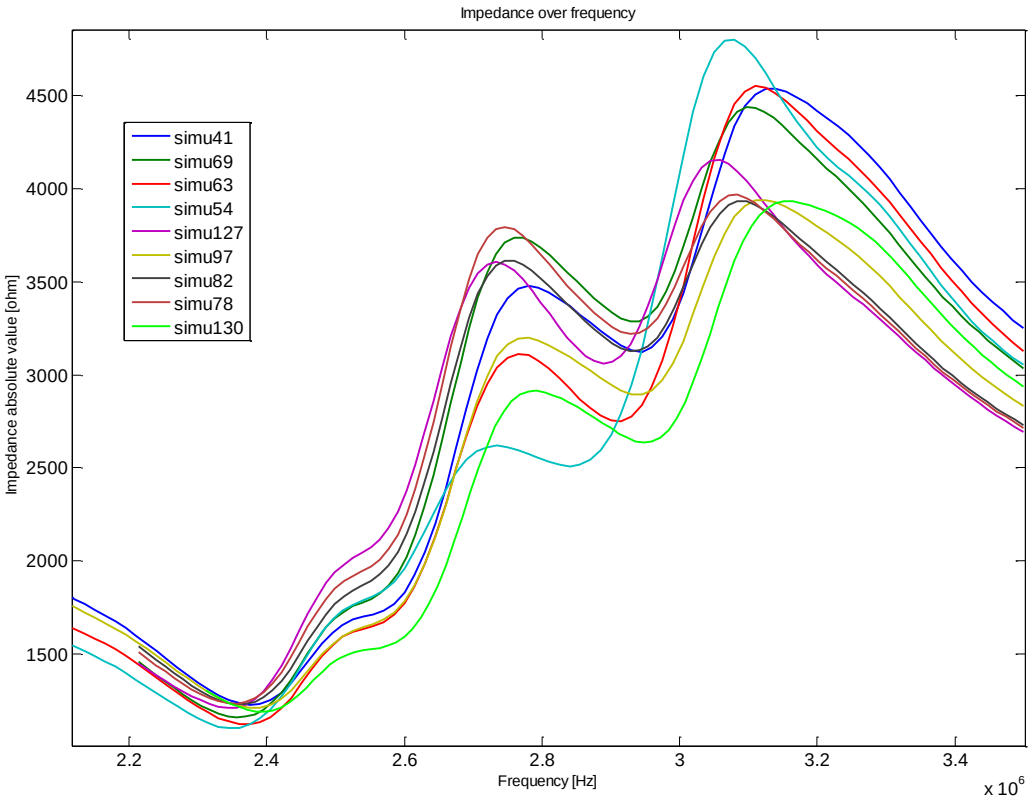

FIGURE 25. Example impedances from different material parameter datasets

TABLE 4. Optimized material dataset

Parameter		Unit	Variation from datasheet
PZT			
ρ	= 7956	kg/m³	+2%
ε11	= 942.7		-
ε33	= 989,835		+10%
e13	= -7.15	N/Vm	-
e15	= 11.9	N/Vm	-
e33	= 12.33	N/Vm	-10%
C11	= 1.23E11	N/m²	-
C12	= 8.0535E10	N/m²	+5%
C13	= 6.67375E10	N/m²	-5%
C33	= 10.19655E10	N/m²	+5%
C44	= 2.226E10	N/m²	-
C66	= 2.315E10	N/m²	-
PU			
ρ	= 1600	Kg/m³	-
E-Modulus	= 1.579E9	N/m²	-
Poisson-ratio μ	= 0.45		-
εr	= 4.0		-
TMM4			
ρ	= 2105	Kg/m³	-
E-Modulus = 800E6		N/m²	-
Poisson-ratio μ	= 0.43		-
εr	= 4.5		-

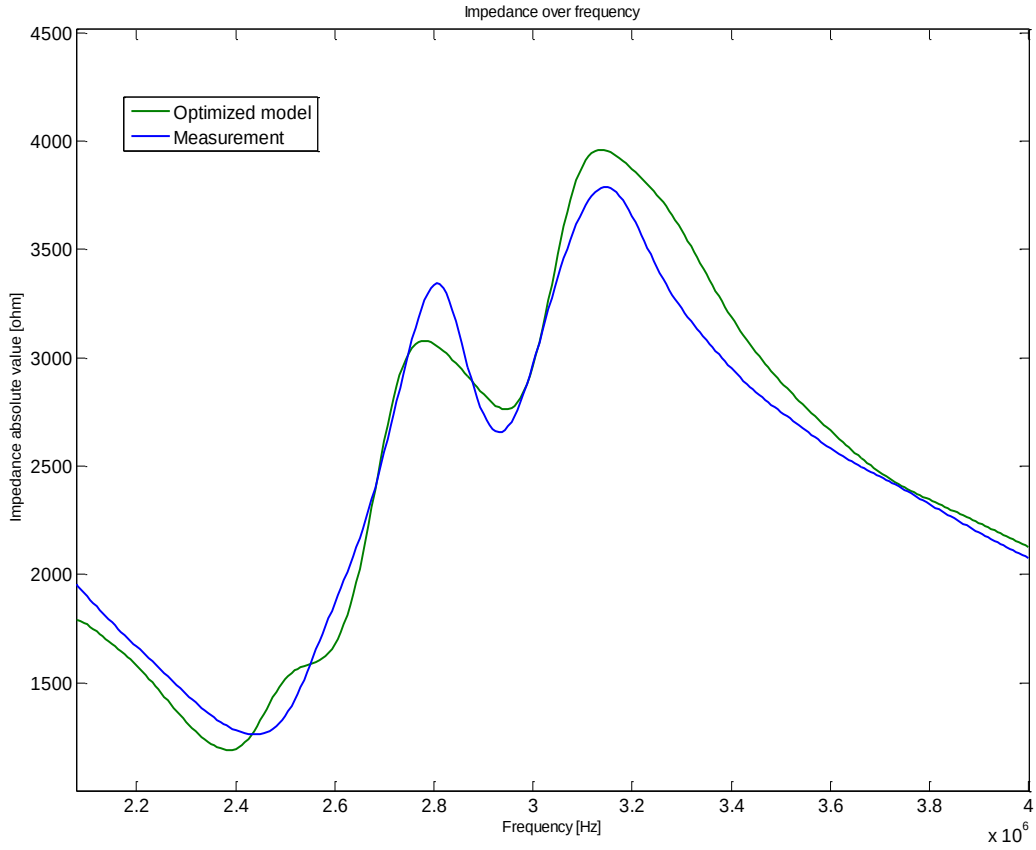

FIGURE 26. Impedance absolute value from measurement and optimized simulation model

Finding the optimal dataset with a trial and error method proved to be a time consuming task. Changing a single parameter has a big effect on the impedance curve and predicting the effects accurately is challenging. The optimized parameter dataset is optimum for the limited amount of time consumed in varying the parameters, but could be bettered with more time and effort. However the chosen dataset is accurate and can be considered as a good improvement to the model which is to be used in upcoming simulations.

5.2 Varying the Spacing

The spacing between rods in an ultrasound transducer matrix is one element that can influence the operation of the transducer. Aside from material parameters the spacing of the rods affects the occurrence of lateral resonances in the transducer. Lateral resonances in the transducer matrix occur as so-called *inter-pillar modes*, because of Lamb wave mode generation. [19]

If the filler and PZT are regarded as a composite, when the spacing of the matrix is changed, the volume fraction in the composite also changes. The change in volume fraction affects the acoustical impedance. [20]

The coupling effect also differs between different spacings since it is proven that the presence of filler has notable influence on electrical coupling. Increasing the spacing and so thickening the filler obviously decreases the coupling. [21]

The effect of the space between PZT elements in the matrix structure (Figure 27) to the behaviour of ultrasound transducer was studied with ANSYS simulations with varied spacing. The simulations were done over the frequency area of interest which was from 1.5 MHz to 3.3 MHz. From each simulation the electrical impedance values were recorded and analysed. Also the power values and deformation behaviour was studied.

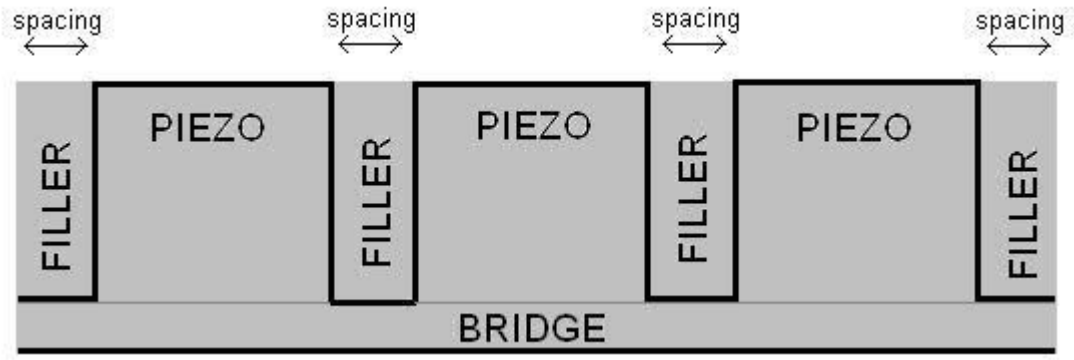

FIGURE 27. The structure of the PZT matrix

The initial structure had a spacing measuring 100 µm between the elements and on the outer edges. Simulations were done varying the spacing from 30 to 200 µm, the extremes illustrated in Figure 28. The PZT rod size stayed constant thus the size of the whole transducer was also varied.

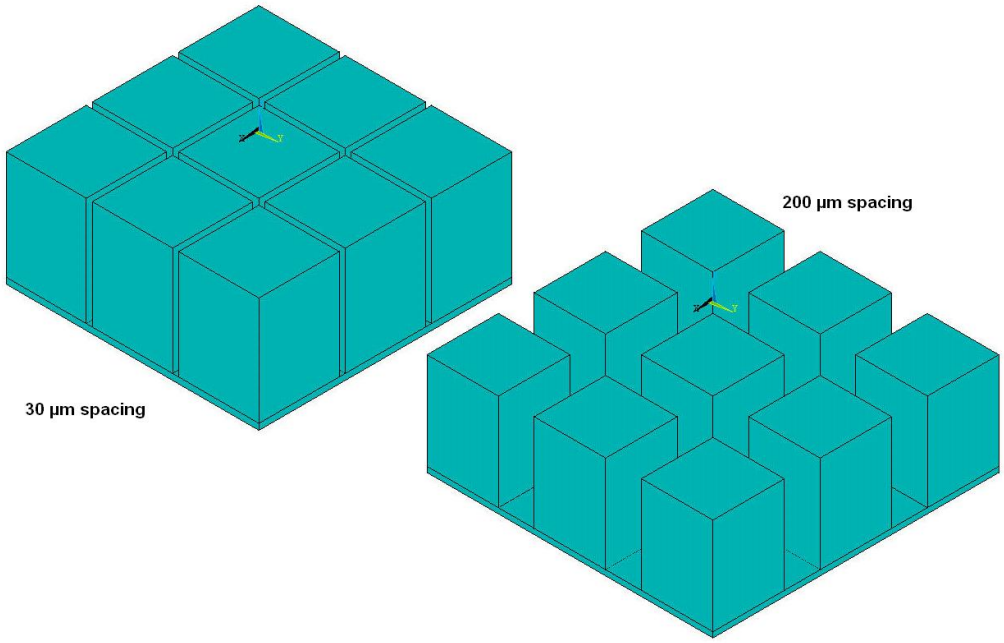

FIGURE 28. Smallest spacing of 30 µm and the largest of 200 µm

In the simulations a quarter model of 5x5 matrix could be built and simulated due to symmetry. Electrodes were placed on top of the middle elements and one under the bridge. A voltage of 40 V was then applied between the electrodes on top and the electrode on the bottom as is shown in Figure 29.

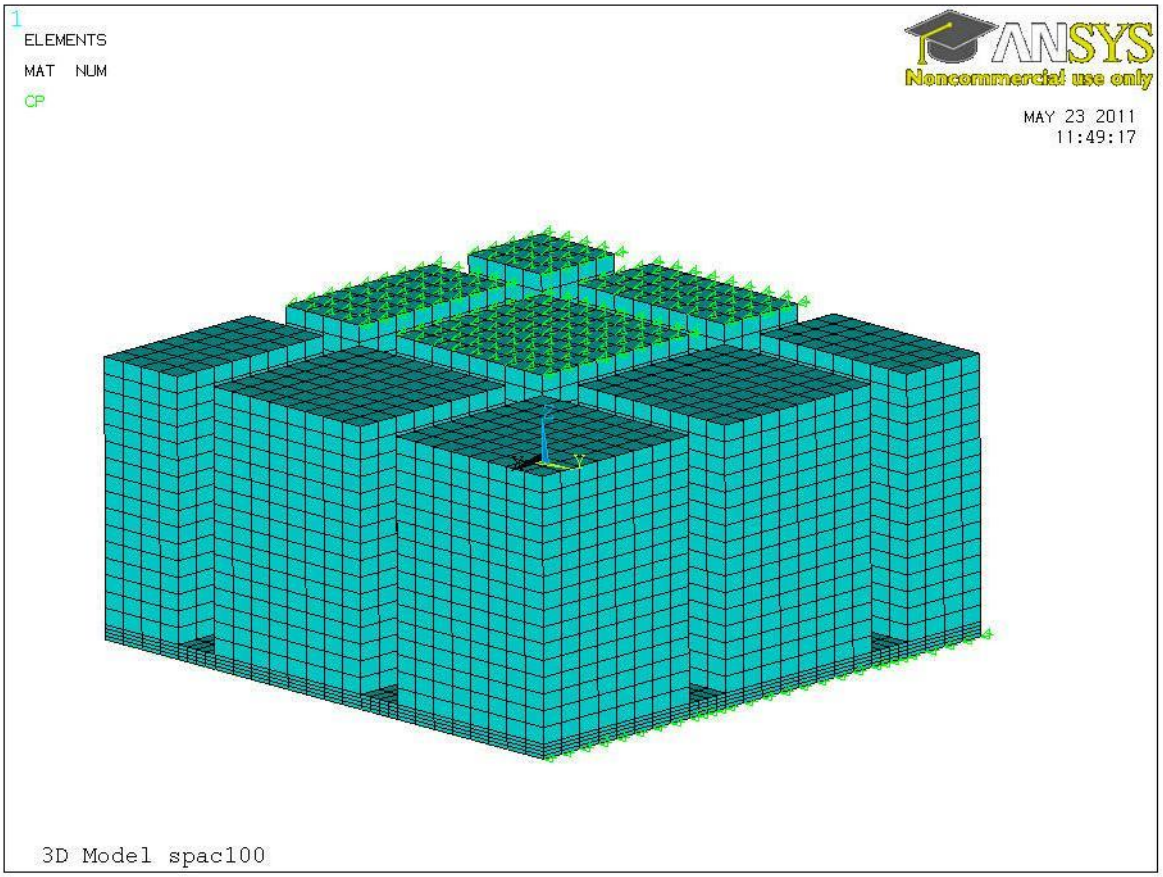

FIGURE 29. ANSYS plot of the piezo elements in blue and applied voltages in green

5.2.1 Impedance

Simulations showed that the spacing has an effect on the absolute value and the phase of the electrical impedance. Overall the effects were greater on the absolute value of the impedance. Largest differences in absolute value were shown to occur between the resonance and the anti-resonances of the transducer. Also the 3 dB bandwidth was studied. The impedance curves are shown in Figures 30 and 31.

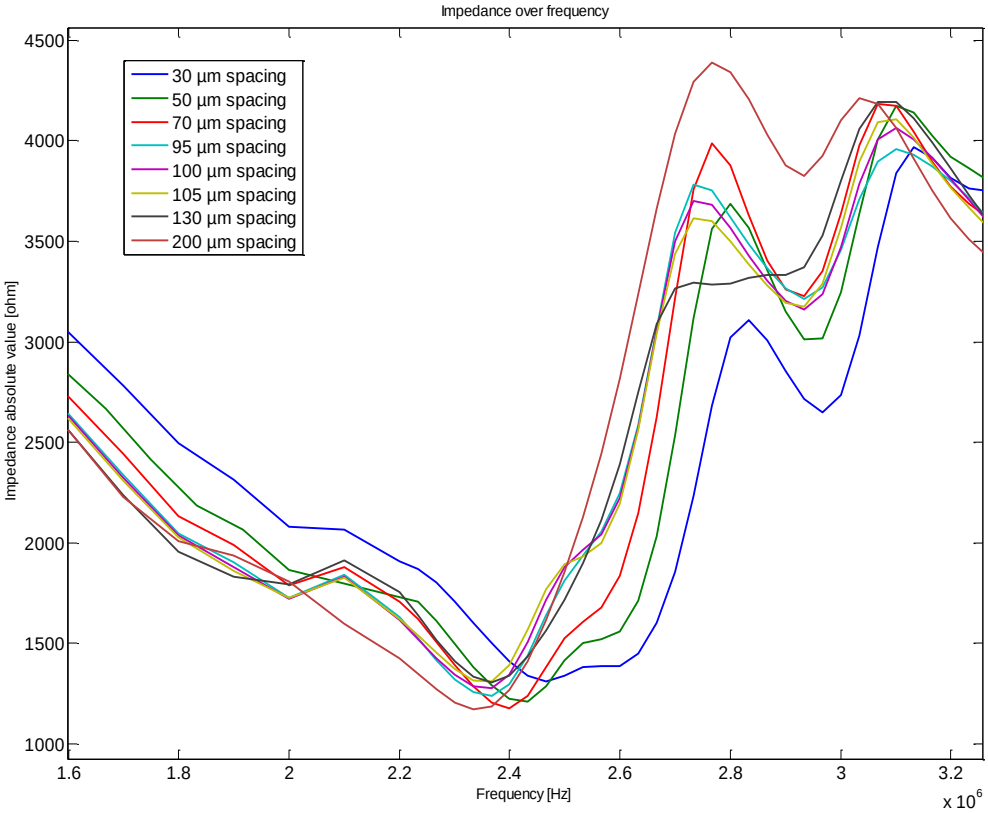

FIGURE 30. Impedance absolute value graph

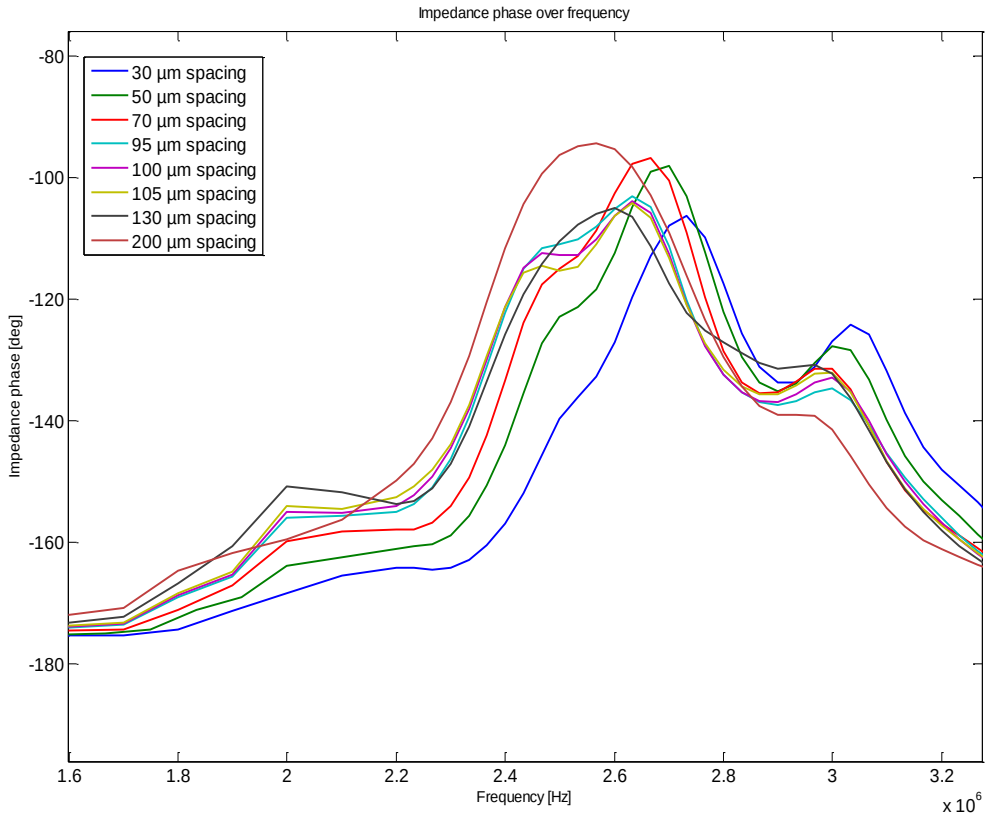

FIGURE 31. Impedance phase graph

The different models have similar average impedances over the frequency area of interest, which implies that the changes happen more in time than in magnitude. Apart from the smallest and the largest spacing all the others fall inside 10 Ω deviation of average impedance absolute value. It is also noted that the impedance from the model with 70 µm spacing has a low minimum and also peaks strongly at the first maximum at anti-resonance area. The average total impedance absolute values and average phase from 45 measurement points in the frequency between 1.1-3.3 MHz are shown in Table 5.

TABLE 5. Impedance characteristics

Spacing / µm	Average impedance / Ω	Average phase / °	Peak value / Ω	Lowest value / Ω
30	2 628	146.9	4 963	1 309
50	2 789	144.7	4 646	1 210
70	2 786	143.1	4 361	1 177
95	2 787	142.5	4 227	1 241
100	2 787	142.4	4 212	1 275
105	2 786	142.4	4 197	1 313
130	2 795	142.0	4 193	1 305
200	2 930	140.1	4 387	1 174

In Table 6 are the bandwidths and resonance points for different spacings. Also the average absolute value in the respective 3 dB impedance bandwidth area is marked in the table. The resonance frequency seems to be dependent of the spacing size; the smaller the spacing, the larger the resonance frequency. Models with spacing of 105 µm and 130 µm resulted with widest 3 dB bandwidths, while the models with small spacings had the narrowest 3 dB bandwidths. The impedance inside the 3 dB area is more dispersed than within the whole frequency area, which is helpful when evaluating the models.

TABLE 6. 3 dB bandwidths

Spacing / µm	3 dB bandwidth / kHz	Resonance point / MHz	Average impedance in 3 dB / Ω
30	933	2.47	1 716
50	767	2.43	1 638
70	833	2.40	1 617
95	900	2.37	1 704
100	900	2.37	1 719
105	1 033	2.37	1 814
130	1 000	2.37	1 774
200	833	2.33	1 592

It was also confirmed that the differences in impedance came from varying the spacing and not from the change in the size of the whole transducer. This was done by doing simulations where the spacing was varied ± 5% and the size of the whole transducer remained original. The size change from spacing was compensated with changing the size of the piezo elements. Results from these simulations followed the results from simulations where the spacing was varied without varying the piezo size. The change in absolute value is only about 1.8%, when the piezo width and length is changed 1%.

5.2.2 Power

Total transducer power was calculated from the simulations. It was calculated from the total transducer impedance and current using formula

$$\underline{P}(f) = \underline{Z}(f)\underline{I}^{*}(f)^{2} \tag{5}$$

where $\underline{P}$ is the power from all active rods, $\underline{Z}$ is the complex impedance from all active rods, $\underline{I}^{*}$ is the complex conjugated current from all active rods and f is frequency.

Resulting power absolute value curves are in Figure 32. Comparing the results in Table 7, it can be seen that overall the difference between the models is rather small. The power bandwidth corresponds to the impedance bandwidth, and again the spacings of 105 µm and 130 µm have the widest bandwidth. The spacings of 70 µm and 200 µm had the highest peak values.

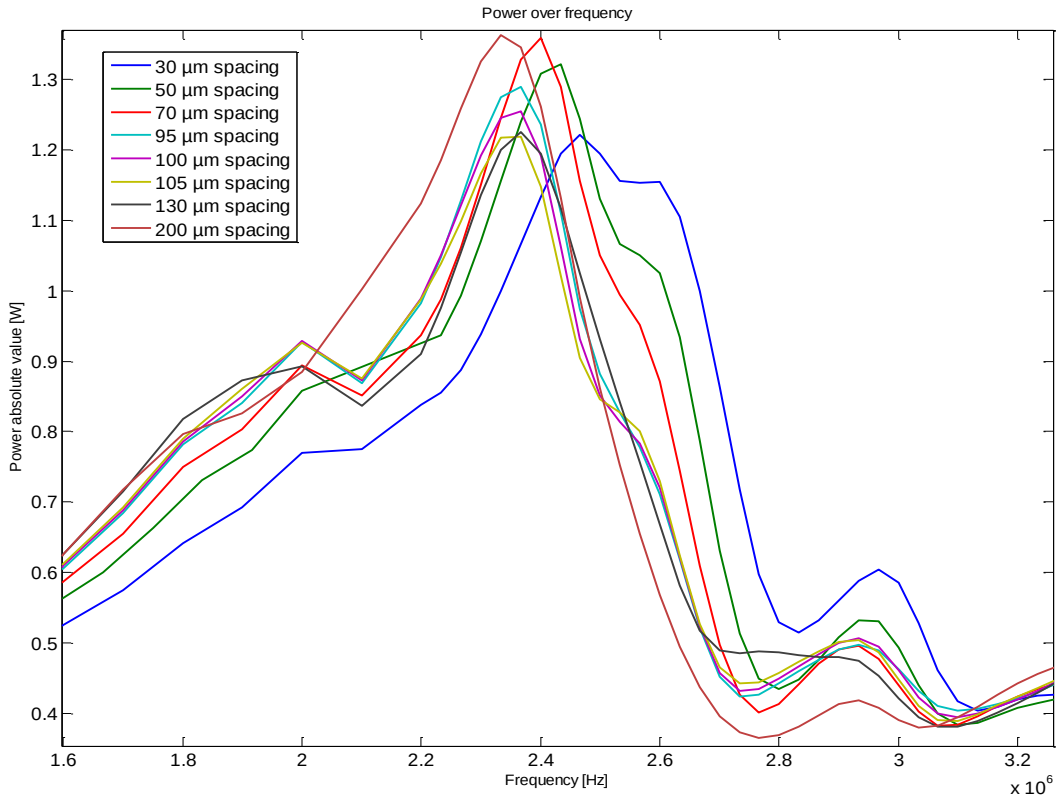

FIGURE 32. Power absolute value graph

TABLE 7. Power charasteristics

Spacing / µm	Average power / mW	Max power / mW	-3 dB bandwidth / kHz	Average power in -3 dB / mW
30	709	1 222	933	969
50	682	1 322	767	1 016
70	684	1 360	833	1 024
95	668	1 289	900	975
100	664	1 254	900	963
105	660	1 219	1 033	919
130	660	1 226	1 000	937
200	662	1 362	833	1 052

5.2.3 Displacement Behaviour

The resonance frequency was determined from the impedance graph. Studying the displacement in these points revealed that the larger the pitch was, the greater the movement was in the bridge of the transducer. Therefore in larger spacings the electrical energy applied to the transducer was directed in unwanted movement, e.g.

lamb waves, rather than to the rods creating pressure. Figures 33 and 34 show the displacement vector sum magnified by a factor of 5000 for a better view.

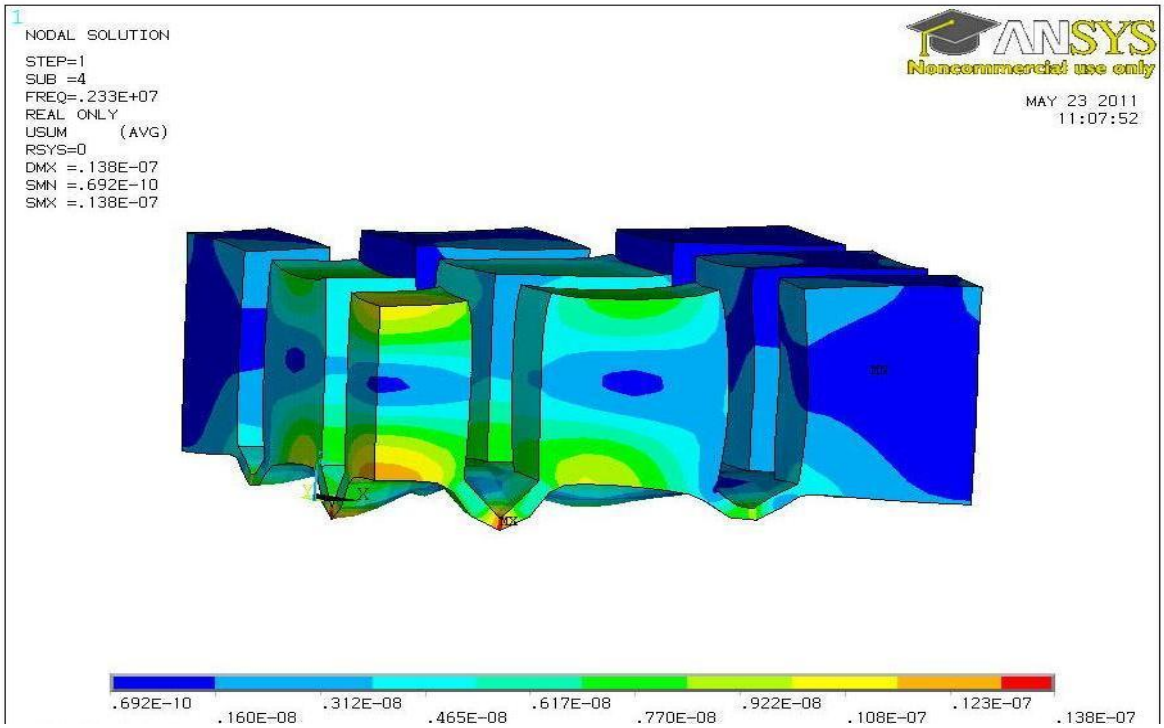

FIGURE 33. PZT matrix with 200 µm spacing at resonance

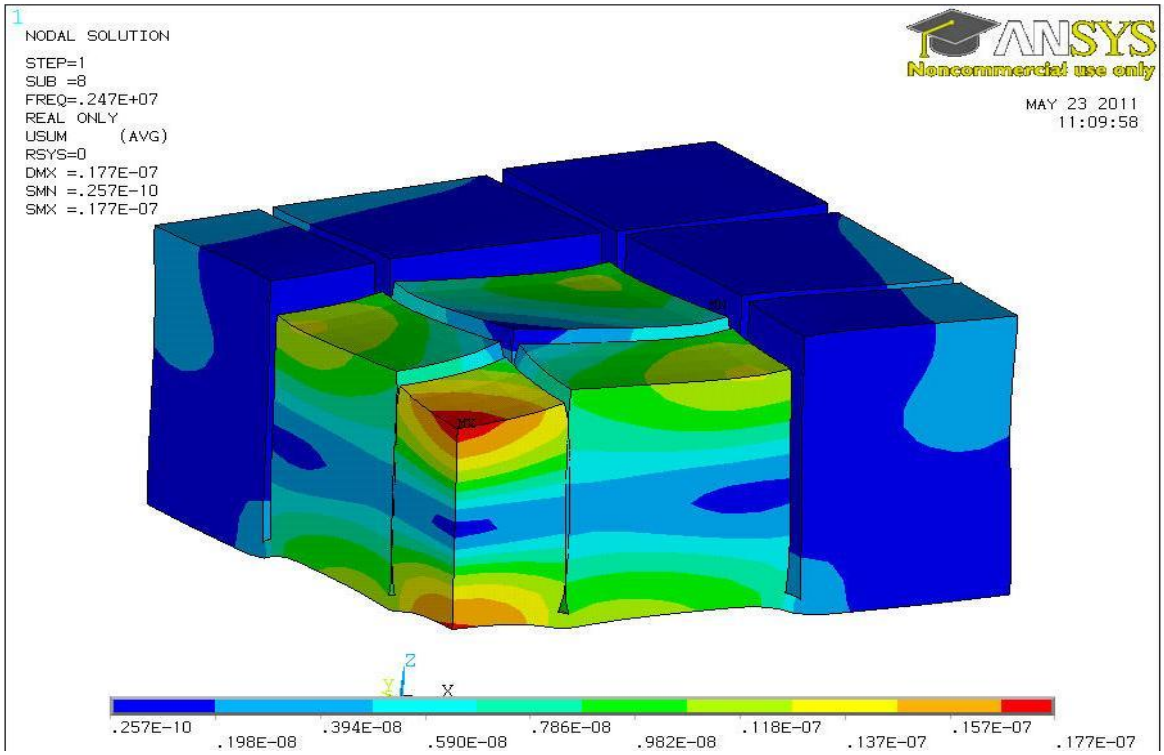

FIGURE 34. PZT matrix with 30 µm spacing at resonance

Displacement was also studied by recording the displacement from total of nine nodes in the bottom surface of the matching layer. The nodes were selected to cover the area of an active rod in the corner of active rods and surrounding filler as shown in Figure 35.

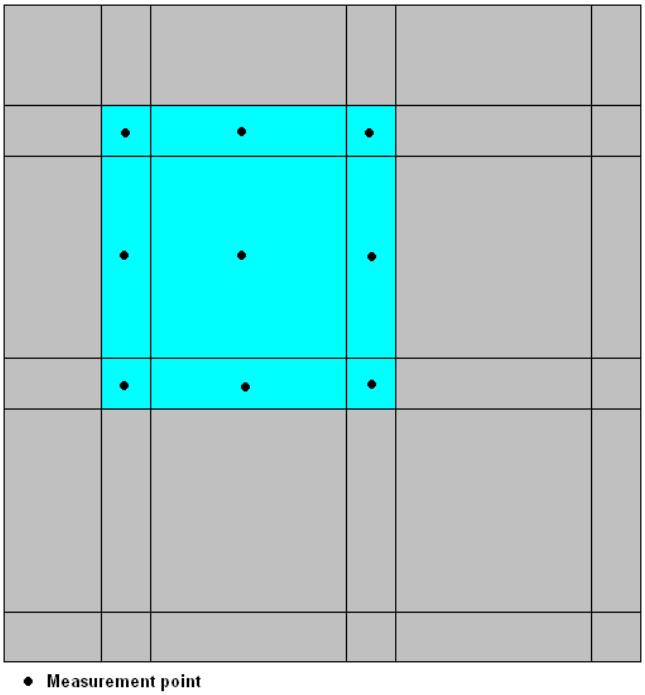

FIGURE 35. The location of measured displacement on the bottom of the matching layer

The amplitude of average displacement was regarded to have an impression of potential sound pressure to be achieved. Average displacement from the nine measuring point over the frequency area of 1.1-3.3 MHz was calculated. In Table 8 there is the average displacement and the maximum displacement from the average of the nine nodes with according frequency. It was seen that high electrical power does not always correspond to high displacement.

TABLE 8. Displacement characteristics

Spacing / µm	Average displacement / nm	Max displacement / nm	Peak point / MHz
30	9.7	16.5	2.7
50	9.7	16.0	2.2
70	11.7	19.7	2.4
95	8.5	18.9	2.0
100	9.4	18.7	2.0
105	9.3	18.5	2.0
130	8.7	16.9	2.0
200	7.8	16.0	2.3

It can be seen from the average displacement that smaller spacing seems to indicate bigger displacement in the matching layer even though the differences are not very large. It is notable to compare it in the before said behaviour in the bridge. The displacement between the models with 95, 100, 105 and 130 µm spacing over the frequency area of interest is distinctively similar as can be seen in Figure 36 where their average displacement from the 9 nodes is plotted. The displacement figure also brings out the lateral resonances at 2.4, 2.6 and 3.0 MHz. It can be seen that the model with 95 µm spacing has least effective lateral resonances.

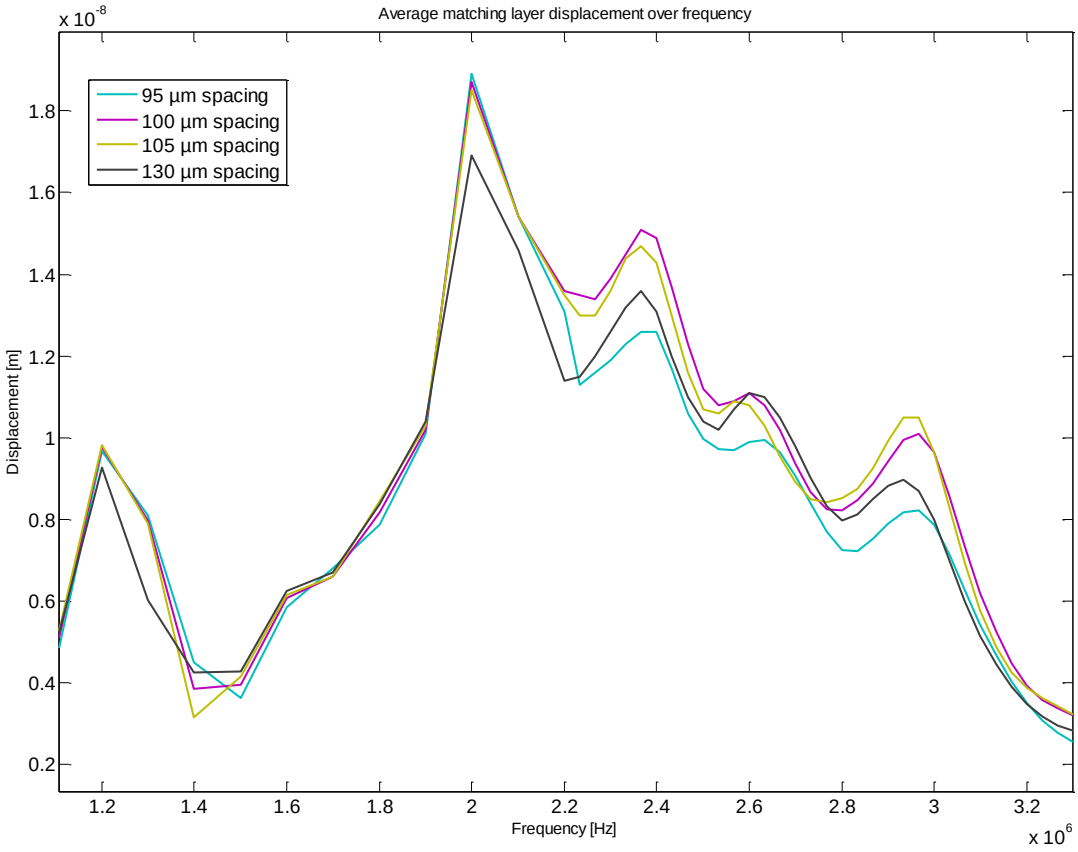

FIGURE 36. The average displacement of the nodes from matching layer for spacings of 95, 100, 105 and 130 µm

The displacement for the rest of the models is plotted in Figure 37. From the curves it can be seen that the models with smaller spacings have multiple and mixed lateral resonances and the displacement behaviour is seemingly random. With spacing as large as 200 µm, the lateral resonances almost disappear and merge to thickness mode resonance and the peak displacement becomes wide in shape.

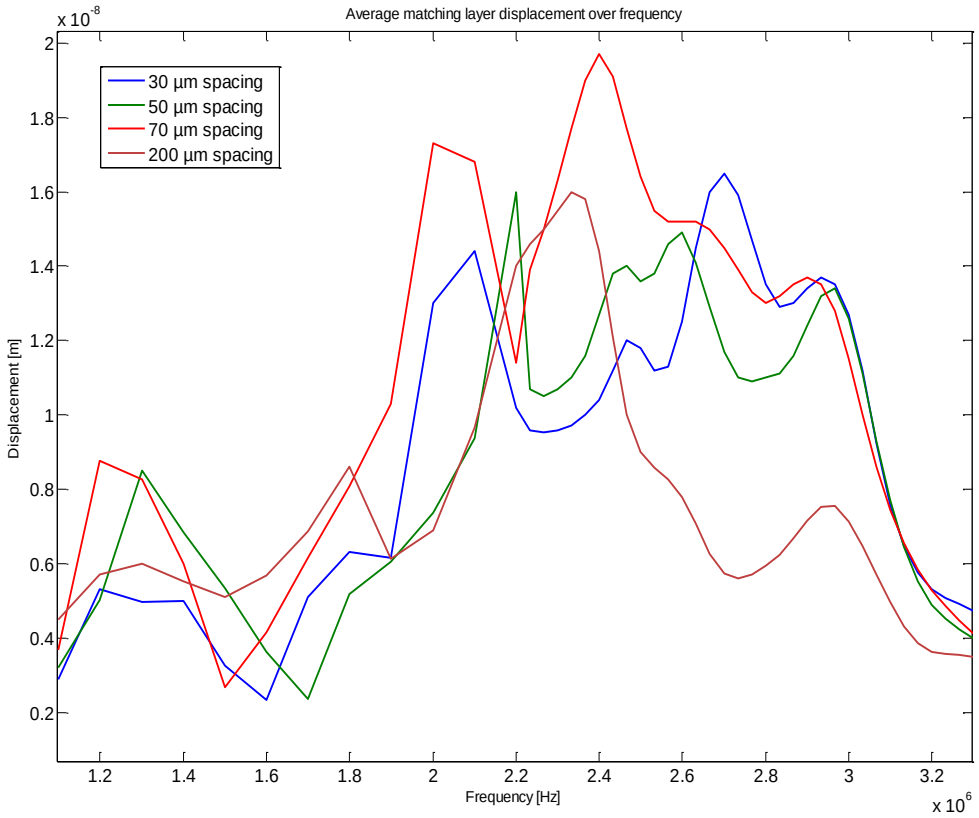

FIGURE 37. The average displacement of the nodes from matching layer for spacings of 30, 50, 70 and 200 µm

5.2.4 Summary of the Results

When averaging the results over a larger frequency area the differences tend to die out. This is because the simulation model can be regarded as an isolated system and the models differ only a fraction in terms of size and shape. A curve with a large extreme also tends to peak narrowly and a curve with a smaller extreme widely thus compensating the average absolute values to the same level. The width of the peak compared to its absolute value can be described with a quality factor; the higher the quality factor the sharper the peak. One approach is to compare the models based on their quality factor.

Quality factor of a resonating circuit comes from the ratio of the resonance frequency to the -3 dB power bandwidth:

$$Q = \frac{f_{res}}{\Delta f_{-3dB}} \tag{6}$$

When the applied voltage in circuit is constant, the current has its maximum value at resonance when the impedance is minimum and equal to resistance because at

resonance the imaginary parts of the impedance are cancelled out. Therefore the power has its maximum value at resonance. The -3 dB bandwidth is the frequency area where the power is half of the maximum power or more. [22]

Having a low Q-factor is generally good for a transducer used in imaging. The lower the Q-factor, the shorter the “ringdown time”, the time a transducer vibrates at its resonance frequency before the vibration decreases to negligible level. So, low Q-factor means short pulse duration which means good axial resolution. The Q-factors are listed in Table 9. The simulations show that having a spacing of 105-130 µm in the USCT transducer could result in good Q-factor and might be beneficial to the imaging resolution. [23]

TABLE 9. Q-factors

Spacing / µm	Q-factor
30	2.64
50	3.17
70	2.88
95	2.63
100	2.63
105	2.29
130	2.37
200	2.80

Aside from low Q-factor, wide bandwidth of low impedance and high power are wanted features for ultrasound transducers that are used with multiple frequencies or over a specified frequency area. In some applications however a single good frequency is in search. From the spacing sizes simulated, apart from the massive model, all of them could be used and they would work fine although the large effect of the lateral resonances for the smaller spacings has to be taken in to concern. If some specific feature is wanted, changing the spacing of the matrix could be helpful.

5.3 Varying Bridge

The effect of transducers bridge thickness to the behaviour of the transducer was examined by doing ANSYS simulations. Simulations were done over the frequency area of interest. Electrical impedance, power and displacement were studied.

The original transducer model has 30 µm thick bridge and 540 µm thick rods; making the whole piezo 570 µm thick in the position of the rods. Bridge thickness was varied from zero to 570 µm (massive plate) in the simulations. Figure 38 illustrates the growing of the bridge. Simulations were done with keeping the overall piezo thickness constant.

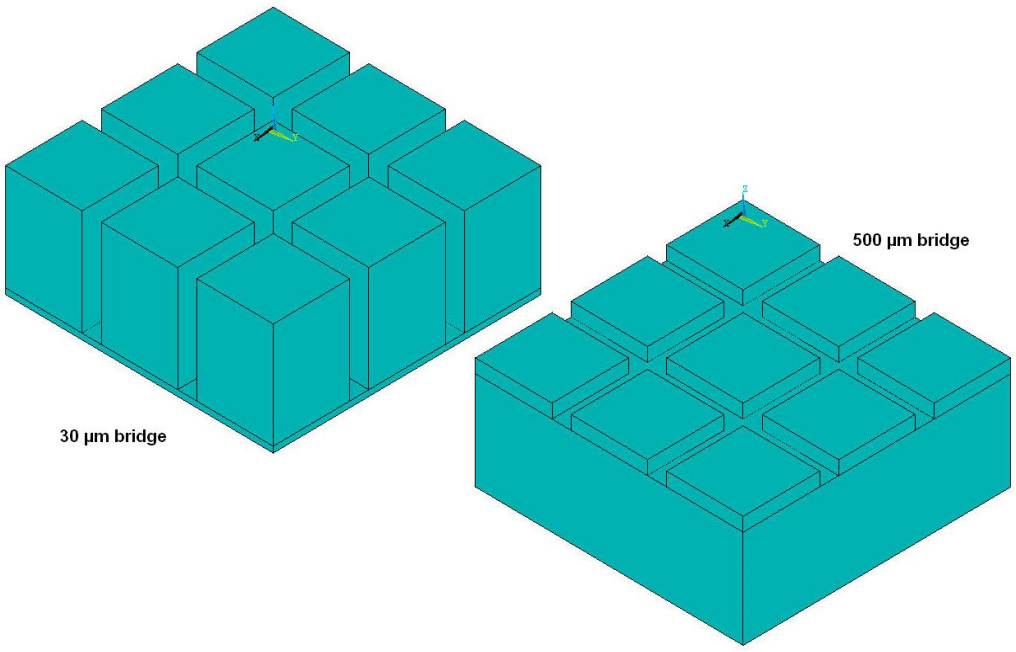

FIGURE 38. Thinnest bridge of 30 µm and the thickest bridge of 500 µm.

5.3.1 Impedance

Varying the bridge thickness and keeping the overall piezo thickness constant affects the impedance clearly at specific frequency areas. It can be seen from Figure 39 how at approximately 300 kHz area at the resonance minimum the impedance grows as the bridge of the transducer is thickened from 0 up to 100 µm. Simulation with 200 µm bridge results with lower impedance at resonance area than with 100 µm, so at some point the direction of the absolute value change turns. Another interesting area is the anti-resonance area where thickening the bridge decreases the impedance. The model with no bridge behaves differently in the anti-resonance area having low impedance on the first peak and very high impedance on the second.

Looking at the phase of the impedance at Figure 40, it can be seen how the thickness of the bridge affects it in the frequencies larger than the resonance frequency. When the

bridge is thicker than 100 µm, the phase is constantly later in the frequency area of interest. It can be also easily noted how thickening the bridge up to 500 µm disposes the resonating effect in the frequency area of interest.

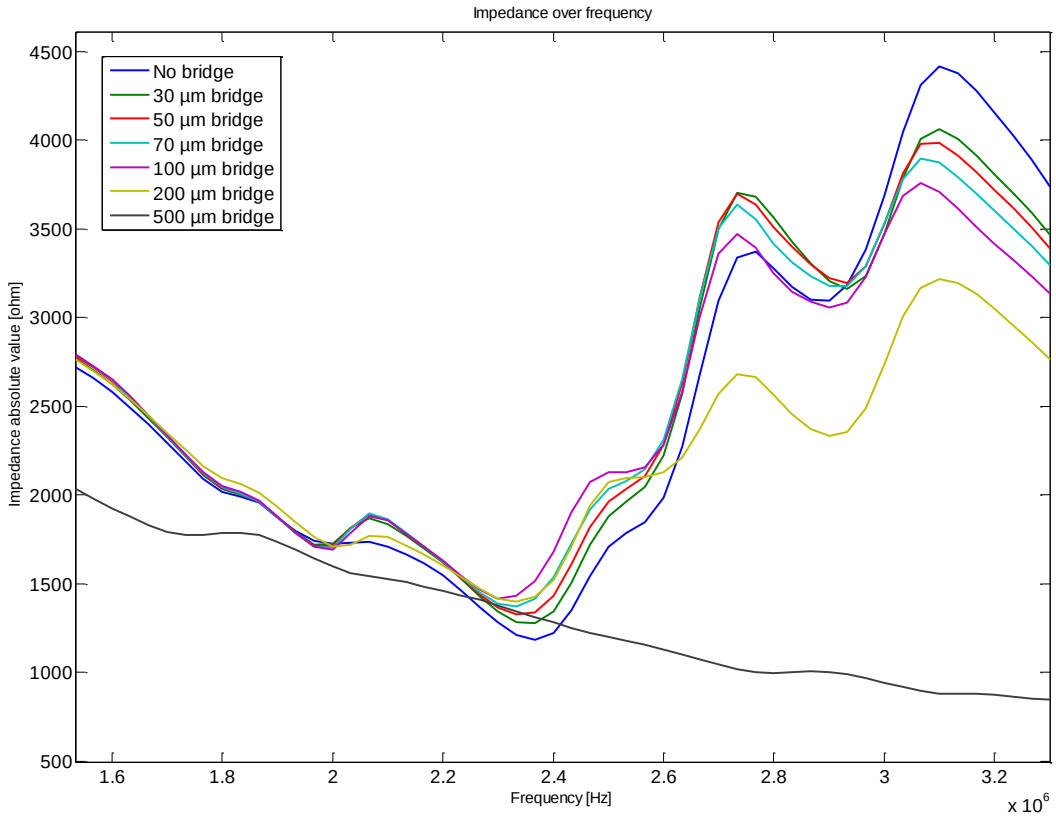

FIGURE 39. Impedance absolute value

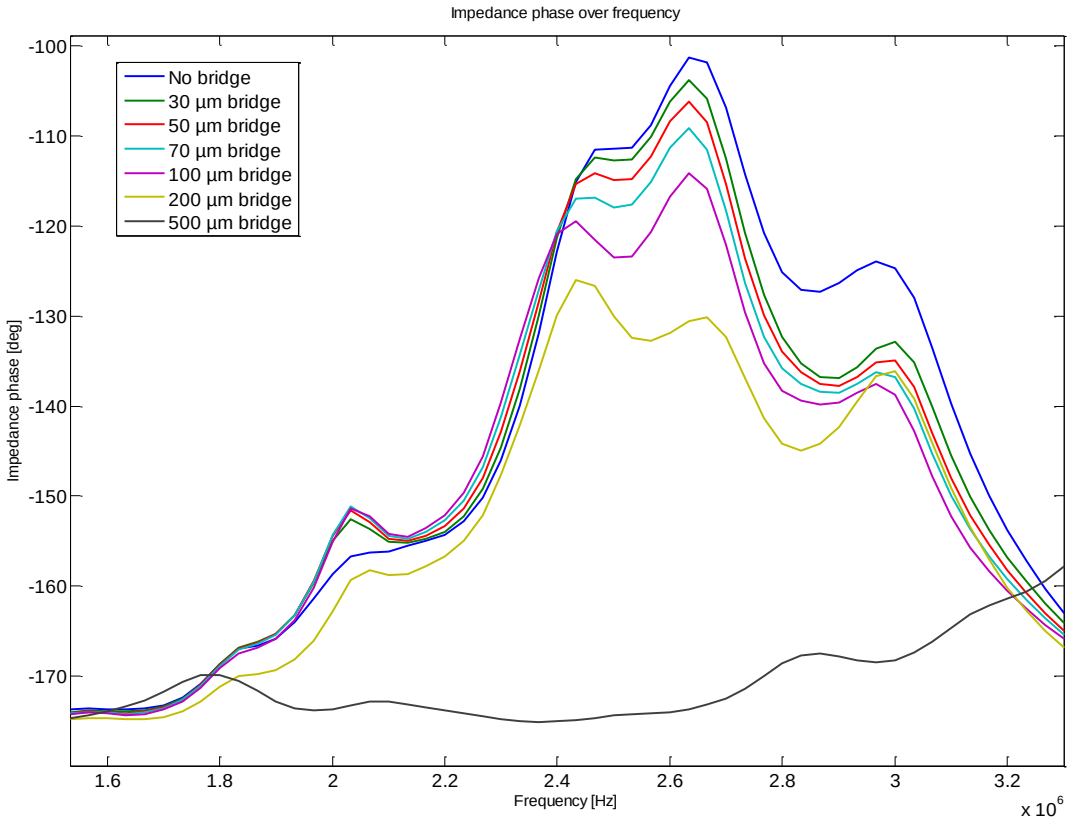

FIGURE 40. Impedance phase

5.3.2 Power

The power behaviour corresponds to the impedance behaviour. Thickening the bridge up to 100 µm affects negatively to the maximum power area near the resonance frequency. It is worth to note that while the absolute values differ at the maximum power area, the shape of the curves do not.

Enlarging the bridge thickness up to 100 µm, the power absolute value decreases. Simulation of a transducer with no bridge especially stands out with larger power absolute value in the Figure 41. After 100 µm the power turns to increase again and at 200 µm the absolute value is larger than with the bridge thickness of 100 µm.

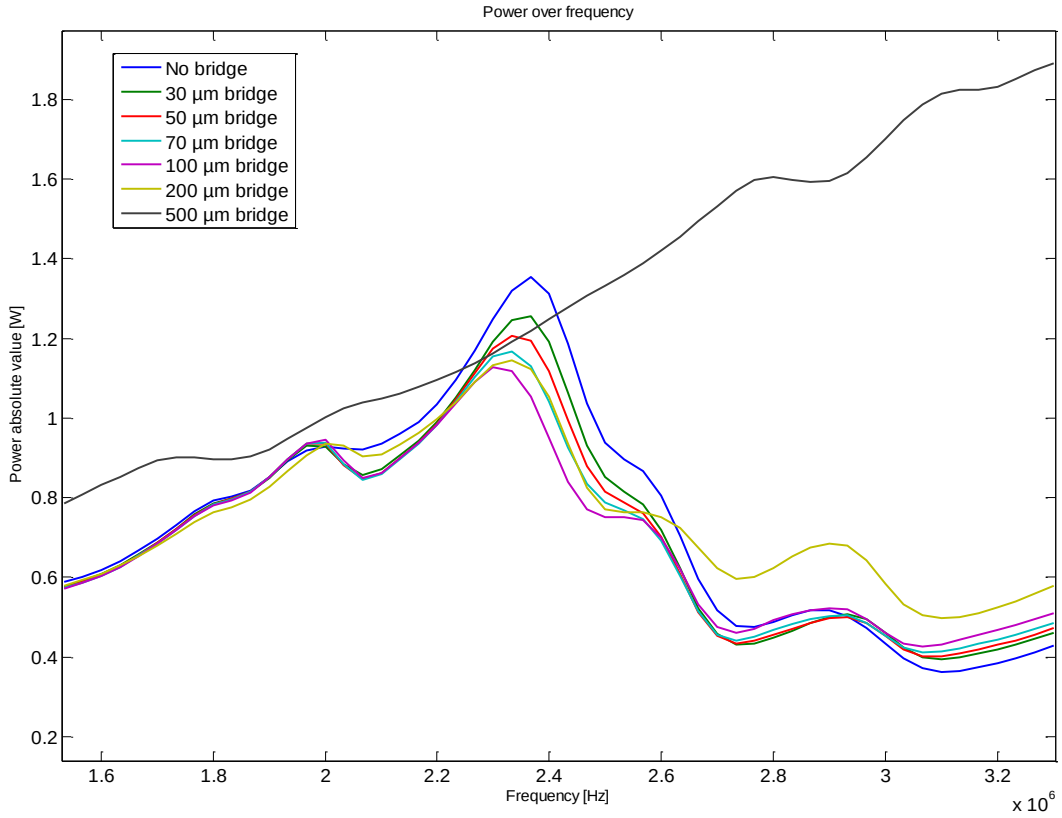

FIGURE 41. Power absolute value

5.3.3 Displacement

Displacement was studied by recording the displacement from total of nine nodes in the bottom surface of the matching layer. The nodes were selected to cover the area of one active rod and surrounding filler (see Figure 35) as was done in the spacing variation section.

When varying the bridge between 30-100 µm, the differences in the displacement were also small. Without the bridge the displacement curve is slightly different and the maximum displacement is smaller than for the other variations. In the Figure 42 it can be seen that growing the bridge larger than 100 µm has undesirable effect as the displacement in the matching layer decreases significantly.

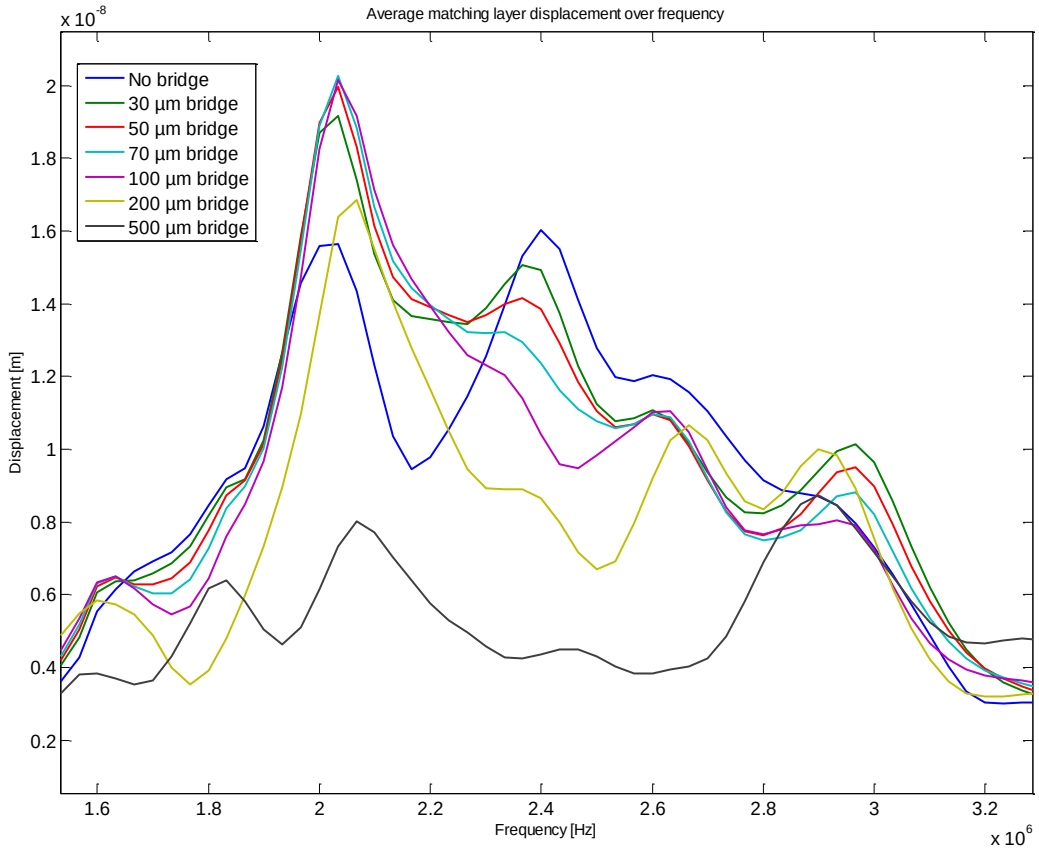

FIGURE 42. Matching layer average displacement

5.3.4 Varying the Bridge Thickness while the Rod Thickness Stays Constant

When varying the bridge thickness while the rod thickness is constant means that the overall piezo thickness is varied also. This has way bigger effects for the behaviour of the transducer than just changing the ratio of the bridge and the rods. The negative effects of growing the bridge are multiplied if the whole transducer thickens as well. This can be seen in Figure 43 where the bridge is grown from 30 µm to 70 µm with and without growing the whole transducer.

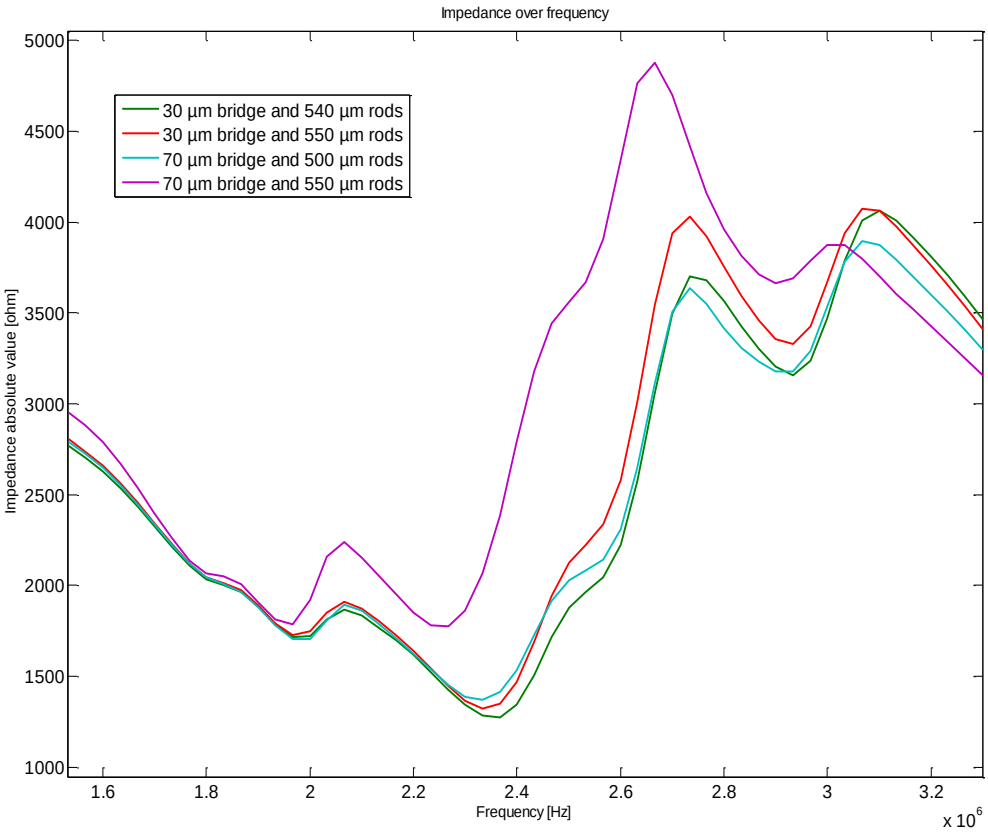

FIGURE 43. Impedance absolute value graph

5.3.5 Varying the Rod thickness while the Bridge Thickness Stays Constant

The thickness of the rods was varied between 450 and 550 µm, while the bridge was constantly 30 µm thick. In Figures 44 and 45 you can see how the rod thickness affects the impedance and the matching layer displacement of the transducer. Looking at the impedance curves it would seem that decreasing the rod thickness would decrease the resonating effect of the transducer, but looking at the Figure 45 we see that there still is a good amount of displacement in the matching layer for the thinnest rods.

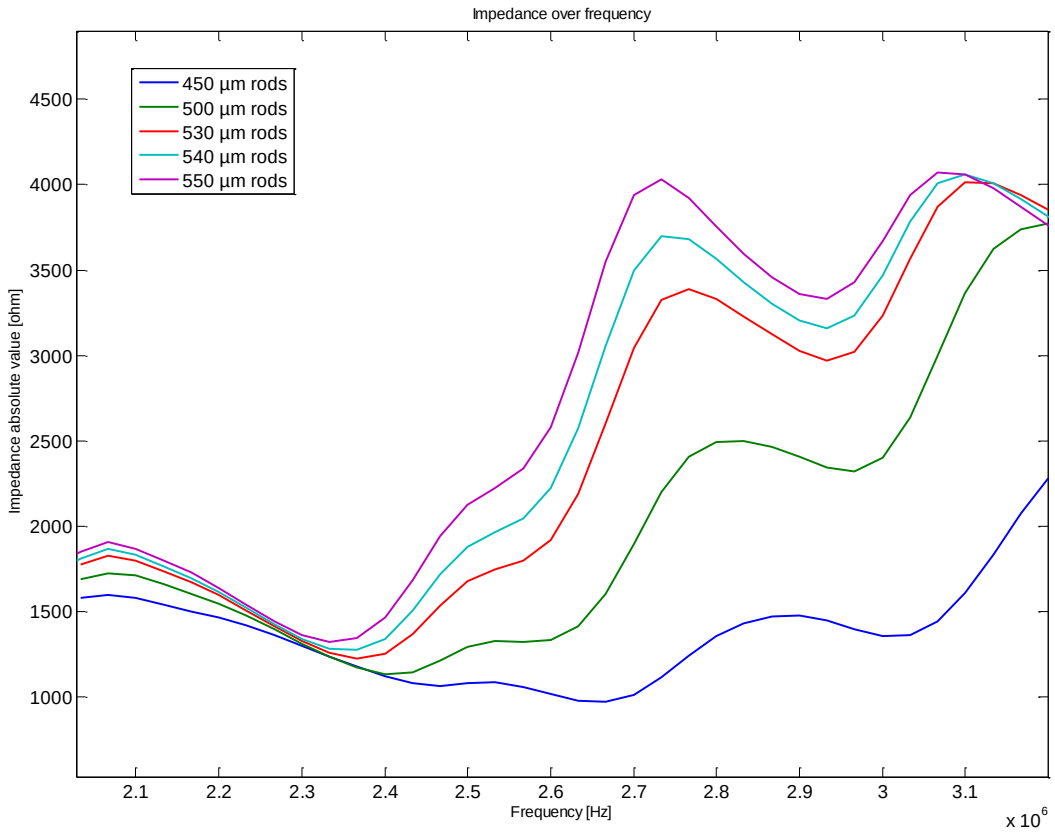

FIGURE 44. Impedance absolute value graph

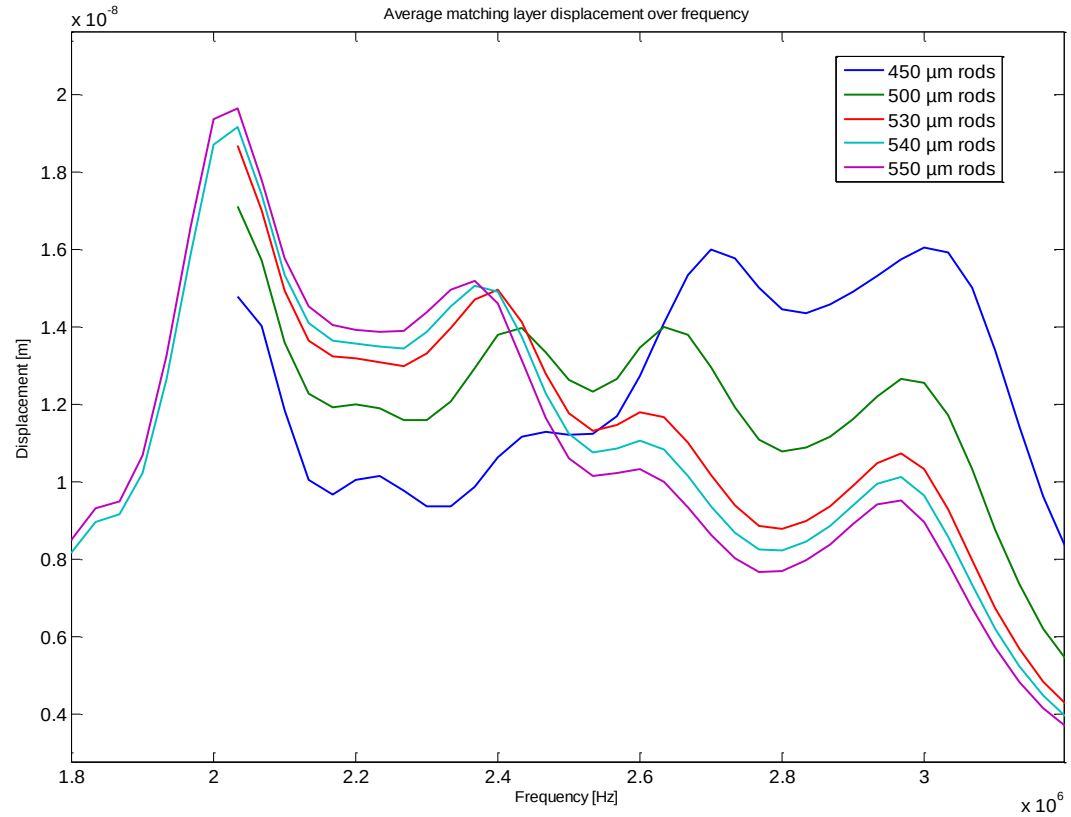

FIGURE 45. Average matching layer displacement graph

5.3.6 Results for Varying the Bridge Size

Simulation results show that the thickness of a transducer piezo matrix bridge has an effect on the impedance and power and the matching layer displacement. When the bridge thickness is between 30 µm and 100 µm, the differences stay relatively small. However between these measures, a thinner bridge has larger power and displacement and also lower impedance near resonance frequency. Especially the model without a bridge had good characteristics in the simulations. Models with bridge thicker than 100 µm had much larger power, much lower impedance and lower displacement. This suggests that when the bridge is grown too large, the transducer starts acting like a massive PZT plate. Then, in the frequency area of interest, the given electrical energy is transformed into different displacement modes that do not produce the desired ultrasound.

It can be determined from the results that when the thickness of the whole piezo stays constant, the thinnest bridge that can be fabricated would suit best for medical imaging in the frequency area of interest. If the fabrication process would allow the bridge to be left out completely, it could also be a good option although the displacement data seems to indicate that having a bridge under the piezo rods increases the matching layer displacement.

5.4 Massive Plate Transducer

While decreasing the pitch down to 30 µm did not have negative effects to the behaviour of the transducer, it is not efficient to decrease the spacing to nonexistent. Same results come when the bridge thickness is increased to make in fact a single massive plate. Simulation done with one massive rod the size of matrix of regular rods with 100 µm spacing showed that by not having spacing at all results as somewhat inactive transducer in the frequency area of interest. In Figure 46 is comparison of impedance from original matrix and massive rod. It can be seen that the massive rod has no clear resonance in the frequency range of interest so the distributed power shown in Figure 47 does not generate sound pressure. Low displacement for massive model seen in Figure 48 implies it as well.

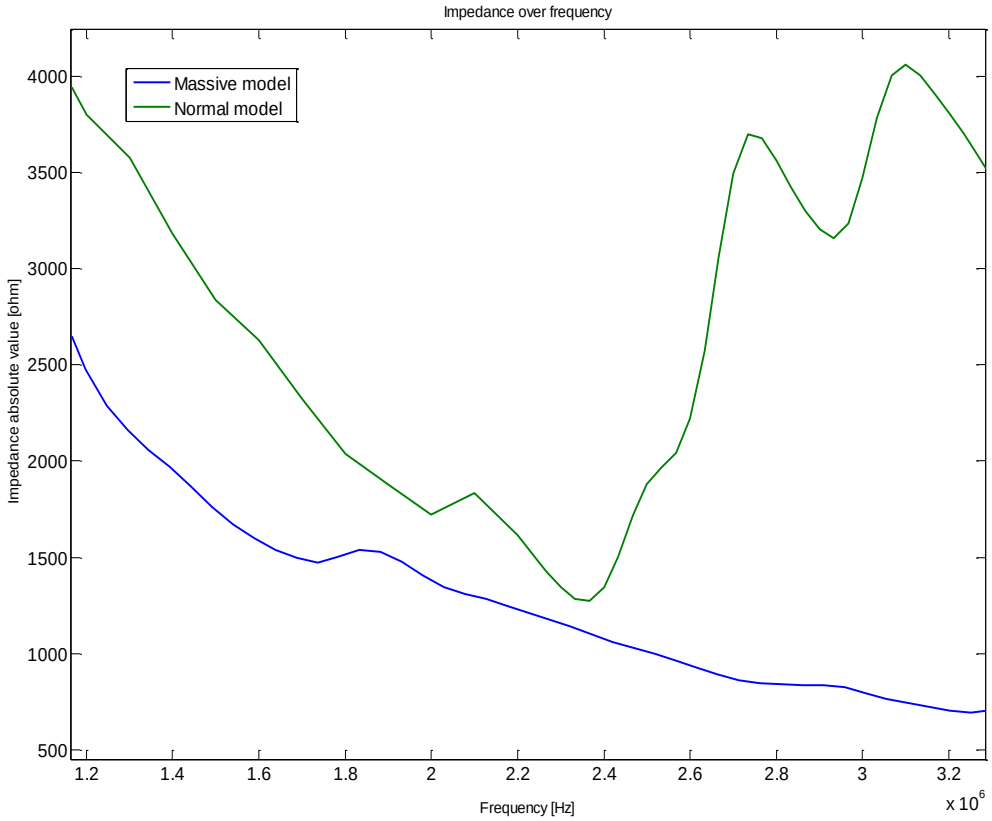

FIGURE 46. Impedance absolute value of original matrix with 100 µm spacing with 30 µm bridge and massive rod.

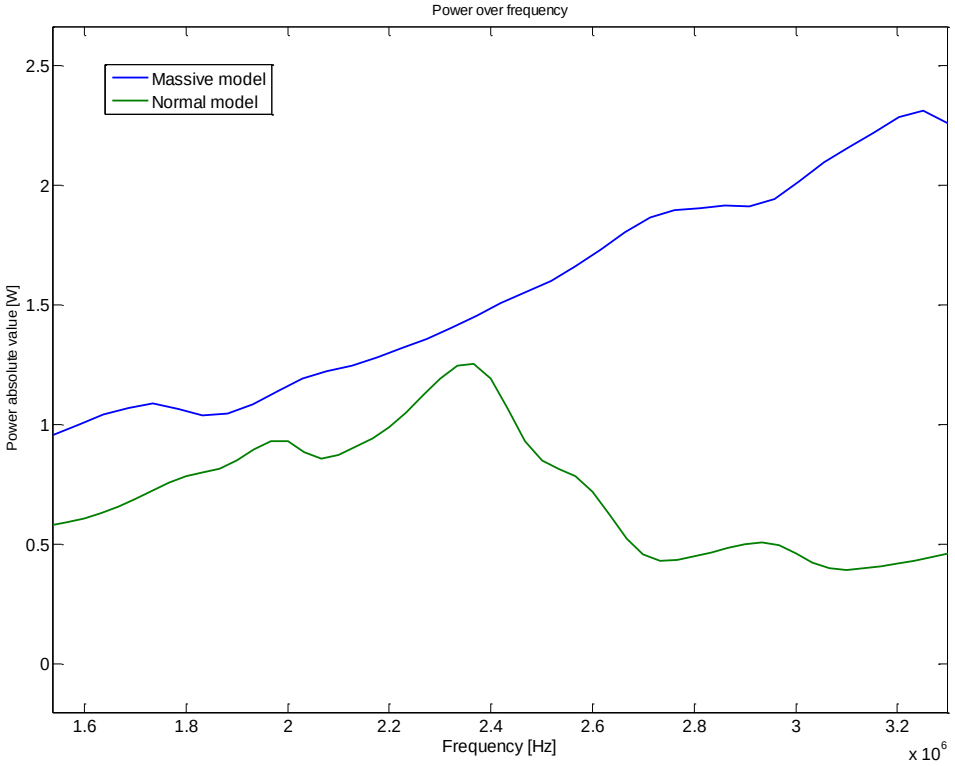

FIGURE 47. Power absolute value of original matrix with 100 µm spacing with 30 µm bridge and massive rod.

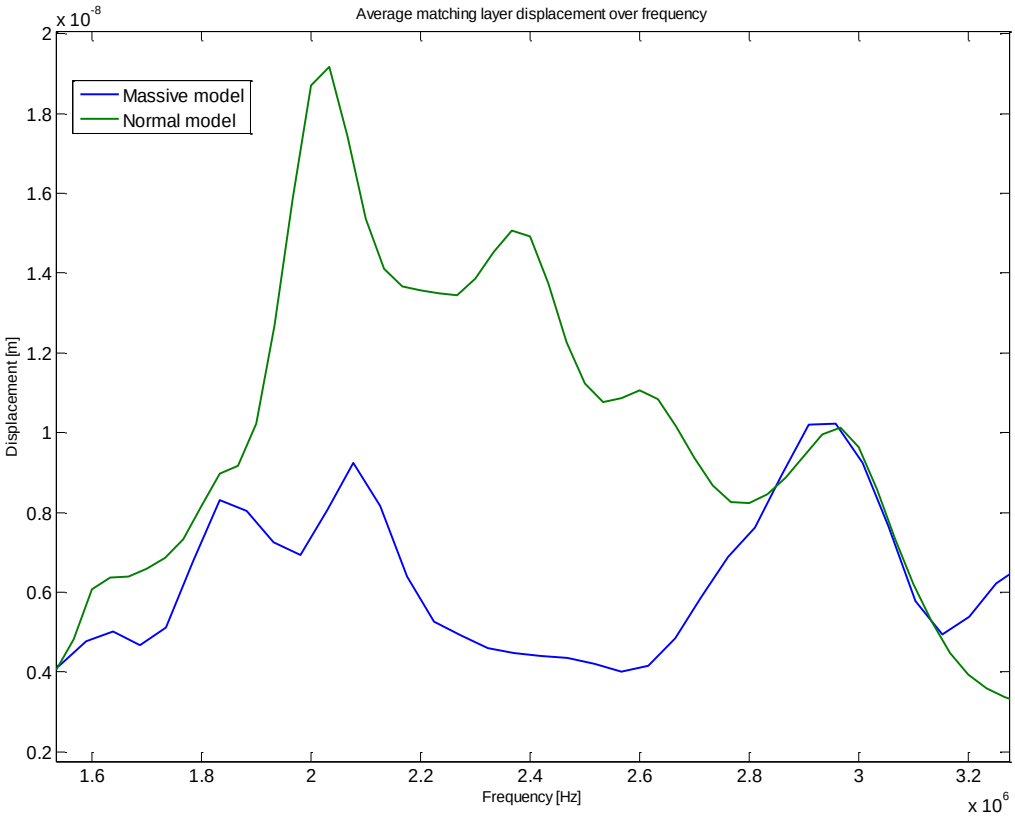

FIGURE 48. Average matching layer displacement

5.5 Real Life Transducers

After the simulations two real life transducers with 50 µm spacing with 30 µm bridge were fabricated. For this thesis, it was not possible to have transducers that were exactly the same as the simulated models and with the fabrication methods used, the final measurements varied somewhat from the simulation model.

Measurements were done with the transducers with 50 µm spacing (transducers 1 and 2) as well as with two earlier fabricated transducers with 100 µm spacing (transducers A and B). The older transducer also differed in bridge size, having 70 µm thick bridge versus the 30 µm in the newer ones. This does have an effect, comparable to the results seen earlier when bridge thickness was varied.

5.5.1 Differences in Fabricated Transducers

In the impedance measurements it has to be taken into account that even the differences between the two new transducers is notable. The difference can come from various sources. The two transducers, although fabricated the same way, may have differences originated from the fabrication due to non-factory fabrication. Also the transducers differ in the number of rods that have readiness to be excited i.e. the connections made to rods are different.

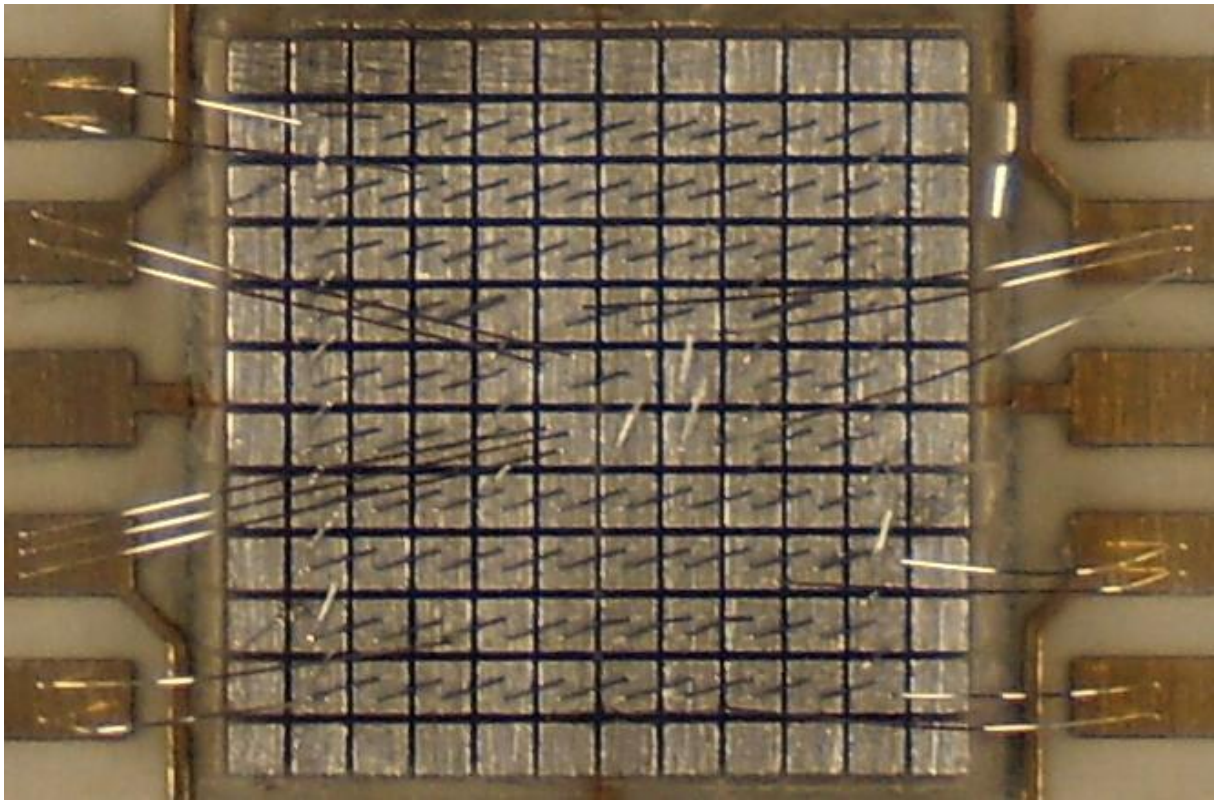

FIGURE 49. Test transducer 1 with 50 µm spacing and bonded connections to all but outmost rods

As can be seen from the Figure 49, test transducer 1 has bonded connections to all but the outer rods, but in the measurements, only 9 rods in the middle were excited.

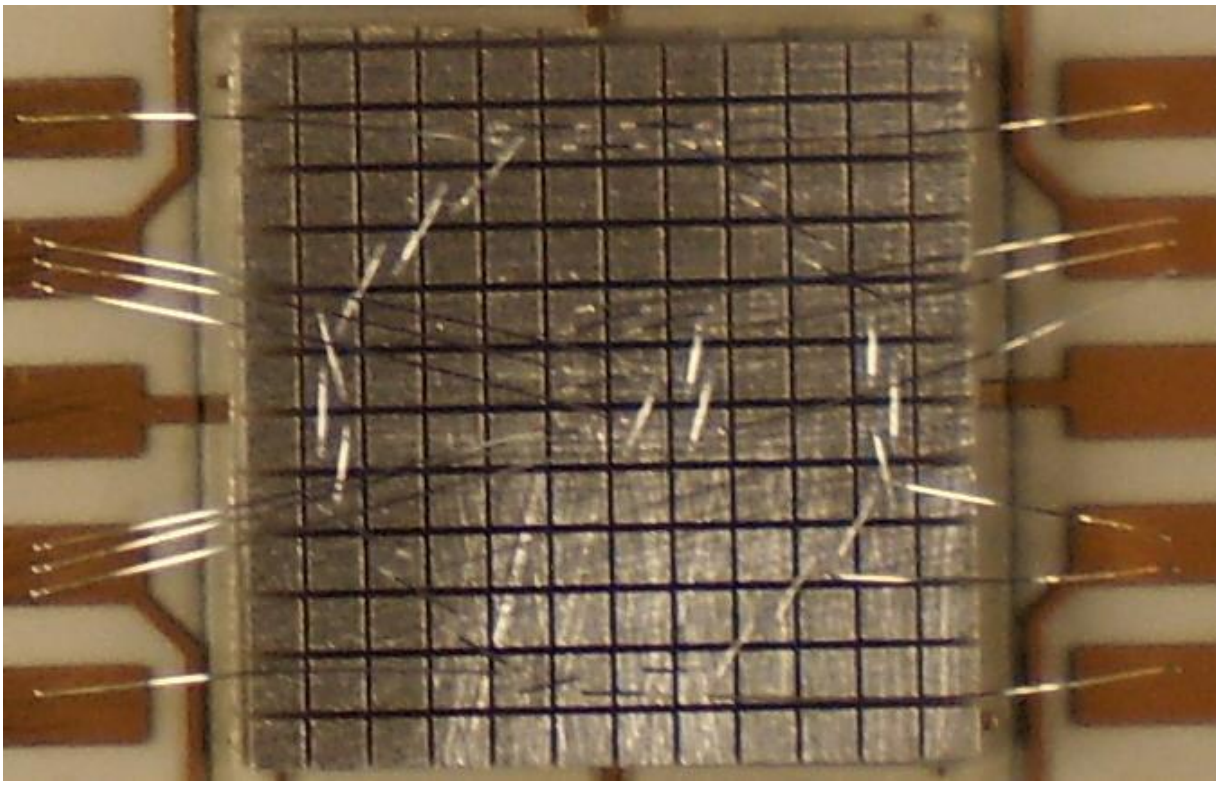

FIGURE 50. Test transducer 2 with 50 µm spacing and bonded connections to 9 rods in the middle and to surrounding annular pattern

As can be seen from the Figure 50, test transducer 2 has bonded connections made to the middle 9 rods and to an annular pattern circulating the middle rods. In the measurements, only 9 rods in the middle were excited.

Different bonding leads to difference in coupling and mass of the rods. When voltage is applied to the transducer, there is electrical coupling between the rods. In the transducer with connections to all rods, the electrical coupling advances mainly galvanically conducting through the connections. In the transducer with the connection to the annular set of rods, the electrical coupling advances from the middle rods to the annular set mainly statically, inductively or capacitively. Similarly, the mechanical coupling also travels differently in the rods of the two transducers. Mechanical coupling produces electrical charges, which in turn is again coupled and so on.

The connections to the rods are made with 20 µm silver wires. The transducer with connections made to all rods obviously has more mass in the rods which can have a small effect in the measurements.

5.5.2 Impedance Measurements

Keeping all this in mind, the impedance measurements from the new transducers with 50 µm spacing were compared to the old transducers with 100 µm spacing and to the simulation results. Impedance absolute values are in Figure 51. Comparison was done using 9 active rods. In the measurements it can be seen that the resonance point is drifted to larger frequency point for the transducers 1 and 2 as predicted by the simulations. Also the impedance seems to be much lower near anti-resonance, behaviour that was not visible in the simulated impedance. Reason for this behaviour cannot be concluded without making a larger proto-series, but the impedance measured from the test transducer 2 indicates that a lateral resonance occurs nearer to the thickness mode resonance than for the other transducers and the impedance measured from the test transducer 1 indicates a presence of a powerful lateral resonance between the anti-resonance peaks.

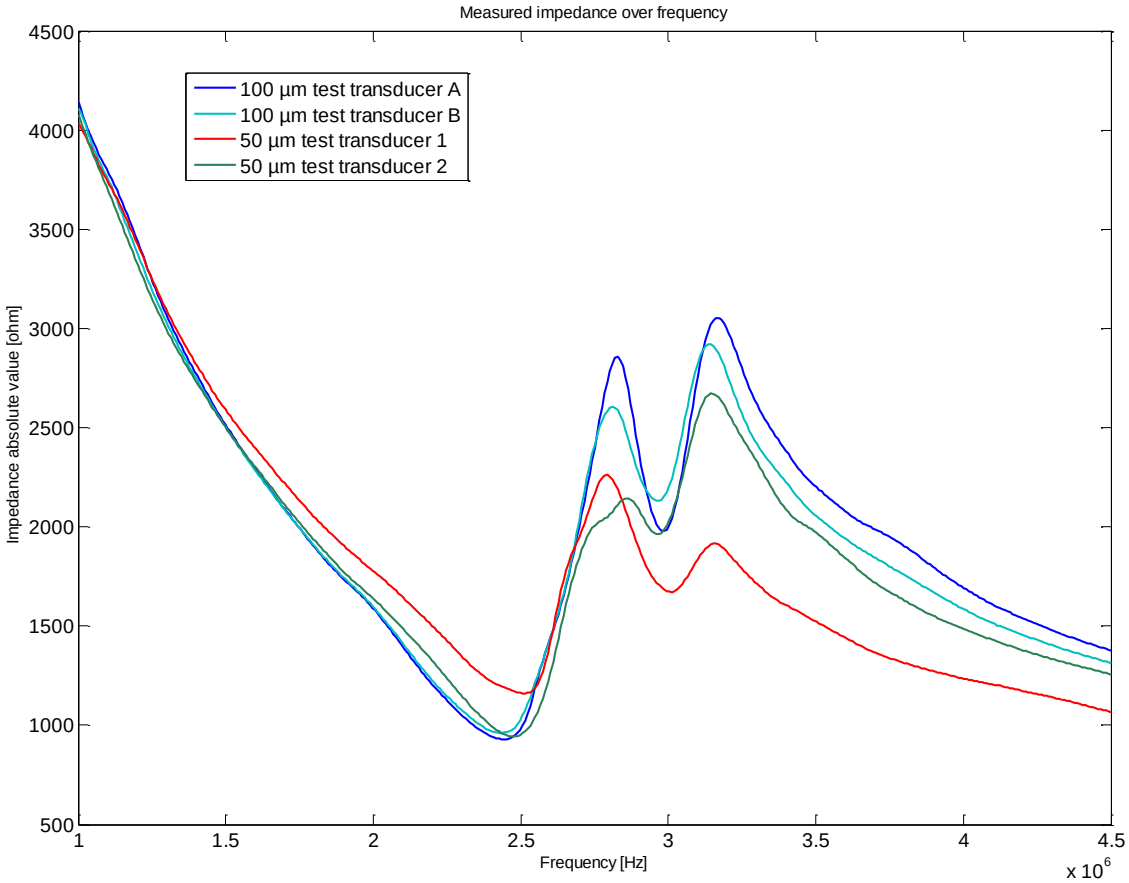

FIGURE 51. Figure 16. Measured impedance absolute value of the test transducers

From the measurements it can be suggested that there is no positive effect in decreasing the spacing of the matrix too much. Decreasing the bridge size however should be researched by fabricating test transducers with 100 µm spacing and 30 µm bridge.

6 OUTLOOK

To make the simulation model even more precise and comprehensive, an option to simulate also the sound pressure would be effectible. This would require a media of propagation (e.g. water) to be modelled to follow-on the matching layer. The problem is that the volume of the simulated media would need to cover an area of beyond the near field to get comparable results. The model would have to be done so that the simulation time would not increase too much. It would require compromising in the meshing, but it can be done. Sound pressure simulation would be a good additional method to investigate the transducer along the existing methods and to compare to measurements.

The same methods used in this thesis can be used to further examine the transducer. Completely changing the materials or even the structure of the transducer could be beneficial future research to be done. The effects on modifying the matching layer and the backing is widely researched in scientific world and surely these methods could be used on that as well. One example is how regarding the PZT matrix and the filler as composite material changes the optimal matching layer material.

6.1 PZT Matrix and Filler as Composite Material

Earlier in this thesis, the three principles for designing a matching layer for ultrasound transducer were presented. The first one, telling that the acoustic impedance of the matching layer should be the square root of the product of the characteristic acoustic impedances of the PZT-matrix and the target medium, is now discussed.

The characteristic impedance of a medium is a material property depending on the material density and the speed of sound in material, being the product of the two. Water, which is the target medium in this case, has an acoustic impedance of ~1.5 MRayls and the PZT has an acoustic impedance of ~28 MRayls. However, because the PZT is not a solid plate, but a matrix of rods filled with polyurethane, the impedance for the PZT-matrix and filler composite can be calculated. [19]

The structure of the PZT matrix with the filler has a connectivity pattern of a material called a 1-3 composite. A 1-3 composite has one material connected to itself in one dimension and another material connected to it in three dimensions, illustrated in Figure 52. [19]

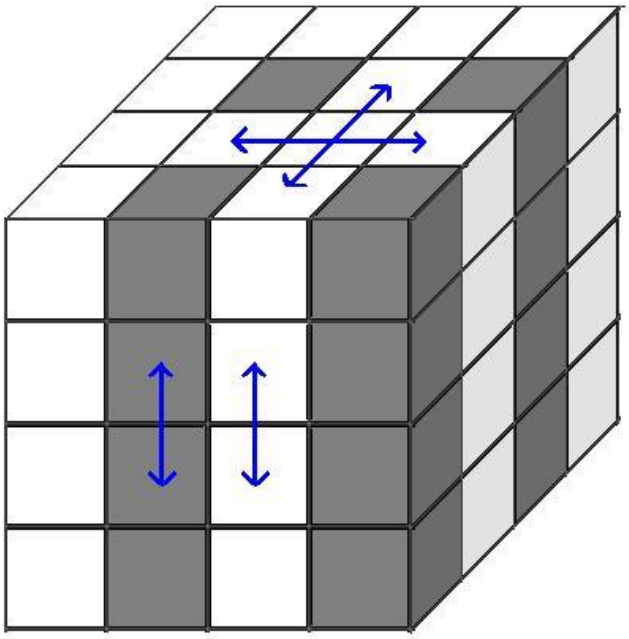

FIGURE 52. The white material is connected in three dimensions whereas the shaded material is connected only in one, making the structure 1-3 composite

In the transducer, the PZT is connected to itself in one dimension and the filler in three. So, looking at the PZT and filler as a single composite material, it is proposed that an acoustic impedance for the composite structure can be calculated.

The acoustic impedance Z is related to the material density ρ and elastic bulk modulus K as follows:

$$Z = \sqrt{K\rho} \tag{7}$$

The density of the composite can be calculated using

$$\rho_{comp} = \rho_{PZT} V_{PZT} + \rho_{PU} V_{PU} \tag{8}$$

where ρ_{PZT}, ρ_{PU}, V_{PZT} and V_{PU} are the densities and volume fractions of PZT and polyurethane. In the USCT test transducer the PZT has a volume fraction of 0.64 and the polyurethane 0.36. The density of a PZT is 7900 kg/m^3 and of a polyurethane it is 1600 kg/m^3. Hence the density of the composite is

$$\rho_{comp} = 7900 \ \frac{kg}{m^3} * 0.64 + 1600 \ \frac{kg}{m^3} * 0.36 = 5632 \ \frac{kg}{m^3} \tag{9}$$

For elastic properties of components, three methods of calculation are available. Reuss method:

$$K_{\mathrm{Reuss}} = \left(\frac{K_1 K_2}{V_1 K_2 + V_2 K_1} \right) \tag{10}$$

Voigt method:

$$K_{Voigt} = V_1 K_1 + V_2 K_2 \tag{11}$$

and logarithmic method:

$$\ln(K) = V_1 \ln(K_1) + V_2 \ln(K_2) \tag{12}$$

where K_1 and K_2 are the elastic bulk modulus of each composite material and the V_1 and V_2 are the volume fractions for each composite material. The logarithmic model is an empirical model giving values between the lower bound Reuss and upper bound Voigt models. [19]

PZT has bulk modulus of $9.833*10^{10}$ N/m^2 and the polyurethane has bulk modulus of $5.966*10^9$ N/m^2. Calculating the composite bulk modulus with the logarithmic model gives:

$$\begin{aligned} \ln(K_{comp}) &= 0.64 \ln(9.833*10^{10} \ \frac{N}{m^2}) + 0.36 \ln(5.966*10^9 \ \frac{N}{m^2}) \\ &= 24.30278 \ \frac{N}{m^2} \\ \Rightarrow K_{comp} &= 3.58563*10^{10} \ \frac{N}{m^2} \approx 3.59*10^{10} \ \frac{N}{m^2} \end{aligned} \tag{13}$$

Inserting the values to formula 7 gives acoustic impedance for the composite:

$$\begin{aligned} Z_{comp} &= \sqrt{3.59*10^{10} \ \frac{N}{m^2} * 5600 \ \frac{kg}{m^3}} = 14210646 \ \ Rayl \\ &\approx 14.2 \ \ MRayl \end{aligned} \tag{14}$$

Now using this value for the first principle in designing matching layer we get:

$$\begin{aligned} Z_{ML} &= \sqrt{14.2 \ \ MRayl * 1.5 \ \ MRayl} = 4.616922 \ \ MRayl \\ &\approx 4.6 \ \ MRayl \end{aligned} \tag{15}$$

The TMM4-material, used for the matching layer has characteristic acoustic impedance of 6.4 MRayl. Therefore the TMM4 is not a perfectly suitable material for the matching layer of USCT transducer. On the other hand, the polyurethane used in the backing and filler has impedance that, although not perfect, is still closer to the calculated optimal

acoustical impedance. Simulation with polyurethane as a matching layer material was conducted to examine the feasibility of regarding the PZT matrix with filler as a composite. [16] [19] [24]

In Figure 53 there is the simulated resulting electrical impedance of the transducer with TMM4 matching layer and PU matching layer. It can be seen how the resonance area is very different for the PU matching layer. It is much wider, but also has larger amplitude, which suggests larger bandwidth but lower sound pressure. The acoustical impedance of the material parameters is not the only one affecting the impedance, but the results show that it would be feasible to study further the material of the matching layer for the USCT transducers.

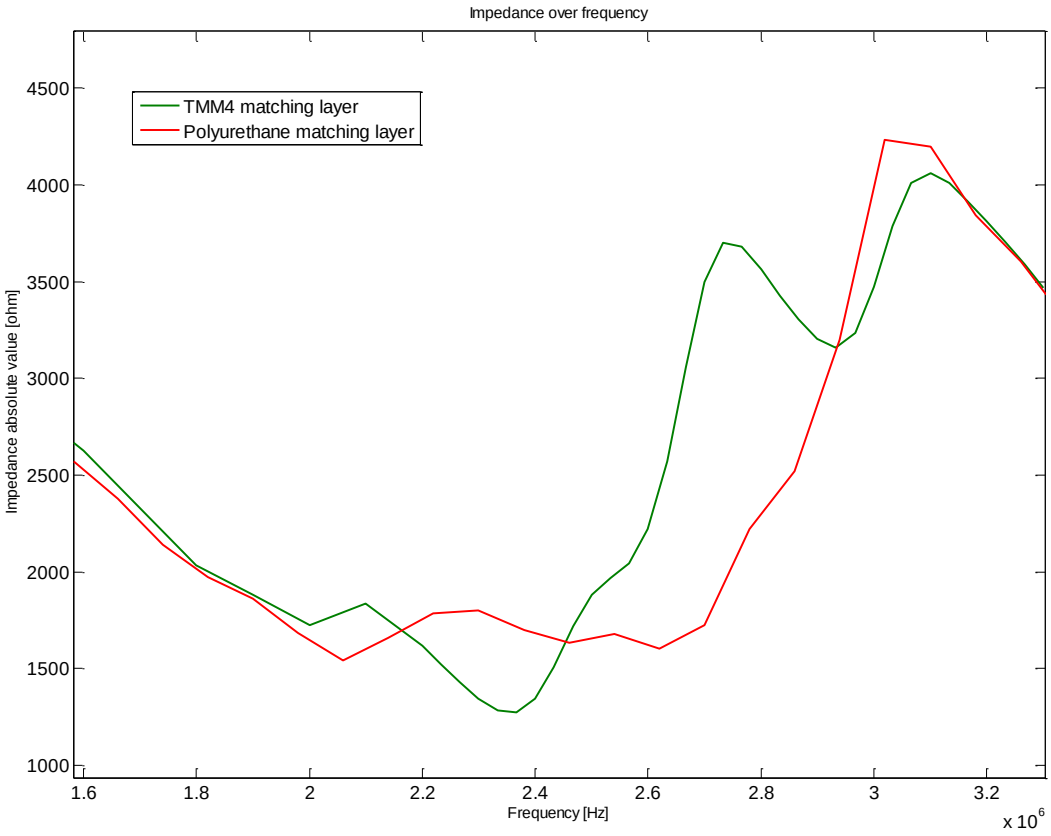

FIGURE 53. Comparison of the impedance absolute values between TMM4 matching layer and polyurethane matching layer

6.2 Smaller Transducer Models

Since the simulations done with the quarter model of the 5x5 matrix are still quite time consuming, it would be useful to fabricate 3x3 matrix and 2x2 matrix transducers. Then

the measurements could be compared to a quarter model of a 3x3 matrix simulating behaviour of one active rod with the coupling effects from surrounding rods and to a quarter model of 2x2 matrix simulating just one rod in the matrix. The smaller models could be used at least for preliminary simulations, using the larger models and fabricated transducers then if the results necessitate so.

7 CONCLUSION

The ultrasound transducers used in the USCT project were examined in this thesis. The using environment for the transducers was reviewed and the basic theory of operation of the transducers was processed. Moreover, the behaviour of the transducers was examined and simulated. The simulation model was optimized and effects on changing the parameters of the transducer were researched.

Fine tuning a transducer is precision art and using simulation software with FEA turned out to be a feasible method to predict and research the behaviour, provided that the used model is accurate and matching.

Although there was time to research only a couple of affecting changes in the transducer, it can be concluded that the groundwork on aiming to optimize the transducer is a valuable effort in possible future research. Also many of the transducer features got characterized and as a result of this thesis understanding of the transducers used in USCT was enhanced.

REFERENCES

1. GLOBOCAN (IARC) 2008. *Section of Cancer Information*. [online] [referred 28.06.2011] http://globocan.iarc.fr/factsheets/populations/factsheet.asp?uno=900
2. KIT webpages. [online] [referred 28.06.2011] http://www.ipe.kit.edu/english/
3. Kohout, B. 2010. *Finite Elemente Simulation von Ultraschallwandlersystemen für die Ultraschall Computertomographie.* Diploma Thesis.
4. Müller, T-O., Stotzka, R., Ruiter, N., Schlote–Holubek, K. and Gemmeke, H. 2004. *3D Ultrasound Computer Tomography: Data Acquisition Hardware.* IEEE Xplore. [online] [referred 28.06.2011] E-ISBN: 0-7803-8701-5.
5. Jirik, R., Peterlik, I., Jan, J., Ruiter, N. and Zapf, M. 2009. *3D Regularized Speed-Map Reconstruction in Ultrasound Transmission Tomography.* IEEE Xplore. [online] [referred 28.06.2011] ISSN: 1948-5719.
6. Ruiter, N., Schwarzenberg, G., Zapf, M. and Gemmeke, H. 2008. *Conclusions from an Experimental 3D Ultrasound Computer.* IEEE Xplore. [online] [referred 28.06.2011] ISSN: 1082-3654.
7. Birk, M., Koehler, S., Balzer, M., Huebner, M., Ruiter, N. and Becker, J. 2010. *FPGA-based Embedded Signal Processing for 3D Ultrasound Computer Tomography.* IEEE Xplore. [online] [referred 28.06.2011] Print ISBN: 978-1-4244-7108-9.
8. Hunt, J., Arditi, M. and Foster, F. 1983. *Ultrasound Transducers for Pulse-Echo Medical Imaging.* IEEE Xplore. [online] [referred 28.06.2011] ISSN: 0018-9294
9. Vives, A., Arnau, A. 2004. *Piezoelectric Transducers and Applications – Chapter 3*. [online] [referred 28.06.2011] ISBN: 3-540-20998-0.
10. Kocbach, J. 2000. *Finite Element Modeling of Ultrasonic Piezoelectric Transducers.* [online] [referred 11.07.2011] http://web.ift.uib.no/~jankoc/thesis/diss.pdf
11. Krimholtz, R., Leedom, D., Matthaei, G. 1970. *New equivalent circuits for elementary piezoelectric transducers*. IEEE Xplore. [online] [referred 11.07.2011] ISSN: 0013-5194
12. APC International Ltd. Webpages, Knowledge Center. [online] [referred 11.07.2011] http://www.americanpiezo.com/knowledge-center/

13. Piezocryst Advanced Sensorics GmbH webpages. [online] [referred 28.06.2011] http://www.piezocryst.com/
14. The Morgan Crucible Company plc webpages. [online] [referred 11.07.2011] http://www.morganelectroceramics.com/
15. Kossof, G. 1966. *The Effects of Backing and Matching on the Performance of Piezoelectric Ceramic Transducers.* IEE Xplore. [online] [referred 11.07.2011] ISSN: 0018-9537
16. Reynolds, P., Hyslop, J. and Hayward, G. 2003. *Analysis of spurious resonances in single and multi-element piezocomposite ultrasonic transducers.* IEEE Xplore. [online] [referred 28.06.2011] Print ISBN: 0-7803-7922-5
17. Kohout, B. 2010. *Optimierung von Anpassschichten für Ultraschallwandler.* Studienarbeit.
18. ANSYS Inc. Webpages. [online] [referred 28.06.2011] http://www.ansys.com/
19. ANSYS Inc. 2010. *ANSYS 13.0 Help.*
20. Grewe, M., Gururaja, T., Shrout, T., Newnham, R. 1990. *Acoustic Properties of Particle/Polymer Composites for Ultrasonic Transducer Backing Application.* IEE Xplore. [online] [referred 11.07.2011] ISSN: 0885-3010
21. Reynolds, P., Hyslop, J. and Hayward, G. 2003. *Analysis of spurious resonances in single and multi-element piezocomposite ultrasonic transducers.* IEEE Xplore. [online] [referred 28.06.2011] Print ISBN: 0-7803-7922-5
22. Lamberti, N., Gori, P., Caliano, G., Iula, A. and Carotenuto, R. 2000. *Radiation pattern distortion caused by the inter-element coupling via the backing and the matching layers in linear array transducers.* IEEE Xplore. [online] [referred 28.06.2011] ISSN: 1051-0117.
23. Medcyclopaedia. Webpages. [online] [referred 12.07.2011] http://www.medcyclopaedia.com/
24. Open Book Project. Webpages. [online] [referred 12.07.2011] http://openbookproject.net/electricCircuits/
25. Göbel, G. Diplomarbeit 2002. *Entwicklung von Ultraschallsensorarrays mit miniaturisierten Komponenten.*

```
%----------------- MATLAB ListPlotter by Juhana Pirinen -------------------- %

%----------------- Operation sliders ---------------------------------------- %
save    = 0;          %Turn 1 to save
versus  = 0;          %Number of data to compare to
phase   = 0;                    %Turn 1 for easy phase plotting
                      %(2,4,6,.. for parallel data in list file)

%----------------- Data multipliers for scaling ----------------------------- %
multiplier1  = 1;
multiplier2 = 1;
multiplier3 = 1;
multiplier4 = 1;
multiplier5 = 1;
multiplier6 = 1;
multiplier7 = 1;
multiplier8 = 1;
multiplier9 = 1;
multiplier10 = 1;

%----------------- Filenames ------------------------------------------------ %
name1   = 'file1';              %Name of the list file
name2   = 'file2';              %Name of the second list file…
name3   = 'file3';
name4   = 'file4';
name5   = 'file5';
name6   = 'file6';
name7   = 'file7';
name8   = 'file8';
name9   = 'file9';
name10  = 'file10';

folder  = 'save_folder';        %Folder to save to (has to exist)

%----------------- Folder paths --------------------------------------------- %
load_path1  = fullfile('Drive:', 'Folder_name1','Folder_name2','/');
load_path2  = fullfile('Drive2:', 'Folder_name3','Folder_name4','/');
load_path3           = load_path1
load_path4           = load_path1;
load_path5           = load_path1;
load_path6           = load_path1;
load_path7           = load_path2;
load_path8           = load_path2;
load_path9           = load_path2
load_path10 = load_path2;
save_path  = fullfile('Drive:', 'Folder_name5,'Folder_name6', folder,'/');

%----------------- File init -----------------------------------------------%
ext = '.lis';   %File extension
headers = 7;    %No. of headerlines in files
letters = 6;    %No. of letters from file to display in plot legend
```

```
%---------------- Program code ------------------------------------------%


colororder = [                  %MATLAB RGB values for colours
    0.00  0.00  1.00    %#1 blue (standard)
    0.00  0.50  0.00    %#2 green, darker
    1.00  0.00  0.00    %#3 red (standard)
    0.00  0.75  0.75    %#4 cyan, darker
    0.75  0.00  0.75    %#5 magenta, darker
    0.75  0.75  0.00    %#6 ocker, navi
    0.25  0.25  0.25    %#7 black (standard)
    0.75  0.25  0.25    %#8 braun
    0.95  0.95  0.00    %#9 yellow (standard)
    0.25  0.25  0.75    %#10 blue, darker
    0.75  0.75  0.75    %#11 grey
    0.00  1.00  0.00    %#12 green, lighter
    0.76  0.57  0.17    %#13 ocker, brown
    0.54  0.63  0.22    %#14 olive
    0.34  0.57  0.92    %#15 blue, lighter
    1.00  0.10  0.60    %#16 pink
    0.88  0.75  0.73    %#17 rose
    0.10  0.49  0.47    %#18 turquoise
    0.66  0.34  0.65    %#19 violett
    0.99  0.41  0.23    %#20 orange
];

legends = '';                   %Initializing variables for legend
save_name = '';                 %and save names

for i=1:(versus+1),   %Handling commands to strings

     cat_load = ['load_path' int2str(i) ' = strcat(load_path' int2str(i) ',name'
     int2str(i) ',ext);'];

     open_file = ['fid = fopen(load_path' int2str(i) ' , ''r'');'];

     get_data = ['data' int2str(i) ' = textscan(fid, ''%f %f %f %f %f %f %f'',
     ''CollectOutput'', 0,''headerlines'', headers);'];

     plot_data = ['plot(data' int2str(i) '{1},(data' int2str(i)
     '{2+phase})*multiplier' int2str(i) ',''Color'',['
     num2str(colororder(i,1:3)) '],''LineWidth'',1.5);'];

     create_legend = ['legends = strcat(legends, ''name' int2str(i)
     '(1:letters),'');'];

                                          %Evaluating commands
     eval(create_legend);
     eval(cat_load);
     eval(open_file);
     eval(get_data);
     eval(plot_data);
     fclose(fid);
     hold on;
```

```
if(save)
          create_save_name = ['save_name = strcat(save_name, name' int2str(i)
          '(1:letters), ''-vs-'');'];
          eval(create_save_name);
     end;
end;

hold off;
legends(i*17) = 0;
save_name(((i-1)*12+1):i*12) = 0;
create_save_name = ['save_name = strcat(save_name, name' int2str(i) ');'];
eval(create_save_name);
save_name = strcat(save_name, '.fig');
ins_legend = strcat('legend(', legends);
ins_legend = strcat(ins_legend, ');');
eval(ins_legend);

if(save)
    save_path = strcat(save_path, save_name);
    hgsave(save_path);
end;

                  %Handling the labelling
 if(phase)
     phaselabel = ' (phase)';
 else
     phaselabel = ' absolute value';
 end;

xlabel('Frequency');

a = findstr(name1, 'imp');
if(a)
    ylabel(strcat('Impedance',phaselabel));
    a = 0;
else
    a = findstr(name1, 'pwr');
end;
if(a)
    ylabel('Power');
    a = 0;
else
    a = findstr(name1, 'disp');
end;
if(a)
    ylabel('Displacement');
    a = 0;
end;
```

Piezotechnology PI

Material coefficients PIC255

Coeffcient	Unit	Value	Coefficient	Unit	Value
Densitiy	kg/m³	7,80E+03	N1	Hzm	1420
Qm		80	N3	Hzm	1710
			N5	Hzm	1125
ε 11Tr		1649	Np	Hzm	2000
ε 33Tr		1750	Nt	Hzm	2000
ε 11Sr		930			
ε 33Sr		857	d31	m/V	-1,74E-10
			d33	m/V	3,94E-10
β 11T	Vm/As	6,85E+07	d15	m/V	5,35E-10
β 33T	Vm/As	6,45E+07			
β 11S	Vm/As	1,21E+08	g31	Vm/N	-1,13E-02
β 33S	Vm/As	1,32E+08	g33	Vm/N	2,54E-02
			g15	Vm/N	3,66E-02
tan δ		20,0E-3			
			e31	N/Vm	-7,15
k31		0,351	e33	N/Vm	13,70
k33		0,691	e15	N/Vm	11,90
k15		0,661			
kp		0,620	h31	N/As	-9,43E+08
kt		0,471	h33	N/As	1,81E+09
			h15	N/As	1,45E+09
Poisson (σ)		0,36			
s11E	m²/N	1,590E-11	c11E	N/m²	1,230E+11
s33E	m²/N	2,097E-11	c33E	N/m²	9,711E+10
s55E	m²/N	4,492E-11	c55E	N/m²	2,226E+10
s12E	m²/N	-5,699E-12	c12E	N/m²	7,670E+10
s13E	m²/N	-7,376E-12	c13E	N/m²	7,025E+10
s44E	m²/N	4,492E-11	c44E	N/m²	2,226E+10
s66E	m²/N	4,319E-11	c66E	N/m²	2,315E+10
s11D	m²/N	1,393E-11	c11D	N/m²	1,298E+11
s33D	m²/N	1,096E-11	c33D	N/m²	1,220E+11
s55D	m²/N	2,532E-11	c55D	N/m²	3,949E+10
s12D	m²/N	-7,660E-12	c12D	N/m²	8,345E+10
s13D	m²/N	-2,945E-12	c13D	N/m²	5,729E+10
s44D	m²/N	2,532E-11	c44D	N/m²	3,949E+10
s66D	m²/N	4,319E-11	c66D	N/m²	2,315E+10

Values are only for information - no specification!
Simulation purpose

The data in the table was determined using testbodies with geometries and dimensions in accordance with European Standard EN 50324 2, and are typical values.

Singular parameters can deviate from catalogue values, because they were measured at samples whith were taken from one block of ceramics according to the sequence of IEC483 to get maximum consistency.
Catalogue values reflect the statistical distribution of each individual specication in prodcution and therefore also take into account spreading from material batch to material batch.

ROGERS CORPORATION

Advanced Circuit Materials

Advanced Circuit Materials Division
100 S. Roosevelt Avenue
Chandler, AZ 85226
Tel: 480-961-1382, Fax: 480-961-4533
www.rogerscorporation.com

Data Sheet
TMM

TMM® Thermoset Microwave Materials

Features:

- Wide range of dielectric constants. Ideal for single material systems on a wide variety of applications.
- Excellent mechanical properties. Resists creep and cold flow.
- Exceptionally low thermal coefficient of dielectric constant.
- Coefficient of thermal expansion matched to copper. High reliability of plated through holes.
- Resistant to process chemicals. No damage to material during fabrication and assembly processes.
- Thermoset resin for reliable wirebonding. No specialized production techniques required. TMM 10 and 10i laminates can replace alumina substrates.

Some Typical Applications:

- RF and Microwave Circuitry
- Global Positioning Systems Antennas
- Power Amplifiers and Combiners
- Patch Antennas
- Filters and Coupler
- Dielectric Polarizers and Lenses
- Satellite Communication Systems
- Chip Testers

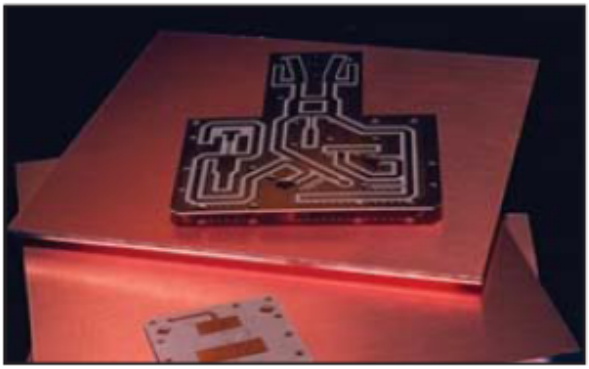

TMM® thermoset microwave materials are ceramic thermoset polymer composites designed for high plated-thru-hole reliability stripline and microstrip applications. TMM laminates are available in a wide range of dielectric constants and claddings.

The electrical and mechanical properties of TMM laminates combine many of the benefits of both ceramic and traditional PTFE microwave circuit laminates, without requiring the specialized production techniques common to these materials. TMM laminates do not require a sodium napthanate treatment prior to electroless plating.

TMM laminates have an exceptionally low thermal coefficient of dielectric constant, typically less than 30 ppm/°C. The material's isotropic coefficients of thermal expansion, very closely matched to copper, allow for production of high reliability plated through holes, and low etch shrinkage values. Furthermore, the thermal conductivity of TMM laminates is approximately twice that of traditional PTFE/ceramic laminates, facilitating heat removal.

TMM laminates are based on thermoset resins, and do not soften when heated. As a result, wire bonding of component leads to circuit traces can be performed without concerns of pad lifting or substrate deformation.

TMM laminates combine many of the desirable features of ceramic substrates with the ease of soft substrate processing techniques. TMM laminates are available clad with 1/2 oz/ft^2 to 2 oz/ ft^2 electrodeposited copper foil, or bonded directly to brass or aluminum plates. Substrate thicknesses of 0.015" to 0.500" and greater are available. The base substrate is resistant to etchants and solvents used in printed circuit production. Consequently, all common PWB processes can be used to produce TMM thermoset microwave materials.

Typical Values

TMM® Thermoset Microwave Materials

PROPERTIES	TYPICAL VALUES					DIRECTION	UNITS	CONDITIONS	TEST METHOD
	TMM3	TMM4	TMM6	TMM10	TMM10I				
[1] Dielectric Constant, ε_r	3.27 ± 0.032	4.50 ± 0.045	6.00 ± 0.080	9.20 ± 0.230	9.80 ± 0.245	Z		10 GHz	IPC-TM-650 method 2.5.5.5
[1] Dissipation Factor, tan δ	0.0020	0.0020	0.0023	0.0022	0.0020	Z		10 GHz	IPC-TM-650 method 2.5.5.5
Thermal Coefficient of ε_r	+37	+15	-11	-38	-43*		ppm/K	-55 to +125°C	IPC-TM-650 method 2.5.5.5
Insulation Resistance	>2000	>2000	>2000	>2000	>2000		Gohm	C/96/60/95	ASTM D257
Volume Resistivity	3X10⁹	6X10⁸	1X10⁸	2X10⁸	2X10⁸		Mohm cm		ASTM D257
Surface Resistivity	>9X10⁹	1X10⁹	1X10⁹	4X10⁷	4X10⁷		Mohm		ASTM D257
Flexural Strength	16.53	15.91	15.02	13.62	-	X,Y	kpsi	A	ASTM D790
Flexural Modulus	1.72	1.76	1.75	1.79	1.80*	X,Y	Mpsi	A	ASTM D790
Impact, Notch Izod	0.33	0.36	0.42	0.43	-	X,Y	ft-lb/in		ASTM D256A
Water Absorption (2X2)							%	D/48/50	ASTM D570
1.27mm (0.050" thk)	0.06	0.07	0.06	0.09	0.16				
3.18mm (0.125" thk)	0.12	0.18	0.20	0.20	0.13				
Specific Gravity	1.78	2.07	2.37	2.77	2.77			A	ASTM D792
Specific Heat	0.87	0.83	0.78	0.74	0.72*		J/g/K	A	Calculated
Thermal Conductivity	0.70	0.70	0.72	0.76	0.76	Z	W/m/K	80°C	ASTM C518
Thermal Expansion	15	16	18	21	19	X,Y	ppm/K	0 to 140°C	ASTM D3386
	23	21	26	20	20	Z			
Td	425	425	425	425	425		°C TGA		ASTM D3850
Copper Peel Strength	5.7 (1.0)	5.7 (1.0)	5.7 (1.0)	5.0 (0.9)	5.0 (0.9)	X,Y	lb/inch (N/mm)	after solder float 1 oz. EDC	IPC-TM-650 Method 2.4.8
Lead-Free Process Capable	YES	YES	YES	YES	YES				

Notes: ASTM D3386 corresponds to IPC-TM-650, method 2.4.4.1
* estimated

Typical values are a representation of an average value for the population of the property. For specification values contact Rogers Corporation.

(1) Prolonged exposure in an oxidative environment may cause changes to the dielectric properties of hydrocarbon based materials. The rate of change increases at higher temperatures and is highly dependent on the circuit design. Although Rogers' high frequency materials have been used successfully in innumerable applications and reports of oxidation resulting in performance problems are extremely rare, Rogers recommends that the customer evaluate each material and design combination to determine fitness for use over the entire life of the end product.

AVAILABLE THICKNESS:		STANDARD PANEL SIZE:	STANDARD COPPER CLADDING:
0.015" (0.381mm)	0.125" (3.175mm)	18" X 12" (457 X 305mm)	½ (17µm), 1 oz (35µm), 2 oz. (70µm) electrodeposited copper foil. Heavy metal cladding available. Contact Rogers customer service.
0.020" (0.508mm)	0.150" (3.810mm)	18" X 24" (457 X 610mm)	
0.025" (0.635mm)	0.200" (5.080mm)		
0.030" (0.762mm)	0.250" (6.350mm)		
0.050" (1.270mm)	0.275" (6.985mm)		
0.060" (1.524mm)	0.300" (7.620mm)		
0.075" (1.905mm)	0.500" (12.70mm)		
0.100" (2.540mm)			

Revised 05/2008 0797-0508-0.5CC Publication #92-108

Technisches Merkblatt

99/01
POLYURETHANE Juli 1999

FLEXOVOSS K 6 S + K 6 T

FLEXOVOSS K 6 S bzw. K 6 T ist eine lösungsmittelfreie zweikomponentige Verguß- bzw. Streichmasse auf Basis Polyurethan. Die Typen K 6 S und K 6 T unterscheiden sich nur in ihrer Konsistenz.
K 6 S ist selbstverlaufend (Vergußkonsistenz), K 6 T ist thixotrop eingestellt (Streichkonistenz)

Anwendung:

K 6 S und K 6 T werden als Verguß- bzw. Beschichtungsmaterial auf Holz, Metall, Beton, Glasfaserkunststoff, Polystyrolschaum, Polyurethanschaum sowie auf einigen Thermoplasten eingesetzt. K 6 S kann darüber hinaus als Vergußmasse zum Bau zähelastischer Formen verwendet werden.

Spezielle Einsatzgebiete:

K 6 S:	Zähelastischer Verguß von elektronischen Schaltungen und Maschinenteilen.
K 6 T:	Beschichtungen von Polystyrol- und PUR-Schaum, Holz und Metall, (mit Haftvermittler G 4), Beton (mit Haftvermittler G 4), Thermoplasten (eingeschränkt), Glasfaserkunststoffen.
K6 S und K6 T:	Zähelastische Formen für Fertigbeton-Teile und als Beton-Matrizen.

Kenndaten des flüssigen Produktes:

	A-Komponente	B-Komponente
Aussehen	Grau	braun
Viskosität	ca. 7000 mPa.s bei K 6 S; thixotrop bei K 6 T	ca. 150 mPa.s
Flammpunkt	> 200° C	> 200° C
Spezifisches Gewicht	1,5 g/cm³	1,2 g/cm³
Lagerfähigkeit	Mindestens 6 Monate	unter Ausschluß von Feuchtigkeit zwischen +5° C und +20° C

Kenndaten des Gemisches:

Mischungsverhältnis A:B	= 4:1 Gew.-Teile bzw. 3,2:1 Vol.-Teile
Verarbeitungszeit bei 20° C	= ca. 30 Minuten
Mischviskosität (RV 3/10) K6S	= 2550 mPa.s

Kenndaten des ausgehärteten Produktes:

Zugfestigkeit	7,0 N/mm2		
Shore A (DIN 53 505)	95		
Shore D (DIN 53 505)	50		
Reißdehnung	65 %		
Wasseraufnahme (DIN 53 471)	0,45 %		
Spez. Widerstand (DIN 53 482)	5,8 x 1014 W x cm		
Spez. Oberflächenwiderstand (DIN 53 482)	3,6 x 1013 W		
Durchschlagfestigkeit (DIN 53 481)	172 kV/cm		
Kriechstromfestigkeit (DIN 53 480)	KA 3c		
Dielektrizitätszahl (DIN 53 483)	5,2	4,5	4,0
trocken bei	50 Hz	1 kHz	1 MHz
Dielektrischer Verlustfaktor tan Delta (DIN 53 483)	0,115	0,059	0,024
Abrieb nach Taber-Abraser 1000 Zyklen, Steine: CS 10, Gewicht 1000 g	100,8 mg		

FLEXOVOSS K 6 ist gegen verdünnte Säuren und Laugen und Wasser gut, sowie kurzfristig gegen Heizöl beständig. K 6 ist bis zu 120° C temperaturbeständig, wobei jedoch ab 60° C eine zunehmende Erweichung zu verzeichnen ist.

Verarbeitung:

Beschichten

Voraussetzung für die Verarbeitung als Beschichtungsmasse ist ein sauberer, fettfreier und trockener Untergrund. Eine Vorbehandlung des Untergrundes kann ggf. mit G 4 erfolgen. Das angemischte K 6 wird mit einem Pinsel oder Roller aufgetragen. Die Type K 6 S wird dabei für selbstverlaufende Beschichtungen verwendet, während K 6 T als thixotrope Einstellung für senkrechte Flächen und dickere Schichten geeignet ist. Die Type K 6 S kann mittels einer Spritzpistole (4-mm-Düse, 6 bar) verspritzt werden (wegen der hierbei auftretenden Nebel ist unbedingt eine Schutzmaske zu tragen).

Vergießen

FLEXOVOSS K 6 S eignet sich infolge seiner günstigen Konsistenz sehr gut als Vergußmasse zum Fixieren und Einbetten der verschiedensten Objekte. Infolge seiner Dauerelastizität kann es als Formenmaterial eingesetzt werden. In diesen Fällen ist wegen der guten Haftung von FLEXOVOSS beim Vergießen mit Trennmitteln zu arbeiten.

Auf eine gleichmäßige Vermischung der Komponenten A und B im entsprechenden Mischungsverhältnis ist größte Aufmerksamkeit zu richten, da nur so eine richtige Aushärtung erfolgen kann. Die Gebinde sind so befüllt, daß die beiden Komponenten im vorgeschriebenen Mischungsverhältnis vorliegen.

Werden Teilmengen entnommen, so ist auf jeden Fall vorher gut aufzurühren, da die Komponenten zum Absetzen neigen.

Die Verarbeitungszeit bei 20° C beträgt ca. 30 Minuten, wobei höhere Temperaturen eine Verkürzung und niedrigere eine Verlängerung der Topfzeit ergeben. Ebenso hat die Ansatzmenge einen Einfluß auf die Verarbeitungszeit; große Mengen verkürzen infolge der Reaktionswärme die Topfzeit im Mischgefäß.

Die Aushärtung erfolgt nach ca. 12 Stunden, und die völlige Endhärte ist nach 7 Tagen erreicht.

Für die Verarbeitungstemperatur kann eine Spanne von +5° bis +30° C gesetzt werden, wobei die vorstehenden Punkte berücksichtigt werden sollten. Die o.g. Zeiten können durch Zugabe von PUR BESCHLEUNIGER verkürzt werden (eine Zugabe von 0,15 % halbiert die Topfzeit).

Feuchtigkeit jeder Art ist bei der Verarbeitung auszuschließen, da dieses zu Blasenbildung führen kann.

Der Verbrauch an K 6 S bzw. K 6 T beläuft sich auf ca. 1,5 kg/l bzw. 1,5 kg/m² bei 1 mm Dicke.

Vorsichtsmaßnahmen:
Hinweise zum Umgang mit den Produkten und zur Entsorgung entnehmen Sie bitte dem gültigen Sicherheitsdatenblatt und den entsprechenden Merkblättern der Berufsgenossenschaft der Chemischen Industrie.

Die Ausführungen in unseren Informationen dienen der anwendungstechnischen Unterweisung und sind nach bestem Wissen zusammengestellt. Eine Verbindlichkeit kann hieraus jedoch nicht hergeleitet werden.

www.savonia.fi